UNIVERSITEIT VAN PRETORIA
UNIVERSITY OF PRETORIA
YUNIBESITHI YA PRETORIA
Faculty of Natural and Agricultural Sciences

Metal organic frameworks as electrocatalysts for CO_2 reduction

By

Saraswati Sharma

(19096306)

Submitted in fulfilment of the requirements for the degree

Master of Science in Chemistry

In the Faculty of Natural & Agricultural Sciences

University of Pretoria

November 2024

Declaration

I, Saraswati Sharma (19096306) declare that the thesis, which I hereby submit for the degree Master of Science in Chemistry, at the University of Pretoria, is my own work and has not previously been submitted by me for a degree at this or any other tertiary institution.

Signature: 

Date: 11 November 2024…….

Dedication

To my dear husband,

Sunil Sharma,

for his love, encouragement, and constant support throughout this journey. Thank you for believing in me and inspiring me to reach new heights.

Acknowledgements

I am deeply grateful to God for His grace, mercy, and love, which have sustained me throughout this journey. Without His blessings, I would not have had the strength to complete this work.
My sincerest appreciation extends to my supervisor, **Prof Nolwazi Nombona**, for welcoming me into her research group and providing invaluable guidance at every step. Her dedication, regular discussions, and steadfast support have significantly contributed to my growth as a researcher, enabling me to achieve new levels of proficiency in my work. Her encouragement has been instrumental in inspiring me to reach my fullest potential.

I am also immensely thankful to my lab colleagues for their camaraderie, support, and assistance. The experience of working alongside such dedicated and insightful individuals has been truly enriching.

Finally, I wish to express my gratitude to the **University of Pretoria**, particularly the Faculty of Agriculture and Natural Sciences, for creating a nurturing and supportive environment for research. The warmth and kindness of the people in South Africa have been a constant source of inspiration throughout my time here, making this journey a truly memorable experience.

Research outputs

PREPARED MANUSCRIPTS

Exploiting metal organic frameworks for CO_2 electrochemical reduction

Saraswati Sharma and Nolwazi Nombona

Target Journal: Talanta

Abstract

Metal-Organic Frameworks (MOFs) have received significant attention as porous and crystalline materials with potential in gas storage, catalysis, and separation due to their high surface area, tuneable porosity, and various structural characteristics. MOFs have recently emerged as potential candidates for the electrochemical reduction of CO_2, an essential process in mitigating the negative consequences of increasing atmospheric CO_2 levels, which contribute to global warming, desertification, and ocean acidification.

Electrochemical CO_2 reduction offers an environmentally friendly approach to converting CO_2 into valuable compounds such as methanol, hydrocarbons, and formic acid. In this study three MOF electrocatalysts were synthesised using a solvothermal method, these were MOF-5, Cu-BTC MOF, and Ir(III)CpCl@COMOC-4 MOF. The synthesized MOFs were characterized using various techniques; including Fourier transform infrared spectroscopy (FT-IR), X-ray diffraction (XRD), scanning electron microscopy (SEM), energy dispersive X-ray spectroscopy (EDX) and Brunauer-Emmett-Teller (BET) analysis. The XRD results revealed diffractogram patterns consistent with previously reported results for the MOFs. SEM analysis showed distinct morphologies for the MOFs. MOF-5 had a cubic morphology, Cu-BTC MOF had an octahedral morphology and Ir(III)CpCl@COMOC-4 MOF displayed irregular structure characterized by visible pores on the surface. The Cu-BTC MOF had the highest specific surface area of 634 m^2/g followed by MOF-5 at 630 m^2/g and lastly Ir(III)CpCl@COMOC-4 MOF at 273 m^2/g.

Electrochemical catalysis using cyclic voltammetry, revealed CO_2 reduction capabilities across all three MOFs. The CO_2 reduction process was indicated by a shift in the MOF redox peaks in the presence of CO_2 with increase currents. Differential electrochemical mass spectrometry (DEMS) is required to validate the product(s) formed. The findings indicate that the MOFs show promise as electrocatalysts for CO_2 reduction underscoring their potential as candidates for environmentally friendly CO_2 conversion technology.

Table of contents

List of abbreviations

BDC	Benzene-1,4-dicarboxylate
BET	Brunauer-Emmett-Teller
CO_2	Carbon dioxide
COMOC	University of Ghent's Centre for Ordered Materials Organometallics, and Catalysis,
CO_2RR	Carbon dioxide reduction reaction
CV	Cyclic Voltammetry
EDX	Energy dispersive X-ray spectroscopy
eCO_2RR	Electrochemical CO_2 reduction reaction
FT-IR	Fourier transform infrared spectroscopy
GCE	Glassy carbon electrode
HER	Hydrogen evolution reaction
HOMO	Highest Occupied Molecular Orbital
LUMO	Lowest Unoccupied Molecular Orbital
MOFs	Metal-Organic Frameworks
PXRD	Powder X-ray diffraction
SEM	Scanning electron microscopy
XRD	X-ray diffraction

List of Figures

List of Schemes

List of Tables

Chapter 1: Introduction

1.1 Background

A major challenge in the 21st century is the high level of anthropogenic carbon dioxide (CO_2) emissions in the atmosphere, which harm the ecosystem and significantly contribute to global warming (*1*, *2*). According to the 5th Intergovernmental Panel on Climate Change (IPCC) report, climatic changes have an impact on extreme weather, ocean warming, sea level rise, and ocean acidification. These climate change effects accelerate the development of deserts and the extinction of species (*3*, *4*).

According to a recent study, there is about 3.9% excess CO_2 when compared to the "carbon cycle" in nature. To resolve this, new technologies must be invented, and they must have the ability to capture, convert, and use CO_2 before it enters the natural "carbon cycle" (*5*, *6*). The carbon cycle occurs naturally and involves the exchange of carbon between the atmosphere, the oceans, and the fixation of CO_2 by plants and microbes. The release of CO_2 by various species and elements of nature, such as plants, animals, and volcanoes, is balanced through this exchange (*5*, *7*). Man-made as well as natural sources are the main causes of rising CO_2 emissions. Deforestation and volcanoes are examples of natural processes that produce CO_2; estimates of their emissions range from 10% to 30% (*8*). Man-made sources include industries that produce cement, limestone, hydrogen, ammonia, soda, and chemicals through oxidation. These industries produce 25% of all CO_2 emissions (*8*, *9*). Power plants are another illustration of man-made energy sources that are efficient at producing energy through the combustion of fossil fuels, that produce 33–40% of CO_2 emissions in the atmosphere (*10-12*).

Natural CO_2 fixation is currently not feasible to remove excess CO_2 due to the dramatically increased CO_2 levels in the atmosphere. CO_2 levels increased from 270 to 385 parts per million (ppm) over the past 200 years (*5*). Increased CO_2 concentration is one of the main factors contributing to an increase in atmospheric temperature (*5*). The IPPC predicted that due to current CO_2 emissions, CO_2 levels will reach 570 ppm in 2100 years and that the average world temperature may rise by as much as 1.9 degrees (*11*, *13*).

CO_2 storage, CO_2 collection, CO_2 utilisation and conversion are three useful options to reduce excess CO_2 in the environment (*14-20*). In this study, the third option CO_2 utilisation and conversion strategy are used to reduce CO_2 emissions. There are a variety of alternative methods that exist for utilising and converting CO_2 into useful chemicals. This work is based

on the electrochemical CO_2 reduction reaction (eCO_2RR), which uses electrocatalytic porous material to convert CO_2 chemically into usable compounds.

The eCO_2RR process has many benefits, including a high reaction rate, a relatively simple reaction system in ambient conditions, controllable selectivity, and potential integration with intermittent renewable electricity sources (solar, wind, and hydro) (*21*-*23*). These benefits have caught the attention researchers.

It has a few additional benefits.

1. CO_2 emissions from renewable energy sources could be reduced using electrochemical techniques (*24*, *25*).
2. The reaction temperature and electrode potential can be used to regulate the electrochemical reduction process (*26*).
3. Electrochemical cells can be easily modified (*27*).
4. The supporting electrolyte can be recycled because so little chemical is utilised (*26*).

As a result, the electrochemical CO_2 reduction approach has a lot of potential for producing fuel sources with added value. The CO_2 molecule has a high activation energy barrier and is thermodynamically and chemically inert (*27, 28*). A strong catalyst will break through this energy barrier. A serious challenge that needs to be resolved by scientists is choosing the proper catalyst, one that can activate the chemically inert CO_2 molecules and encourage their conversion during an electrochemical reduction reaction (*27*-*29*).

According to earlier research (*30, 31*), porous materials offer a greater potential for electrochemical energy applications because of their high porosity, specific large surface area, and adaptability in charge and mass transfer. Compared to other porous materials, metal-organic frameworks (MOFs), a crystalline porous material, have demonstrated to be the best candidates for electrochemical reduction processes (*32*).

Metal-organic frameworks (MOFs) are made up of inorganic nodes (metal ions or clusters) and multitopic organic linkers. They are periodic, hybrid, and atomically well-defined porous materials (*33*). Due to their special qualities, which include high crystallinity, ultrahigh porosity, permanent porosity, adjustable pore size, fine-tunable functionality, and attractive frameworks, they or applicable in various fields (*34*), including heterogeneous catalysis,

chemical sensors, gas sorption and separation, proton conductivity, biomedicine, and others (*35–37*). In addition, it possesses a number of additional qualities that make it more appropriate for use in electrochemical energy applications, such as the electrochemical CO_2 reduction reaction (eCO_2RR), which is electrocatalytic.

1. Because of their high porosity, products and substrates can diffuse through their channels extremely quickly. This characteristic of MOF increases the likelihood of effective mass transport and easily accessible active sites for the catalyst (*34*).
2. MOF-active sites must have the ability to encircle extremely concentrated CO_2. Due to these unique properties, a large number of CO_2 molecules adsorb on the surface of MOF. Therefore, MOF is a good material for electrocatalytic CO_2 reduction (*34*).
3. MOF design allows for the modification of linkers, nodes, and pores to meet specific needs. This structural variation and tunability property enable the construction of molecular-level catalysts and MOF-based catalysts (*34*).

Hence, due to the aforementioned properties, MOFs show good performance and have been successfully applied in the atmospheric CO_2 electrocatalytic reduction process.

1.2 Problem Statement:

Coal, oil, and natural gas are still the main sources of energy for humans. Because of this, CO_2 levels in the atmosphere have increased from 280 parts per million (ppm) at the turn of the twentieth century to 400 ppm currently (*35*, *36*).

It is true that when fossil fuels are used for energy, CO_2 is released directly into the atmosphere. Despite being chemically stored in fossil fuels, CO_2 is released into the atmosphere during combustion. The amount of atmospheric CO_2 is significantly impacted by the excessive use of fossil fuels. These anthropogenic activities have disturbed the ecosystem's climatic balance and resulted in the loss of natural energy (fossil fuels) (*37-38*). Excess CO_2 in the atmosphere warms the planet and this result in climate change.

Therefore, both the reduction of fossil fuels and the changing climate are caused by increasing atmospheric CO_2 concentrations. Finding ways to reduce CO_2 emissions is a continuous objective for scientists and academics. In the field of reducing CO_2 emissions, various techniques are employed, including electrochemical CO_2 reduction, cryogenic distillation,

membrane-based separation, and physical and chemical absorption. This research will concentrate on the development of MOFs-based electrocatalysts for CO_2 reduction.

1.3 Motivation:

Fossil fuel consumption causes significant CO_2 emissions and disturbs the environmental balance. As the data collected indicates, figures 1.1(a), the use of fossil fuels by several sources has significantly contributed to the rise in atmospheric CO_2 level. The atmospheric CO_2 level has exceeded 300 parts per million (ppm) for the first time in more than 800,000 years and is currently much higher than 400 ppm (*39*).

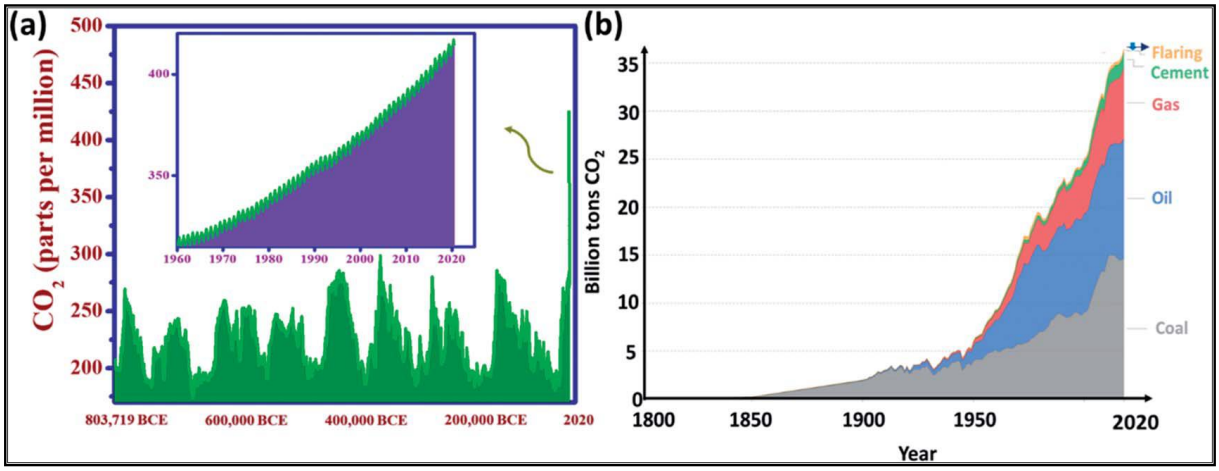

Figure 1.1: (a) The average global atmospheric CO_2 concentrations over 800 000 years, and (b) the average global CO_2 emissions throughout a time period by fuel type (*39*).

It is predicted that it will exceed 500 ppm in 2050 as a result of increased global energy demand and significant coal, oil, and natural gas consumption. Figure 1.1(b) shows the global CO_2 emissions by fuel over a 220-year period (*39*).

In 115 years, the amount of CO_2 released increased from 2 billion tonnes in 1900 years to about 36 billion tonnes. The Global Carbon Project predicts annual increases of 2.7 percent in 2018 and 0.6 percent in 2019. As per recent trends, the reduction of 8% in coal emissions, 2.3% in natural gas emissions, and 4.5% in oil emissions due to the COVID-19 forced confinement resulted in the world's CO_2 emissions being approximately 5% lower in 2020 than in 2019. This shows that CO_2 emissions originate from a range of fuel types as well as energy generation and industrial production (the production of coal, oil, gas, and cement) (*40-41*).

Finding a suitable solution is mostly crucial to addressing the problem of CO_2 emissions based on the above study, which motivates further research on CO_2 reduction.

1.4 Hypothesis:

The synthesised MOFs are expected to serve as efficient electrocatalysts for CO_2 reduction. The materials under investigation include Zn_4O(1,4-benzenedicarboxylate) (MOF-5), Copper(II)-benzene-1,3,5-tricarboxylate (Cu-BTC/MOF-199), and Iridium(III)-bipyridine-metal-organic framework (Ir(III)Cp*Cl@COMOC-4). These MOFs are hypothesized to enhance the sensitivity of electrochemical CO_2 reduction, owing to their distinct structural and catalytic properties.

1.5 Aims and objectives

The aim is to use MOFs as electrocatalysis for CO_2 reduction. The following objectives are proposed in order to accomplish this goal:

- To synthesize and characterize of Zn_4O(1,4-benzenedicarboxylate) MOF/ MOF-5.
- To synthesize and characterize of Copper(II)-benzene-1,3,5-tricarboxylate/MOF Cu-BTC MOF/MOF-199.
- To synthesize and characterize an iridium-based MOF/Ir(III)Cp*Cl@COMOC-4 /iridium(III)-bipyridine-metal-organic framework.
- To investigate the electrochemical behaviour of glassy carbon and modified MOF-based electrodes in aqueous medium and measure the redox behaviour of the electrodes using cyclic voltammetry.
- Use the glassy carbon MOF modified electrodes in the electrochemical reduction of CO_2.

1.6 Research Limitation

- The selectivity of MOFs for CO_2 reduction is relatively low in the presence of moisture, water, and acidic gases, as demonstrated by various investigations (*42*).

- MOFs can be given a unique shape by changing their metal clusters and ligands. Despite these benefits, some MOFs perform poorly due to chemical and physical limitations. For example, in the presence of atmospheric moisture or high temperatures, the crystalline structures of some MOFs may degenerate (*42*).

References

1. Clark, P.U., Shakun, J.D., Marcott, S.A., Mix, A.C., Eby, M., Kulp, S., Levermann, A., Milne, G.A., Pfister, P.L., Santer, B.D., and Schrag, D.P., Consequences of twenty-first-century policy for multi-millennial climate and sea-level change. *Nature Climate Change* **6**, 360-369 (2016).
2. Steffen, W., Grinevald, J., Crutzen, P., and McNeill, J., The Anthropocene: conceptual and historical perspectives. *Philosophical Transactions of the Royal Society A: Mathematical, Physical and Engineering Sciences* **369**, 842-867 (2011).
3. Ishtiaque, A., Estoque, R.C., Eakin, H., Parajuli, J., and Rabby, Y.W., IPCC's current conceptualization of 'vulnerability' needs more clarification for climate change vulnerability assessments. *Journal of Environmental Management* **303**, 114246-114249 (2022).
4. Sage, R.F. Global change biology: A primer. *Global Change Biology* **26**, 3-30 (2020).
5. Mikkelsen, M., Jorgensen, M., and Krebs, F.C. The teraton challenge. A review of fixation and transformation of carbon dioxide. *Energy & Environmental Science* **3**, 43-81 (2010).
6. Poliakoff, M., Leitner, W., and Streng, E.S., The twelve principles of CO_2 chemistry. *Faraday discussions* **183**, 9-17 (2015).
7. Aresta, M., and Dibenedetto, A. Utilisation of CO_2 as a chemical feedstock: opportunities and challenges. *Dalton Transactions* **28**, 2975-2992 (2007).
8. Xiaoding, X., and Moulijn, J.A. Mitigation of CO_2 by chemical conversion: Plausible chemical reactions and promising products. *Energy & Fuels* **10**, 305-325 (1996).
9. Halmann, M., and Steinfeld, A. Fuel saving, carbon dioxide emission avoidance, and syngas production by tri-reforming of flue gases from coal-and gas-fired power stations, and by the carbothermic reduction of iron oxide. *Energy* **31**, 3171-3185 (2006).

10. Carapellucci, R., and Milazzo, A. Membrane systems for CO_2 capture and their integration with gas turbine plants. *Proceedings of the Institution of Mechanical Engineers, Part A: Journal of Power and Energy* **217**, 505-517 (2003).
11. Yang, H., Xu, Z., Fan, M., Gupta, R., Slimane, R.B., Bland, A.E., and Wright, I. Progress in carbon dioxide separation and capture: A review. *Journal of environmental sciences* **20**, 14-27 (2008).
12. Bae, Y.S., and Snurr, R.Q. Development and evaluation of porous materials for carbon dioxide separation and capture. *Angewandte Chemie International Edition* **50**, 11586-11596 (2011).
13. Li, L., Zhao, N., Wei, W., and Sun, Y. A review of research progress on CO_2 capture, storage, and utilization in Chinese Academy of Sciences. *Fuel* **108**, 112-130 (2013).
14. Boot-Handford, M.E., Abanades, J.C., Anthony, E.J., Blunt, M.J., Brandani, S., Mac Dowell, N., Fernández, J.R., Ferrari, M.C., Gross, R., Hallett, J.P., and Haszeldine, R.S. Carbon capture and storage update. *Energy & Environmental Science* **7**, 130-189 (2014).
15. Rubin, E.S., Chen, C., and Rao, A.B. Cost and performance of fossil fuel power plants with CO_2 capture and storage. *Energy policy* **35**, 4444-4454 (2007).
16. Figueroa, J.D., Fout, T., Plasynski, S., McIlvried, H., and Srivastava, R.D. Advances in CO_2 capture technology the US Department of Energy's Carbon Sequestration Program. *International journal of greenhouse gas control* **2**, 9-20 (2008).
17. Gibbins, J., and Chalmers, H. Carbon capture and storage. *Energy policy* **36**, 4317-4322 (2008).
18. Leung, D.Y., Caramanna, G., and Maroto-Valer, M.M. An overview of current status of carbon dioxide capture and storage technologies. *Renewable and Sustainable Energy Reviews* **39**, 426-443 (2014).
19. Yu, K.M.K., Curcic, I., Gabriel, J., and Tsang, S.C.E. Recent advances in CO_2 capture and utilization. *ChemSusChem: Chemistry & Sustainability Energy & Materials*, 893-899 (2008).
20. Al-Mamoori, A., Krishnamurthy, A., Rownaghi, A.A., and Rezaei, F. Carbon capture and utilization update. *Energy Technology* **5**, 834-849 (2017).
21. Zheng, T., Jiang, K., Ta, N., Hu, Y., Zeng, J., Liu, J., and Wang, H. Large-scale and highly selective CO_2 electrocatalytic reduction on nickel single-atom catalyst. *Joule* **3**, 265-278 (2019).

22. Sa, Y.J., Lee, C.W., Lee, S.Y., Na, J., Lee, U., and Hwang, Y.J. Catalyst electrolyte interface chemistry for electrochemical CO_2 reduction. *Chemical Society Reviews* **49**, 6632-6665 (2020).
23. Jouny, M., Luc, W., and Jiao, F. General techno-economic analysis of CO_2 electrolysis systems. *Industrial & Engineering Chemistry Research* **57**, 2165-2177 (2018).
24. Whipple, D.T., and Kenis, P.J. Prospects of CO_2 utilization via direct heterogeneous electrochemical reduction. *The Journal of Physical Chemistry Letters* **1**, 3451-3458 (2010).
25. Ma, S., and Kenis, P.J. Electrochemical conversion of CO_2 to useful chemicals: current status, remaining challenges, and future opportunities. *Current Opinion in Chemical Engineering* **2**, 191-199 (2013).
26. Al-Rowaili, F.N., Jamal, A., Ba Shammakh, M.S., and Rana, A. A review on recent advances for electrochemical reduction of carbon dioxide to methanol using metal–organic framework (MOF) and non-MOF catalysts: challenges and future prospects. *ACS Sustainable Chemistry & Engineering* **6**, 15895-15914 (2018).
27. Albo, J., Alvarez-Guerra, M., Castano, P., and Irabien, A. Towards the electrochemical conversion of carbon dioxide into methanol. *Green Chemistry* **17**, 2304-2324 (2015).
28. Liu, H., Zhu, Y., Ma, J., Zhang, Z., and Hu, W. Recent advances in atomic-level engineering of nanostructured catalysts for electrochemical CO_2 reduction. *Advanced Functional Materials*, **30**, 1910534-1910555 (2020).
29. Shao, P., Yi, L., Chen, S., Zhou, T., and Zhang, J., Metal-organic frameworks for electrochemical reduction of carbon dioxide: The role of metal centers. *Journal of Energy Chemistry* **40**, 156-170 (2020).
30. Baumann, A.E., Burns, D.A., Liu, B., and Thoi, V.S. Metal-organic framework functionalization and design strategies for advanced electrochemical energy storage devices. *Communications Chemistry* **2**, 1-14 (2019).
31. Tajik, S., Beitollahi, H., Nejad, F.G., Kirlikovali, K.O., Van Le, Q., Jang, H.W., Varma, R.S., Farha, O.K., and Shokouhimehr, M. Recent electrochemical applications of metal–organic framework-based materials. *Crystal Growth & Design* **20**, 7034-7064 (2020).
32. Li, J.H., Wang, Y.S., Chen, Y.C., and Kung, C.W. Metal–organic frameworks toward electrocatalytic applications. *Applied Sciences* **9**, 2427-2446 (2019).

33. Islamoglu, T., Goswami, S., Li, Z., Howarth, A.J., Farha, O.K., and Hupp, J.T. Postsynthetic tuning of metal–organic frameworks for targeted applications. *Accounts of chemical research* **50**, 805-813 (2017).
34. Li, X. and Zhu, Q.L., MOF-based materials for photo-and electrocatalytic CO_2 reduction. *EnergyChem*, **2**, 100033-100114 (2020).
35. Demirbas, A. Biomass resource facilities and biomass conversion processing for fuels and chemicals. *Energy conversion and Management* **42**, 1357-1378 (2001).
36. Mahasneh, A. Climate change and global warming. *Journal of Industrial Pollution Control* **37**, 1-7 (2021).
37. Keeling, C.D. Industrial production of carbon dioxide from fossil fuels and limestone. *Tellus* **25**, 174-198 (1973).
38. Yu, K.M.K., Curcic, I., Gabriel, J., and Tsang, S.C.E. Recent advances in CO_2 capture and utilization. *ChemSusChem: Chemistry & Sustainability Energy & Materials* **1**, 893-899 (2008).
39. Reddy, M.S.B., Ponnamma, D., Sadasivuni, K.K., Kumar, B., and Abdullah, A.M. Carbon dioxide adsorption based on porous materials. *RSC advances* **11**, 12658-12681 (2021).
40. Le Quere, C., Jackson, R.B., Jones, M.W., Smith, A.J., Abernethy, S., Andrew, R.M., De-Gol, A.J., Willis, D.R., Shan, Y., Canadell, J.G., and Friedlingstein, P. Temporary reduction in daily global CO_2 emissions during the COVID-19 forced confinement. *Nature climate change* **10**, 647-653 (2020).
41. IEA, U.Global energy review. *IEA*, 1-55 (2020).
42. Sosa, J.D., Bennett, T.F., Nelms, K.J., Liu, B.M., Tovar, R.C., and Liu, Y. Metal–organic framework hybrid materials and their applications. *Crystals* **8**, 325-348 (2018).

Chapter 2: Literature review

2.1 Introduction

Since the nineteenth-century, fossil fuels such as coal, natural gas and oil have been utilized as the principal energy source to power our economy and civilization (*1, 2*). The overuse of fossil fuels causes many problems. Despite the fact that the world's population and economy have been expanding rapidly, the demand for energy has been constantly rising (*3, 4*).

Conversely, non-renewable fossil fuel reserves have become depleted, worsening the energy problem. The widespread use of fossil fuels has led to a slow but steady rise in carbon dioxide (CO_2) emissions in the atmosphere year after year (*5*). The overproduction of CO_2 is thought to be one of the main causes of a number of unfavourable environmental changes, including global warming, ocean acidification and desertification. Therefore, reducing the adverse effects of excessive CO_2 emissions has become a top priority for modern society (*6, 7*).

In order to deal with the aforementioned issues and reduce their negative effects, it is required to separate and capture CO_2 from its sources, such as industry and power plants. A variety of methods have been used to capture CO_2. The adsorption process is one of the most well-liked methods that has recently experienced broad application. Chemical and physical adsorption are both commonly used in these methods. Additionally, this adsorption process makes use of a porous medium. But this strategy may impact marine or terrestrial life, in contrast to normal strategies for storing CO_2, which depend on either the geology or the marine environment (*8-10*).

Due to the benefits of environmental health, scientists are looking for a low-cost solution to reducing CO_2 emissions. They are focusing on transforming excess CO_2 into items with additional value, such as fuels and chemicals. Converting CO_2 emissions into chemicals and fuel with additional value is the most effective and economical strategy to minimise them. Research has started to create simple CO_2 conversion technologies as a result of this advantageous viewpoint. In 2013, Quadrelli et al. provided an overview of the most effective techniques for using renewable energy to transform CO_2 (as a carbon source) into useful compounds (*11*).

Currently varieties of methods have been employed to convert CO_2 into useful chemicals and fuels. Some of the most common methods are biological, electrochemical, photochemical, and thermochemical reactions (*12*). Among all of these methods, the CO_2 electrochemical reduction reaction (eCO_2RR) has recently received a lot of interest due to its advantages in terms of straightforward operating conditions at ambient temperature and pressure. Using the eCO_2RR method, energy can be generated by utilising renewable energy sources such as the sun, wind, and tides. Additionally, it reduces CO_2 emissions and offers a practical replacement for intermittent and location-based renewable energy sources for energy storage (*12*). Thus, CO_2 electrochemical reduction offers a practical route towards energy conversion and/or the preparation of high-value chemical compounds. This electrochemical methodology offers a practical way to lessen the negative effects of CO_2 and supplies fine chemicals by converting it into fuels using a range of plentiful renewable energy sources (*13*).

Since the linear CO_2 molecule is highly stable in nature and totally oxidized, in order to produce effective and efficient electrocatalysts, it is required to promote this kinetically slow reduction reaction (*14*, *15*). The properties of the electrocatalysts used have a significant impact on the performance of the CO_2 electrochemical reduction reaction. Due to its high energy barriers and multiple electron transfer steps, eCO_2RR has a sluggish kinetic rate. It is also believed that the CO_2 reduction reaction and the hydrogen evolution reaction (HER) are competing reactions. Hence, the completion of the HER and the prolonged electron and proton transfer processes caused by the sluggish reaction kinetics result in insufficient production (*16*, *17*). An efficient and selective electrocatalyst for the CO_2 reduction reaction (CO_2RR) must be developed that can function at low potential with a good yield of the final products. It is urgently needed because the primary barriers to actually using an electrocatalyst to reduce CO_2 emissions have already been addressed. But this remains a major challenge.

MOFs are a distinct category of porous structural materials that demonstrate notable coordination between metal ions and ligands (*18*). Their unique structural features include a huge porous surface area, strong inorganic and organic catalytic sites, and a programmable post-synthetic structure. MOFs are attractive electrocatalysts and alternatives for CO_2 reduction. All of these MOF characteristics can provide structural modification behaviour, which is especially advantageous for electrochemical applications (*19*). Furthermore, due to their distinct properties, these newly developed MOF materials stand out as important

applications in energy storage, gas storage, hazardous chemical adsorption, photo- and electrocatalysis, and other processes (*20*).

According to Kumar et al. (*21*) MOFs were first employed as an electrocatalyst for the CO_2 reduction process (CO_2RR) in 2012. Hinogami et al. (*22*) noted that the copper rubeanate MOF (CR-MOF) enhanced CO_2RR performance in the same year. The CO_2RR occurs in a complicated three-phase system consisting of a liquid electrolyte, gaseous CO_2, and a solid catalyst. Surface reactions, CO_2 activation, and product desorption are all involved in three-phase interfaces. The three-phase interfaces are mass diffusion, electron transport, and electrochemical processes (*23*). When combined, these three characteristics are referred to as "proficiency of active sites." They are essential for the next catalytic action to take place (*23*).

There are several benefits to using MOFs in the creation of different catalytic materials:

1. Offering effective mass transfer and active site availability (*21*);
2. Changing the electronic structure easily via heteroatom doping (*21*) and;
3. Preserving the properties of pristine MOFs following electrochemical, thermal, or pyrolytic degradation (*21*).

Consequently, MOF-based porous materials that possess the above-described characteristics provide perfect CO_2 electrocatalysts. MOF-based materials maintained their inherited characteristics, including uniform distribution of active sites, porosity, and enhanced surface area, even following rational pyrolysis (*24, 25*). MOFs are distinct from other porous materials due to their numerous benefits, and they have shown effectiveness in the electrocatalytic reduction of CO_2.

2.2 MOF's Historical Background

In 1893, Werner-type complexes were discovered, which marked the beginning of MOFs as we know them today. Werner-type complexes have been found to exist as crystals. These crystals were made by combining metal centres with nitrogen as an organic ligand. These substances usually contain the chemical formula MX_2L_4, where L is an octahedral divalent metal, M is a coordinated pyridine molecule, and X is an anionic ligand (such as NCO^-, CN^-, or NO_3^-), and the gradual evolution of MOF is represented in the figure 2.1 below (the historical context of MOF is depicted in figure 2.1) (*26, 27*).

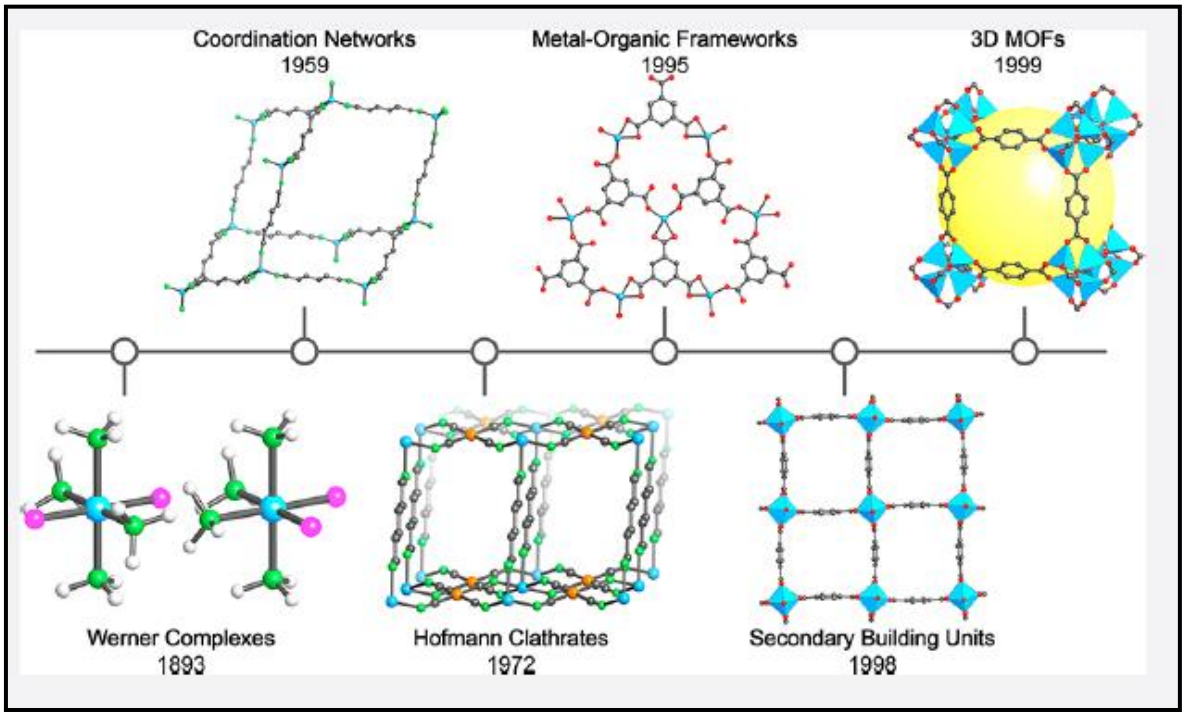

Figure 2.1 Historical background of MOF (*26*)

In 1897, Hofmann et al. used the formula $Ni(CN)_2(NH_3)C_6H_6$ to describe the coordinated network (*28, 29*). After its crystal structure was discovered. Rayner et al. continued to describe it in 1952. The presence of the $Ni(CN)_2(NH_3)$ group is also discovered in the squared-layered Hofmann structure. The benzene group is also present in these channels. The main discovery is that the entire structure looks like a network (*28, 30*).

In 1940, zeolites were the first synthetic crystalline porous materials to receive a detailed examination. Zeolites are entirely composed of inorganic substances like silicates and aluminates, and they contain pores with sizes in the range of 1 nm to 2 nm. Initially, they were discovered in the late 1980s to early 1990s (*31*).

In 1995, Yaghi invented the structure of metal-organic frameworks (MOFs). With a high surface area and consistent porosity. MOFs are crystalline porous materials that arise as a result of strong interactions between charged organic ligands and metal ions (*32, 33–34*).

The study of porous materials and their applications has entered a new age. MOFs are incredibly adaptable inorganic and organic building components. By mixing a variety of other

MOFs with different organic and inorganic building components, each possessing unique geometries and functions, researchers can achieve a great deal of diversity in isoreticular modification. This approach allows for the tailored design of materials with specific properties and applications. Although significant structural and functional modifications can be made during synthesis or by post-synthesis modifications, the underlying topology and design are maintained. The discovery and development of reticular chemistry have had a substantial influence on the synthesis and use of porous crystalline framework materials (*31, 35*).

Over the last few decades, more than 20,000 MOFs have been described in the literature, and Yaghi et al. have substantially improved our understanding by explaining the structural properties of MOFs. However, their studies could only demonstrate that some MOFs have crystalline material-like characteristics. But they were unable to estimate how many MOFs exhibit persistent porosity with accuracy (*36*).

Some of the most typical MOF crystal structures are shown in figure 2.2(a) (*37*). The Cambridge Structural Database (CSD) received 99,075 MOF crystal structures in 2020, highlighting the significant progress made in the field of MOFs over time. The periodic table's rows and columns are represented in these crystal formations (*38*). Figure 2.2(b) displays the estimated number of MOFs listed by year in the Cambridge Structural Database, gathered from the CSD on March 4, 2020 (*38*).

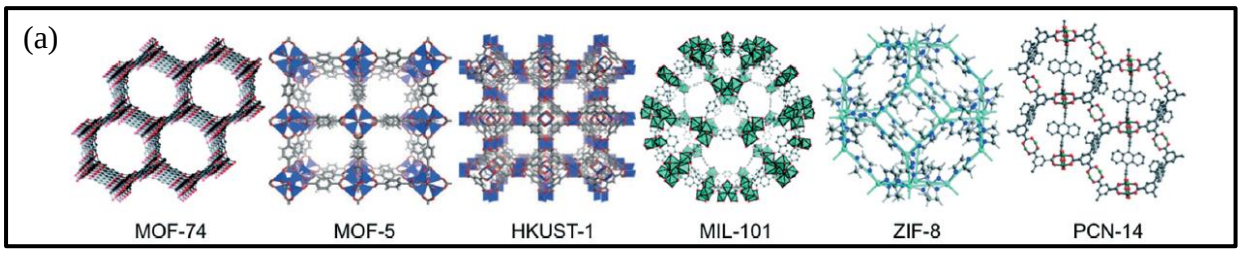

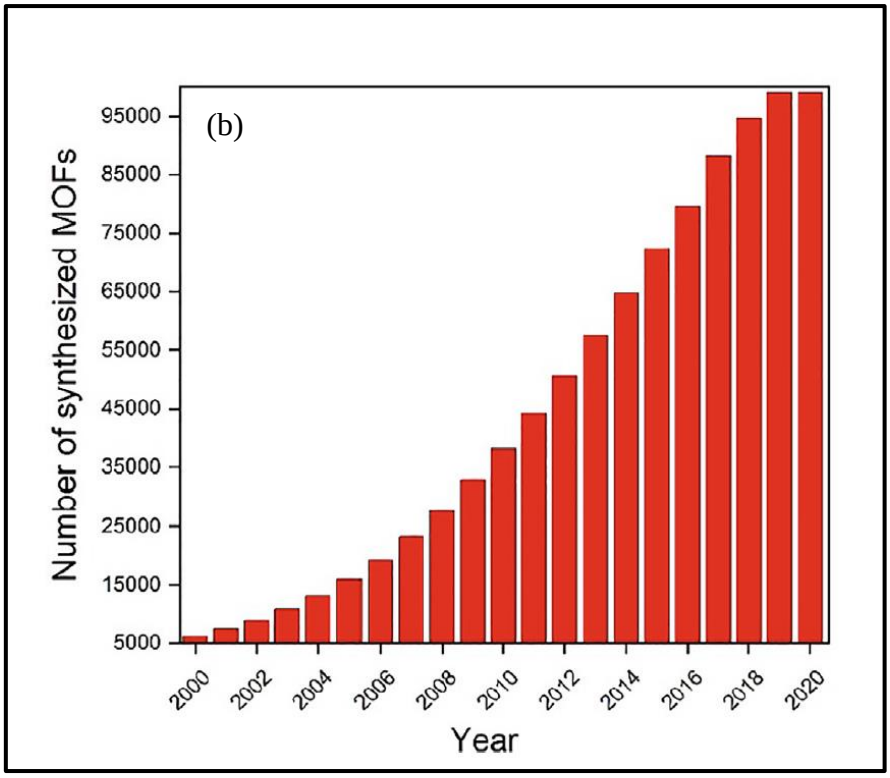

Figure 2.2: (a) Crystal structures of the most prevalent MOFs found in the Cambridge Crystallographic Data Centre (CCDC) database (*37*) and **Figure 2.2:** (b) The number of MOFs synthesized as on the Cambridge Structural Database (CSD) (*38*)

In the late 1980s and early 1990s, the fundamental idea of porosity was developed for metal-organic materials with extended structures (*39*, *40*). Prior to the late 1990s, there were no known experimental gas adsorption data for these inorganic-organic hybrid materials. Kitagawa demonstrated that metal-organic polymers were capable of accepting guest molecules at the gas phase at both room temperature and high-pressure gas adsorption isotherms (*41*).

The first MOF with permanent porosity was reported in 1998 by Yaghi. The method used to examine permanent porosity in other porous materials, such as porous zeolites, silica, and porous carbon, was nitrogen adsorption and desorption isotherms at 77 K and low pressure. He also calculated the apparent surface area and pore volume of the first MOF. Currently, MOFs have attracted interest from a variety of scientific disciplines for a number of applications, as well as the synthesis and production of novel materials (*41*).

Table 2.1 lists some of the MOFs along with their BET area, pore volume, and reported year by different research teams. This data illustrates the several varieties of MOF that have been found and the growth of the MOF field (*41*).

Table 2.1: MOF field progress report (*41*).

MOF Materials	BET area ($m^2 g^{-1}$)	Pore volume ($cm^3 g^{-1}$)	Reported year
MOF-5	3800	1.55	1999, 2007
MOF-177	4750	1.89	2007
MIL-101	4230	2.15	2005, 2008
MOF-200	4530	3.59	2010
NU-100	6140	2.82	2010
MOF-210	6240	3.60	2010
NU-110	7140	4.40	2012
PCN-68	5110	2.13	2010

2.3 Classification and Nomenclature of MOF materials

2.3.1 Classification of MOFs

MOFs are divided into a number of groups according to the parts that make them up. Combining MOF nanocomposites with certain materials, such as metal oxides, polyoxometalates, carbon materials, quantum dots, enzymes, and polymers, can result in functional diversity (*42*, *43*).

2.3.1.1 Porous Coordination Networks (PCNs).

Porous Coordination Networks (PCNs) are three-dimensional stereo-octahedron materials with a hole-cage-hole topology. Some of the PCNs include PCN-333, PCN-222, PCN-224, and PCN-57. One of the PCN MOFs is PCN-222, which is widely used in sensors. Lei et al. developed a sensitive electrochemical sensor for detecting DNA using PCN-222 (*43*, *44*).

2.3.1.2 Isoreticular MOFs

Isoreticular MOFs are made by utilising $[Zn_4O]^{6+}$ Secondary Building Units and a series of aromatic carboxylates. They are octahedral, crystalline, and microporous materials. IRMOF-3 has been widely employed to create sensors in recent years. Zhang and their co-workers

developed IRMOF-3 nanosheets that have exceptional selectivity and sensitivity for finding 2,4,6-trinitrophenol in wastewater (*45*, *46*).

2.3.1.3 Porous Coordination Polymers (PCPs).

In the construction of porous coordination polymer materials, derivatives of carboxylic acid, and pyridine, serve as primary building units (PBU), while transition metal ions serve as secondary building units (SBU). Buser and his colleagues started by building a Prussian blue 3D network. Sumida and his colleagues detected organic vapours using a quartz crystal microbalance (QCM) by immobilising PCP Zn(NO_2-ip)(bpy) (*42*, *47-49*).

2.3.1.4 Zeolitic imidazolate frameworks

Zeolitic imidazolate frameworks are synthesised from imidazole derivatives and other elements having valence electrons. They are topologically organised zeolites. Examples of ZIFs include the ZIF-8, ZIF-90, ZIF-L, ZIF-71, ZIF-67, and ZIF-7. Since the ZIF-8 material performs so well in terms of acid sensitivity, surface area, cytotoxicity, and pore size, it is described in greater detail than the other ZIF materials. Pan and colleagues created a ZIF-8 MOF to detect HIV-1 DNA. ZIFs, which have large pores and excellent chemical and thermal stability, are used as a network to create innovative MOF composites (*42*, *50-53*).

2.3.1.5 University of Oslo (UiO) MOFs.

At the University of Oslo, Lillerud and his co-workers developed the first MOF, using dicarboxylic acid as the PBU and $Zr_6(\mu_3\text{-}O)_4(\mu_3\text{-}OH)$ as the SBU. UiO-66 (Zr) was made using a solvothermal method from $ZrCl_4$ and BDC with octahedral and tetrahedral pore cages. The framework is stable at a pH 14, according to the experimental results, and UiO-66 has good thermodynamic stability. Supercapacitors have successfully used UIO-66 as an electrode material (*42*).

The above-mentioned classification has also resulted in the recent emergence of a large number of MOFs, such as Pohang University of Science and Technology (POST-n), Northwestern University (NU), Dresden University of Technology (DUT-n family), Hong Kong University of Science and Technology (HKUST-n), University of Nottingham (NOTT-n), and Christian-Albrechts-Universitat (CAU) (CAU-n family). A new class of permeable materials known as biological metal-organic frameworks (Bio-MOFs) has recently emerged (*42*).

2.3.1.6 Materials Institute Lavoisier (MIL) MOFs.

Lavoisier created a MOF by combining two carboxylic functional groups and a variety of valence electron-containing elements from the Institute of Materials Research. In response to

external incitation, the pore-size configuration of MIL MOFs can change freely. MIL MOFs include MIL-101, MIL-100, MIL-53, MIL-88, and MIL-125. The highly sensitive resistive humidity sensor MIL-101(Cr) was created by Sun and colleagues using a hydrothermal process. MIL composites act as chemical sensors to immobilise proteins, QDs, and other components. It's important because MILs, with their ultrahigh surface area, homogeneous pores, and permanent porosity, are perfect for a variety of biological and environmental applications due to their unique features. "Transfer capacity" refers to the structure that, in response to external stimuli, stretches between micropores and mesopores (*47-54*, *55)*.

2.3.2 Nomenclature of MOF

The term "MOF" stands for Metal Organic Framework, which is a rigid framework with a specific geometry that facilitates the interconnection of two components during fabrication. It also signifies the presence of a porous structure and strong bonding (*56*). Iso-Reticular Metal Organic Framework (IRMOF), Metal Organic Polyhedra (MOP), Zeolitic Imidazole Framework (ZIF), Porous Metal Organic Framework (PMOF), Coordination Polymers (CP), Porous Coordination Polymers (PCP), and Microporous Metal Organic Framework (MMOF) are some of the MOF's acronyms that have been used in literature (*57*). The acronym "MOF" typically refers to a group of substances. However, it indicates a particular metal-organic framework when it is followed by an ordinal number *(58)*.

The acronyms for the MOF are explained in the following paragraphs.

2.3.2.1 Topology based MOF acronyms

MOF naming is based on the same net, i.e., having the same topology. One form of MOF is called an isoreticular metal-organic framework (IRMOF), which has a similar network layout. By replacing the organic linkers of IRMOF-1 (i.e., MOF-5) with alternative organic linkers, many IRMOFs with distinct properties, such as large BET surface areas and high chemical stability, may be produced (*59*, *60*).

MOF-5, which was initially characterised in 2002 by Eddaoudi, Yaghi, and colleagues, is the most well-known kind of IRMOF. MOF-5's isoreticular series (IRMOFs series) may be constructed utilising hexagonal zinc acetate with six connections, the $[Zn_4O(RCO_2)_6]$ metal cluster, and linear carboxylate-based ligands. Figure 2.3 depicts the MOF-5 (IRMOFs) series. (*61*). Some of the names of the IRMOF MOF series are listed below in Table 2.2.

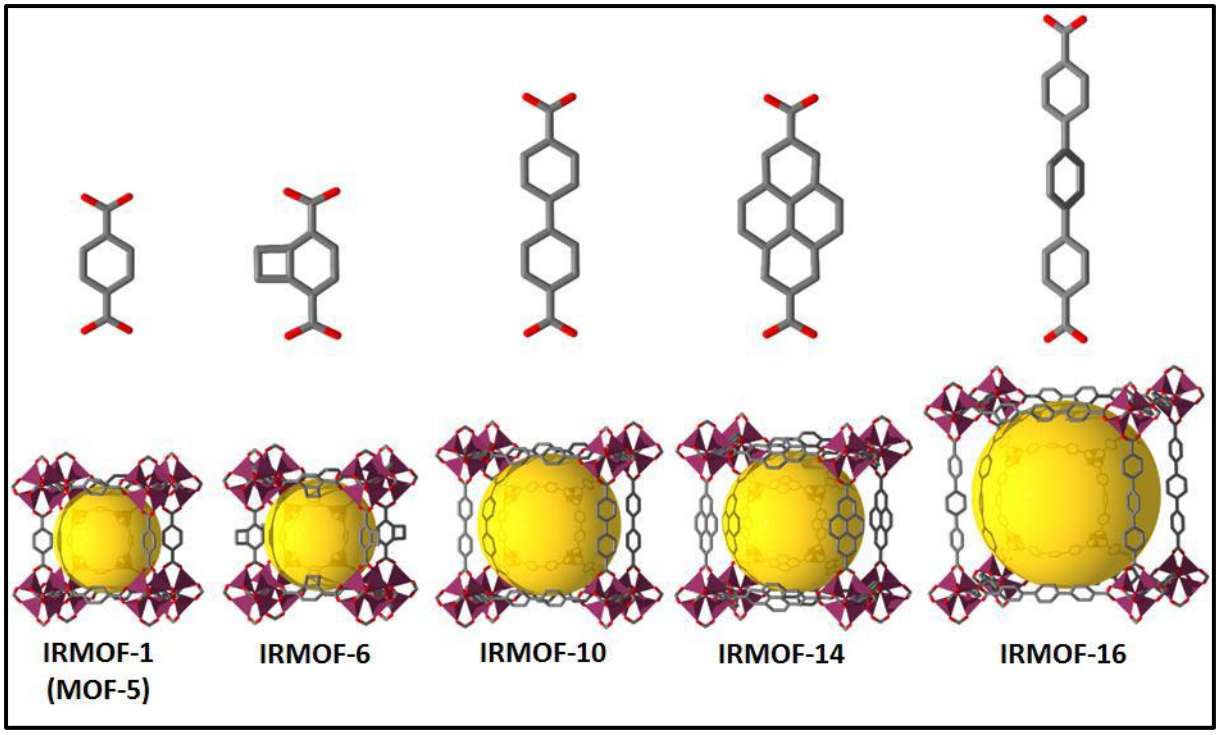

Figure 2.3: Isoreticular sequence of IRMOFs. Colour code: Zn = plum, C = grey, and O = red; hydrogen atoms and solvent molecules have been omitted for clarity (*61*).

2.3.2.2 Discovered site, MOF acronyms

Materials with a specific composition are commonly referred to as "metal-organic coordination polymers" by Chinese and Russian researchers. MOFs are categorised into classes with the same letter designation based on the place of their discovery rather than structural similarity. Among them are UiO, MIL, HKUST, LIC, and other institutions (*62*). Table 2.2 provides a list of a few MOFs by name that are part of this category mention below.

2.3.2.3 Based on zeolite crystal topology

The names of MOFs are represented on the base of the zeolite crystal topology. This particular class of MOFs are called ZIFs (zeolite imidazolate frameworks), which is made up of imidazolate linkers that connect tetrahedrally coordinated transition metal ions (such as Fe, Co, Cu, and Zn). ZIFs exhibit zeolite-like topologies. The angle between the metal and the imidazole is comparable to the 145° Si-O-Si angle in zeolites (*62, 54*). A list of few MOFs by name that belong to the ZIFs category is listed in Table 2.2 below.

Table 2.2: Examples of typical MOF names along with information about their composition (*62*, *63*).

Serial No.	Terms	Formula	Interpretation of acronyms
1	MOF-253	Al(OH)(BPYDC)	**Metal-Organic Framework**
2	MOF-5	$Zn_4O(BDC)_2$	
3	MOF-235	$[Fe_3O(BDC)_3(DMF)_3][FeCl_4](DMF)_3$	
4	MOF-74-Zn	$Zn_2(H_4dhtp)$	
5	MOF-210	$(Zn_4O)_3(BTE)_4(BPDC)_3$	
6	MOF-11	$Co_2(ad)_2(CO_2CH_3)_2$	
7	MOF-200	$Zn_4O(BBC)_2$	
8	MOF-177	$Zn_4O(BTB)_2$	
9	MOF-101	$Cu_2(BDC\text{-}Br)_2(H_2O)_2$	
10	MOF-505	$Cu_2(bptc)(H_2O)_3(DMF)_3$	
11	IRMOF-1 (MOF-5)	$Zn_4O(BDC)_3.7DEF.3H_2O$	IsoReticular Metal-Organic Frameworks
12	IRMOF-16	$Zn_4O(TPDC)_3.17DEF.2H_2O$	
13	IRMOF-20	$Zn_4O(H_2T_2DC)_3$	
14	UiO-66	$Zr_6O_6(BDC)_6$	Universitetet i Oslo
15	UiO-67	$Zr_6O_6(BPDC)_6$	
16	UiO-68	$Zr_6O_6(TPDC)_6$	
17	MIL-53	Al(OH)(BDC)	Materials of Institut Lavoisier
18	MIL-101	$Cr_3O(H_2O)_2F.(BDC)_3.nH_2O$	
19	MIL-53(Al)-NH_2	$Al(OH)(BDC\text{-}NH_2)$	
20	MIL-100-Fe	$Fe_3IIIO(H_2O)_2F.(BTC)_2.nH_2O$	
21	MIL-88A	$Fe_3O(MeOH)_3(O_2CCH{=}CHCO_2)_3.MeCO_2.nH_2O$	
22	MIL-88B-4CH_3	$2Fe_3O(OH)(H_2O)_2(BDC\text{-}Me_2)_3$	
23	LIC-1	$Gd_2(BDC\text{-}NH_2)_3(DMF)_4$	Leiden Institute of Chemistry

24	HKUST-1 (MOF-199)	$Cu_3(BTC)_2$	Hong Kong University of Science and Technology
25	ZIF-90	$Zn(FIM)_2$	Zeolite Imidazolate Framework
26	ZIF-8	$Zn(MIM)_2$	

2.4 MOF Basic Structure

In MOFs metal nodes connect to organic ligands, which act as connectors and form coordination bonds to form 1D, 2D, or 3D networks (*64*) (Scheme 2.1)

Scheme 2.1: Synthetic route of MOF.

K. Meyer et al. (2015) observed that when MOFs are utilised in coordination chemistry to construct organometallic or multidentate organic linkers around metal SBUs, they form well-defined 2D and 3D coordination polymers, as illustrated in figure 2.4. It demonstrates the basic cubic structure of MOF and its components. SBU is represented as a metal node or cluster. The square shape represents the MOF pore, while the black line (*65*) represents the linker (organic or organic-metallic).

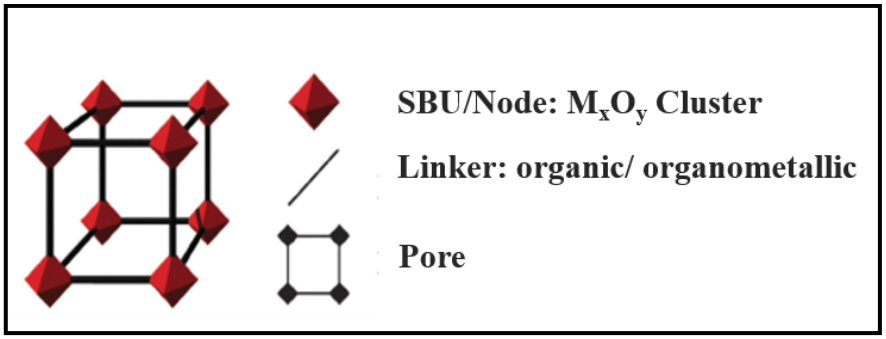

Figure 2.4: The simple cubic structure of MOF. MOFs are made up of two major components: the SBU and the node. The unit SBU, which stands for a node or metal cluster, is shown in red.

The square shape represents the MOF pore, and the black line represents the MOF pore, and the black line represents the linker (organic or organic-metallic) (*65*).

2.4.1 MOF coordination network

MOFs are also stated as components of a coordination polymer. They were classified as a type of coordination network. According to Batten et al.'s study in 2012, the metal-linker combination controls the stability, and the ligand shape controls the MOF structure (*66*). In this study, Stuart R. Batten et al. mentioned the types of MOF networks that correspond to coordination compounds, and the classification of coordination compounds, including MOF which is represented by O'Keeffe et al., as shown in figure 2.5 (a) and (b) (*67*).

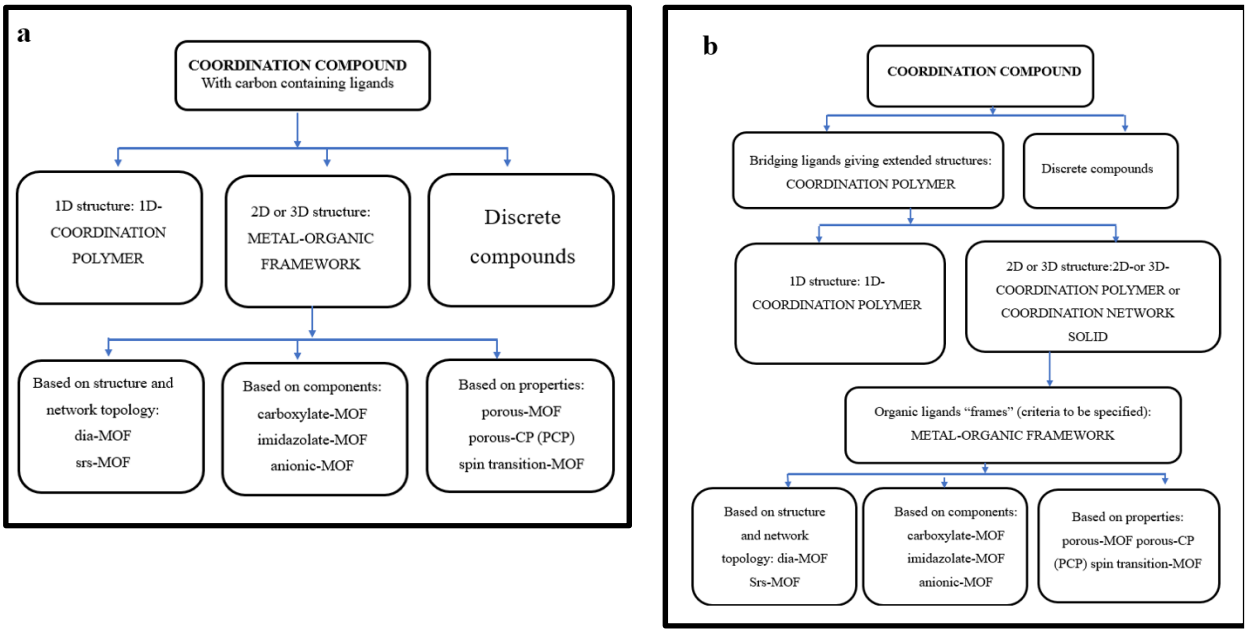

Figure 2.5: Classification of coordination compounds, based on Batten et al's report (2002)

Where (a) is the coordination compound classified based on network structure and (b) the coordination compound classified based on carbon-containing ligands.

MOFs are a broad term for coordination polymers with coordination 2D and 3D networks (*66*). The fundamental structural characteristics of the coordination polymer for its 1D, 2D, and 3D periodic architectures are shown in figure 2.6. On the basis of coordination networks, MOF structure is represented in a simple way in the figure 2.6 (*68*).

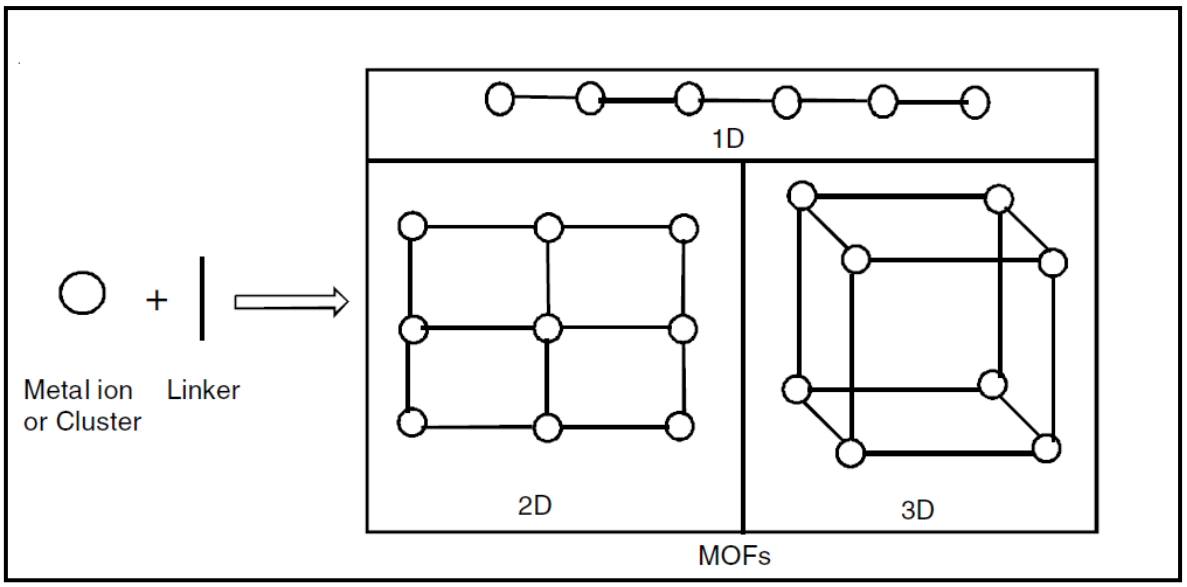

Figure 2.6: Schematic representation of a MOF structure (*68*).

2.5 Properties of MOF

MOFs have promising potential applications in recent energy storage innovations. They are extremely simple to synthesise due to their modular construction, which allows for precise chemical and structural control. Certain properties, such as conductivity, porosity, and stability, can be altered for specific applications (*69*). MOF's unique properties are an important quality for storing and transporting guests and ions. Because of the large number of multidisciplinary characterization techniques available for MOFs, numerous tests can be performed to highlight and provide significant information for the development of next-generation materials. To create functional materials with specific chemical compositions and morphologies. MOFs can serve as precursors and templates. Furthermore, MOF derivatives have shown significant promise in electrocatalysis and energy storage technologies (*70-72*).

2.5.1 Crystallinity

MOFs, like zeolites, are a type of highly crystalline material. Because the range of pore diameters is quite small, it produces bulk property homogeneity (*73, 74*). MOFs are generally produced in amorphous, microcrystalline, or polycrystalline forms. The powder X-ray diffraction (PXRD) and single crystal X-ray diffractometer (SXRD) are two tools used to characterise the crystallinity of MOF. SXRD, as compare to PXRD, allows for very precise and quick structural identification of MOFs (*75*).

MOFs are assumed to form through an equilibrium process due to the labile nature of the covalent bond between the ligand and the metal. This enables scientists to create a single crystalline product. Under ideal synthetic conditions, crystal defects self-correct, resulting in bulk materials composed of single-crystalline particles or polycrystalline with broad crystal domains (*76-78*). Although this equilibrium is often advantageous for the creation of crystals, problems may arise if the ligand-metal combination is unable to generate strong bonds. The MOF may not be water-stable in these conditions because the ligand and water molecules compete for the metal site. To create more resilient, chemically and water-stable frameworks, more oxophilic (trivalent and tetravalent) metals have been used, including titanium, zirconium, and chrome. Owing to the modified equilibrium, these MOFs sometimes need more difficult synthesis conditions and/or only produce microcrystalline powders (*75*).

"Reaction modulators" are a relatively new technique for producing single-crystalline materials from these systems. These reaction modulators, often monofunctional carboxylates, delay the reaction and alter the pH by competing with the polyfunctional ligand (*75*).

2.5.2 Modularity and Tunability

MOFs have many benefits over conventional porous or solid-state materials, including the ability to self-assemble. These advantages are possible due to the high degree of tunability of MOF materials and their hybrid organic and inorganic composition (*75*).

These three variables - Organic ligand, Counterions, and Metal ions can all be altered to achieve this tunability.

i. An organic ligand, which is geometrically equivalent, is made up of functionalized, extended, or contracted ligands (*79, 80*).
ii. Counterions, which can be produced by using different metal salts or by using ion exchange (*81*).
iii. Metal ions are composed of metals, which can group together to create clusters with a recognisable geometrical structure (*82*).

The alterations mentioned above have been shown to allow MOFs to be controlled in terms of pore size, aperture diameters, and porosity (*61, 83*).

Due to advancements in experimentalists' understanding of optimal synthetic conditions and the application of design principles, researchers have been able to accurately control the pore size, properties, and functionality of the finished material.

2.5.3 Mild Synthetic Conditions

One of the well-known advantages of MOFs is the extremely mild conditions required for MOF synthesis. This is evident when compared to the fabrication of MOFs using conventional porous materials such as activated carbons (ACs) and zeolites (*75*).

For instance, ACs can be produced at temperatures between 450 °C and 600 °C using carbon-rich materials. These materials can be produced through pyrolysis, oxidation, or a combination of chemical and thermal processing. On the other hand, MOF can be produced at a maximum temperature of 200 °C under solvothermal conditions in a single pot method (*75*).

2.6 Designing of MOF

MOFs have been constructed using both organic molecules (linkers) and metal ions as connectors. These have been referred to as primary building units. Other MOFs use metal-oxygen-carbon clusters rather than metal ions. The metal oxygen-carbon clusters are referred to as secondary building units (*68*). The SBUs are metal ions or clusters, which are the inorganic elements (*84*).

2.6.1 Primary Building Units

The design and synthesis of MOFs are challenging because the final architecture of MOF materials is totally dependent on the combination of two distinct elements: metal centres and organic ligands, as stated in the previous paragraph (*85*). Some of the factors that influence the composition's form, pore size, and topology are the coordination number quantity and the orientation of the PBUs' bonding sites (coordination geometries). As a result, the PBUs influence the final MOF material dimension, which can be 1D, 2D, or 3D, as shown in figure 2.7 below (*86*).

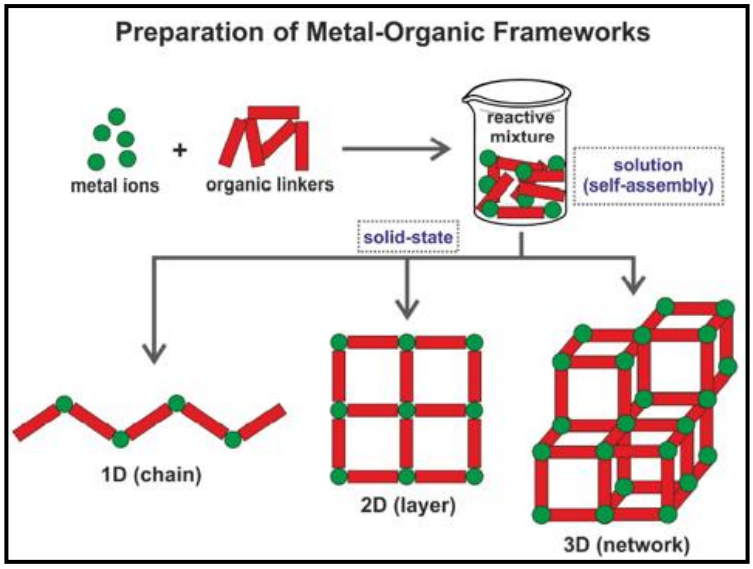

Figure 2.7: Process of creating multidimensional MOFs (*102*).

2.6.1.1 Organic linker

Functional groups that are located in organic linkers that are coupled to metal ions or nodes can create coordination bonds. The names of several organic linkers include nitrile, carboxylate, phosphate, sulfonate, and amine (*85*). The chemical structure of a few organic linkers (*86*) is depicted in the figure below (2.8–2.13).

I. The functional groups that are typically included in the organic linkers used to make MOFs.

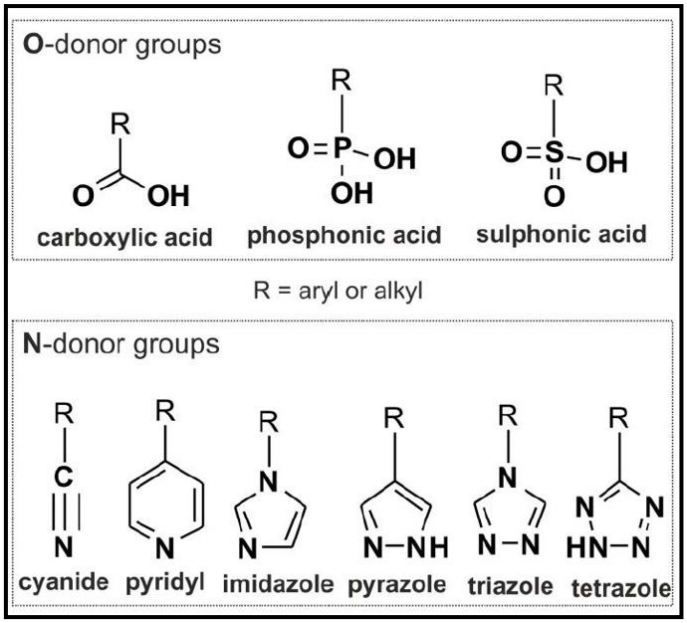

Figure 2.8: Linkers based on O-donor groups and N-donor group (*86*).

II. Organic Ligands with N-Donors for MOF Preparation.

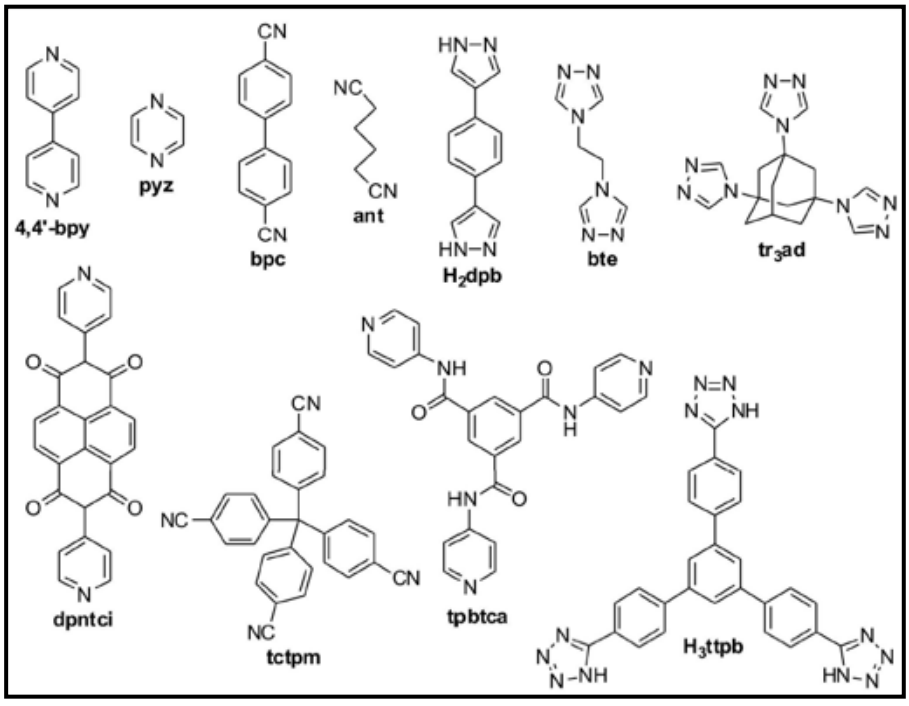

Figure 2.9: Organic ligands with N-donor (*86*).

The terminology used to describe the organic ligands in the figure are defined as follows: 4,4'-bpy is stand for 4,4'-bipyridine, pyz is pyrazine, bpc is 4,4'-dicyanodiphenyl, ant is 1,4-

dicyanobutane, H_2dpb is 1,4-di(1H-pyrazol-4-yl)benzene, bte is 1,2-bis(1,2,4-triazol-4-yl)ethane, tr_3ad is 1,3,5-tris(1,2,4-triazol-4-yl)adamantane, dpntci is N,N'-di(4-pyridyl)-1,4,5,8-naphthalenetetracarboxydiimide, tctpm is 4,4',4'',4'''-methanetetrabenzonitrile, tpbtca is N_1,N_3,N_5-tri(pyridin-4-yl)benzene-1,3,5-tricarboxamide and H_3ttpb is 1,3,5-tris[4-(2H-tetrazol-5-yl)phenyl]benzene.

III. Organic ligands with mixed O- and/or N-donors for MOF synthesis:

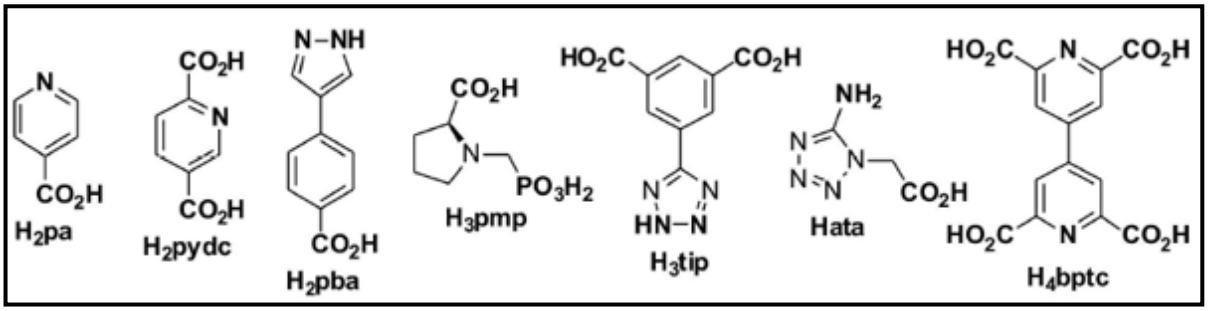

Figure 2.10: Organic ligands with mixed O- and/or N-donors (*86*).

The following terminology is used to describe the mixed O- and/or N-donor organic ligands in the figure2.10 :H_3pmp is (S)-N-(phosphonomethyl)proline, H_3tip is 5-(1H-tetrazol-5-yl)isophthalic acid, Hata is (5-amino-1H-tetrazol-1-yl)acetic acid, and H_4bptc is 4,4'-bipyridine-2,2',6,6'-tetracarboxylic acid.

IV. Organic ligands based on sulfonic acid groups for the preparation of MOFs:

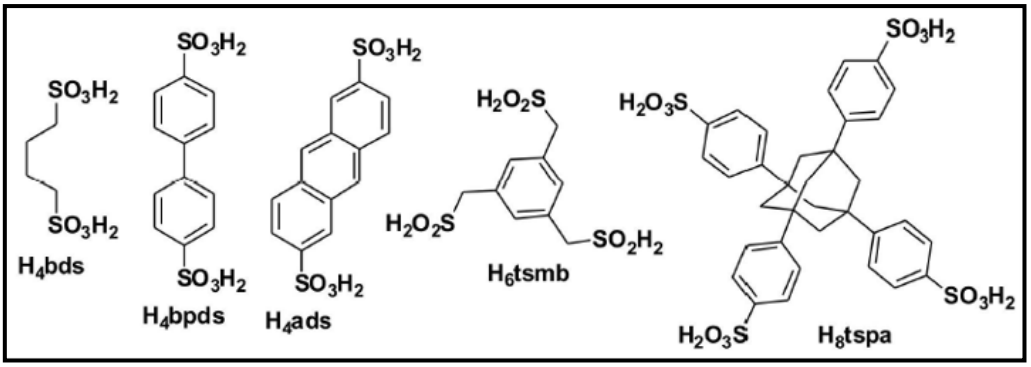

Figure 2.11: Organic ligands based on sulfonic acid groups (*86*).

The organic ligands based on sulfonic acid groups in the figure 2.11 are described using the following terminology: Butane-1,4-disulfonic acid is abbreviated as H_4bds; biphenyl-4,4'-

disulfonic acid is abbreviated as H_4bpds; anthracene-2,6-disulfonic acid is abbreviated as H_4ads; and adamantine is abbreviated as H_6tsmb.

V. Organic ligands based on carboxylic acid groups

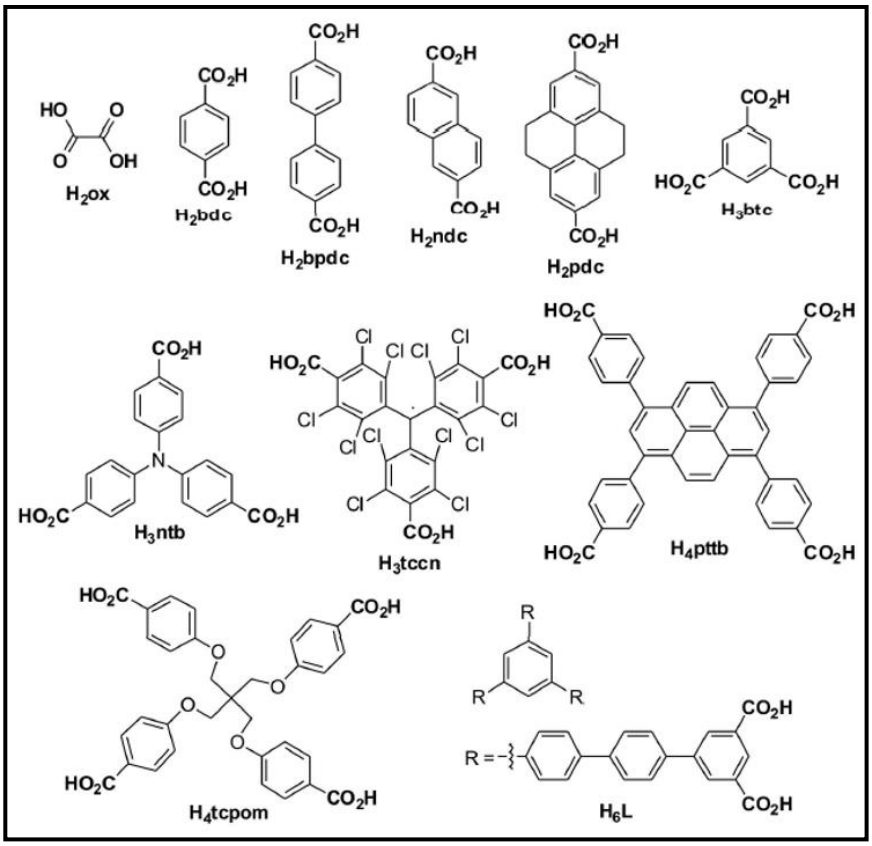

Figure 2.12: Organic ligands based on carboxylic acid groups (*86*).

The following terminology is used to identify the organic ligands in the figure 2.12 based on carboxylic acid groups: H_2ox stands for oxalic acid; H_2ndc for naphthalene-2,6-dicarboxylic acid; H_2bdc for benzene-1,4-dicarboxylic acid (terephthalic acid); and H_2pdc for 4,5,9,10-tetrahydropyrene-2,7-dicarboxylic acid. H_3btc stands for benzene-1,3,5-tricarboxylic acid (trimesic acid), H_4pttb for 4,4',4",4"'-(pyrene-1,3,6,8-tetrayl)tetrabenzoic acid, and H_3ntb for 4,4',4"-nitrilotrisbenzoic acid. Tetrakis[4-(carboxyphenyl)oxymethyl]methane is represented by the symbol H_4tcpom, and tris(2,3,5,6-tetrachloro-4-carboxy)methyl radical is represented by the symbol H_3tccn.

VI. Charged based organic ligands

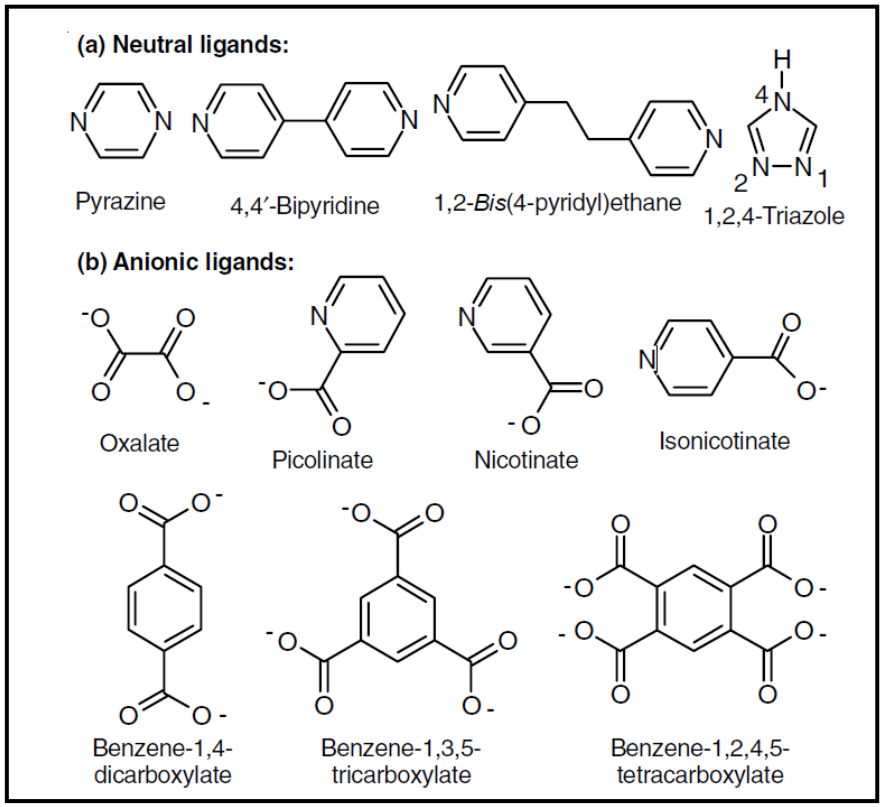

Figure 2.13: Organic ligands based on charge (*68*).

2.6.1.2 More Types of Organic linker

MOF properties can be influenced by both metal nodes and organic linkers. There are several labile or empty locations in the organic linker. Organic linkers are classified into four types based on the number of connections they can form with the metal node: ditopic linkers (two connections), tritopic linkers (three connections), tetratopic linkers (four connections), and multitopic ligands (*87*, *88*). The various types of linkers are depicted in the figure 2.14 (a, b, and c) below.

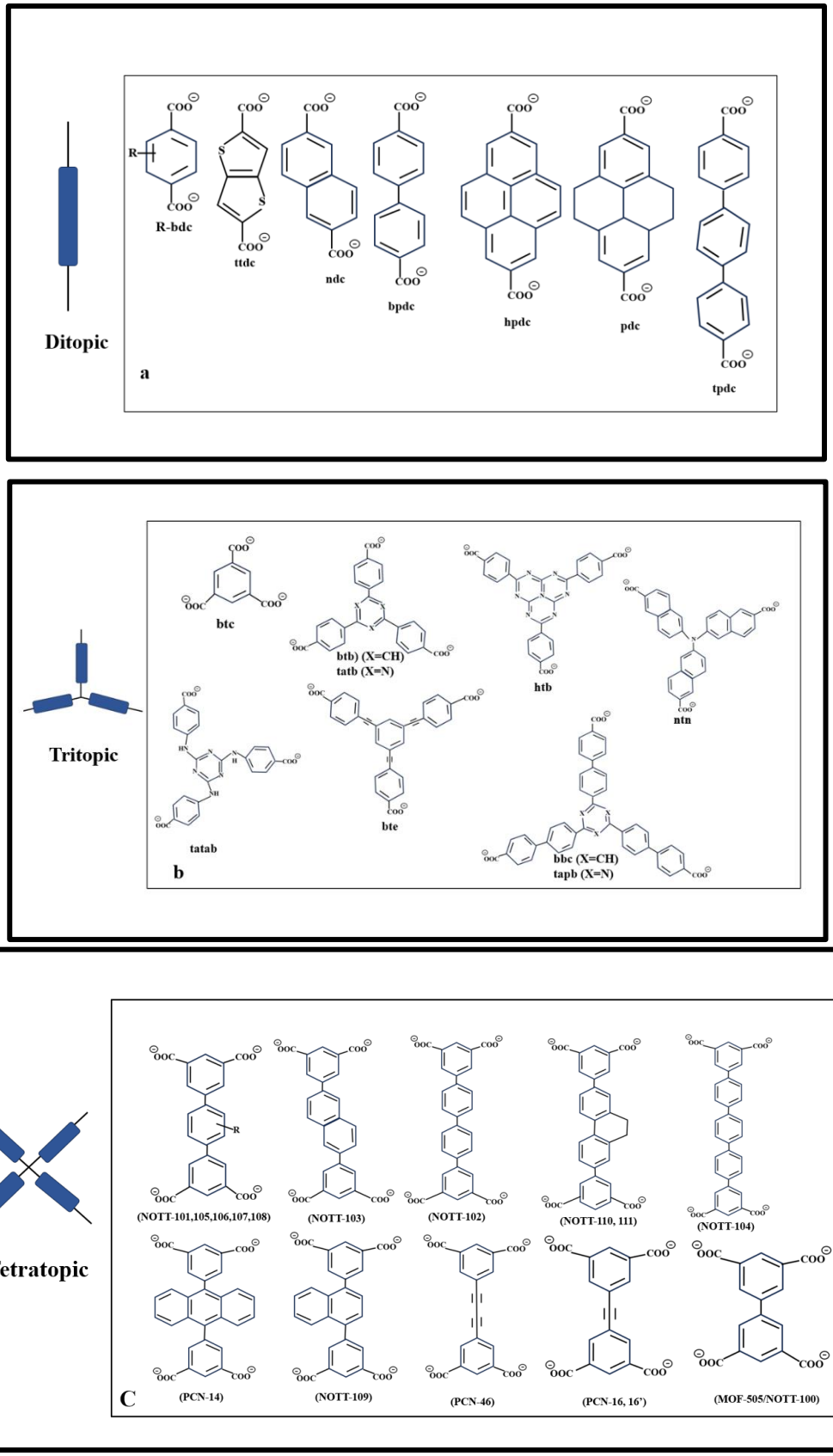

Figure 2.14: Example of Organic linkers (88).

2.6.1.3 Metal ion

MOF connectors are often made of metal ions from the first-row transition series, such as Mn^{2+}, Cr^{3+}, Fe^{3+}, Ni^{2+}, Co^{2+}, and Zn^{2+} (*89, 90*). In the fabrication of MOFs, some alkaline-earth metal ions (*91, 92*), alkali metal ions (*93*), and rare earth metal ions (*94-96*) are employed as metal connectors. Precursors such as metal nitrate, sulphate, acetate, chloride, and oxide are also used in most MOF synthesis processes. The electrochemical synthesis of MOFs also makes use of metal rods (*68, 85*).

Metal ion coordination quantity is crucial in the synthesis of diverse MOFs. The coordinates may be used to generate linear, V-shaped, T-shaped, Y-shaped, tetrahedral, square planar, square pyramidal, or octahedral geometric structures, which are useful for targeting a broad variety of MOF structures (figure 2.15) (*90*).

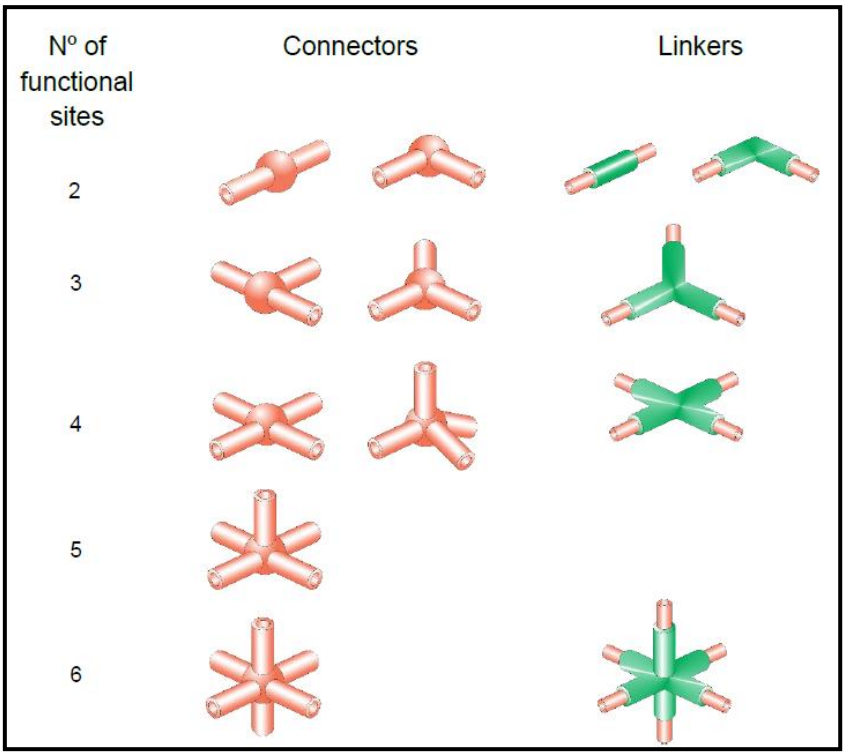

Figure 2.15: Coordination geometries of metal ions; the accompanying numbers show the number of functional sites (*90*).

2.6.2 Secondary Building Unit

MOF geometry is governed by secondary building units (SBUs), which form naturally between the metal precursor and the organic ligand (*61*). SBUs are complexes and cluster entities that

can assemble these fragments into extended porous networks by serving as ligand coordination modes and metal coordination environments. MOF topologies such as tetrahedral, paddle-wheel, and octahedral metal clusters can be generated by different SBUs. Below figure 2.16 (a, b, and c) shows some SBU examples (*88*).

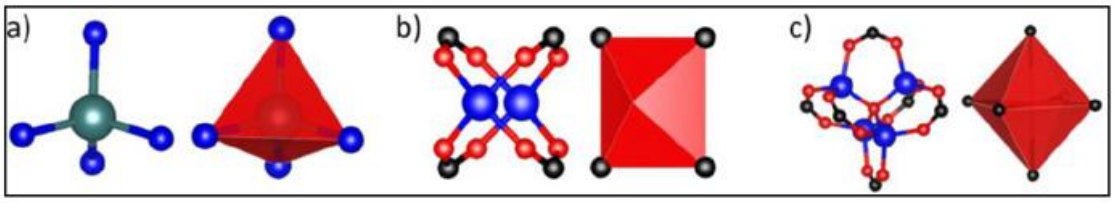

Figure 2.16: Secondary Building Units (SBU): a) tetrahedral, b) paddle-wheel, and c) octahedral (*88*).

The fundamental geometry of SBUs has a significant impact on MOF topology. Figure 2.17 shows some of the geometry of SBUs.

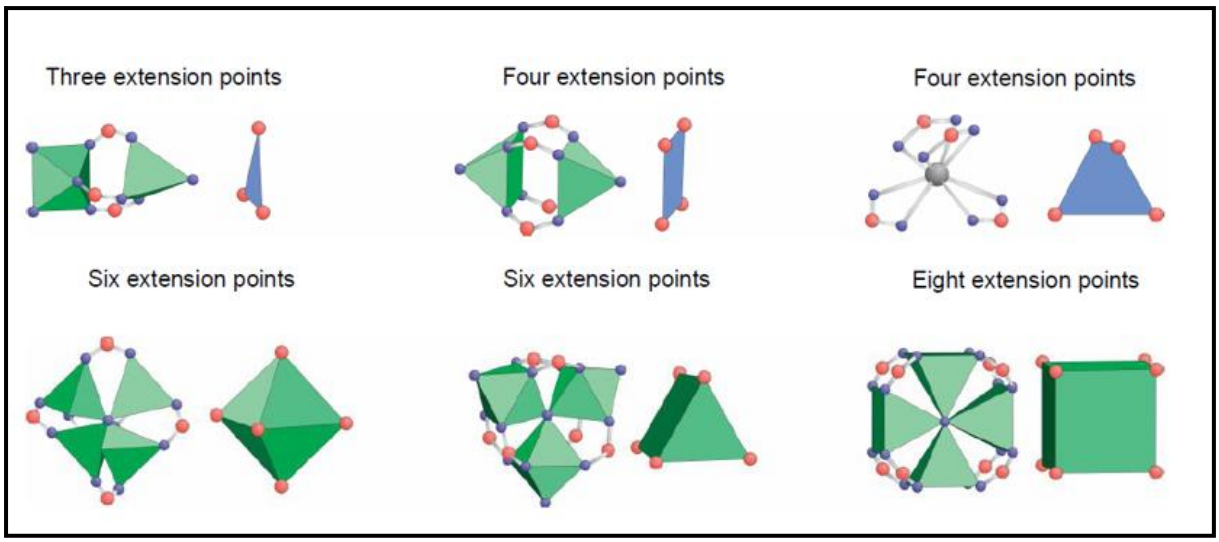

Figure 2.17: The geometry of SBU. In atom labelling for clarity, C (red), O (blue), metals (green), and H atoms are omitted (*90*).

In 2009, Yaghi et al. thoroughly investigated on 131 SBU geometries, which provides a wide range of options for the creation of MOF structures. SBU-based MOFs have extremely high structural stability. The rigidity of these structures is due to metal-carboxylate linkages, which also explains their chemical and thermal durability (*90*).

2.7 Factors affecting MOFs Synthesis

The synthesis factors, as well as the metal ions and organic ligands used, all have an impact on the final structure of MOF. It has been established that synthetic factors have a significant impact on the outcome of a specific reaction (*97*). MOFs are typically formed through hydrothermal or solvothermal methods (*98*).

MOFs are well known for their crystallisation, structure, and morphology, which depend on composition and process parameters. Compositional parameters include solvent, pH, ligand substituents, starting material molar ratio, counterions, concentration, etc. Process parameters include pressure, time, temperature, and others play a vital role (figure 2.18). These parameters greatly affect the structural chemistry of ligands and the assembly of ligands with metal centres, resulting in a large variety of structurally diverse products (*83*).

During MOF synthesis, a variety of factors play a significant role in determining phase development and crystal structure formation. But it can be challenging to follow a methodical investigation that looks at how each factors affects the new MOF structure (*83*). The following are some of the most common factors that influence the MOF phase and crystallization.

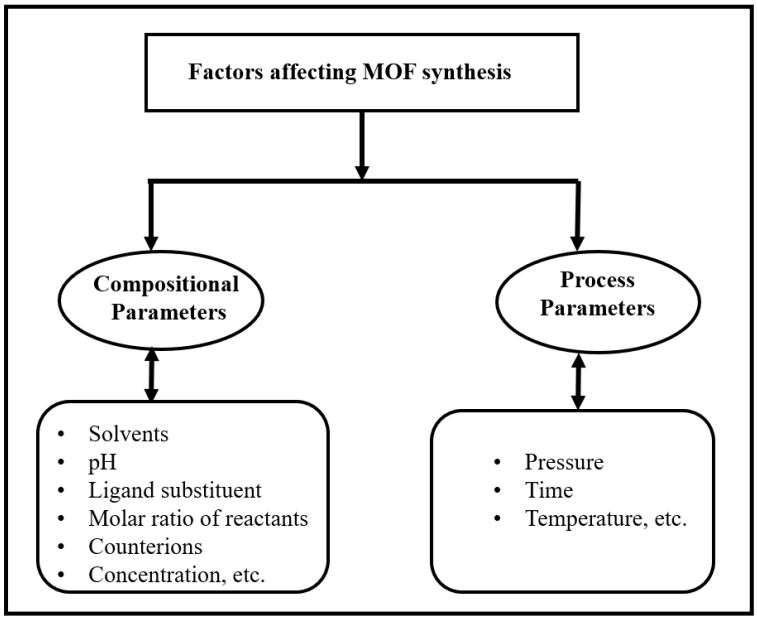

Figure 2.18: Factors that influence the formation of MOFs.

2.7.1 Solvent

The proper selection of solvents is important in MOF synthesis because they can directly or indirectly impact the coordination behaviour of the ligand and metal. Numerous examples of MOF synthesis demonstrate that every solvent system has a significant impact on regulating the formation of various coordination environments, even though the reason for each synthesis solvent selection is still unknown. Solvents utilized in the assembly process either can bind to metal ions, forming coordination complexes or become incorporated as guest molecules within the final crystal structure (*83*).

Generally, the solvents used during synthesis are not considered part of the MOF. Rather, they serve as a crystallisation medium or a structure-directing agent. Another way of controlling the amount of deprotonation of an organic carboxylate ligand is by altering the basicity of the solvent or by employing suitable solvents like DMF, DEF, and DMA. When these solvents are converted into the corresponding amines at higher temperatures, deprotonation of carboxylates occurs (*83*).

2.7.2 Temperature Effect

Temperature is an important factor in the formation of MOF. A wide range of experimental conditions have been discovered that have a significant factor on the MOF crystal and its final structure. In both reaction kinetics and thermodynamics, the temperature has an influence on the reaction energy barrier and the rate of the reaction (*99*).

MOFs are frequently synthesised using hydro or solvothermal methods in these systems. It is obvious that high temperatures will result in high reaction pressure in the sealed system, affecting the assembly and final architecture of MOFs (*100*).

Sun et al. explained how temperature affects MOFs synthesised concluded that changing the temperature range of the reaction can control the dimensionality of MOFs (*99*).

Co(II)-succinate MOF is an excellent example of how temperature range alteration impacts the dimensional frameworks. When the temperatures were altered, the same initial reaction mixture produced completely distinct Co(II)-succinate MOFs. The results show that as the reaction temperature raises, the dimensionality and density of the MOFs increased. Five types of Co(II)-succinate MOFs were isolated at 60, 100, 150, 190, and 250 °C using a 1:1:28 reaction of cobalt hydroxide, succinic acid, and water. At 60 and 100 °C the dimensionality of the resulting Co(II)-MOFs changes from one-dimensional (1D) chains to two-dimensional (2D) chains,

Then to two-dimensional (2D) networks at 150 °C, and three-dimensional (3D) frameworks at 190 and 250 °C (*99*).

2.7.3 Effect of pH

The reaction medium's acidity and basicity have a significant impact on the crystallisation and development of inorganic-organic hybrid materials (MOF). According to the acid-base principle, the production of an OH-ligand will favour the connection of a polycarboxylate ligand to a metal ion. Numerous research groups have carried out some interesting studies on the effect of pH value on MOF synthesis (*83*).

According to Chu et al., at high pH the reaction would result in greater dimensionality, Chu et al. created four different coordination polymers such as [Cd(HL)(H_2O), [Co(HL)(H_2O), [Cd(HL)(H_2O), [Cd(HL)($H_2O)_4$], and [$Cd_3(L)_2(H_2O)_9$].7H_2O at varying reaction pH. The ligand N-(3-carboxyphenyl) iminodiacetic (HL) acid is partly deprotonated in the first three complexes, which are prepared at low pH (approximately 5 or lower), in contrast, at pH 7, all carboxylate groups are fully deprotonated, resulting in a 2D network structure and a more complicated network (*101*).

2.8 Synthesis Methods and Crystallization of MOFs

MOFs were initially formed using solvothermal synthesis. For the synthesis and self-assembly of MOF crystals, organic linkers and metal precursors are typically dissolved in solvent and placed in a closed reaction vessel. N, N-dimethylformamide (DMF), N,N-diethylformamide (DEF), ethanol, methanol, and acetonitrile are some of the most commonly used solvents. The synthesis temperature is usually less than 220°C, and crystallisation times range from a few hours to days (*111*).

Over 20 years of research and development have resulted in significant progress in MOF synthesis. Novel studies on microwave-assisted, microfluidic, electrochemical, and mechanochemical synthesis techniques have been reported. The evolution of the most widely used MOF synthesis methods is depicted in figure 2.19 (*102*).

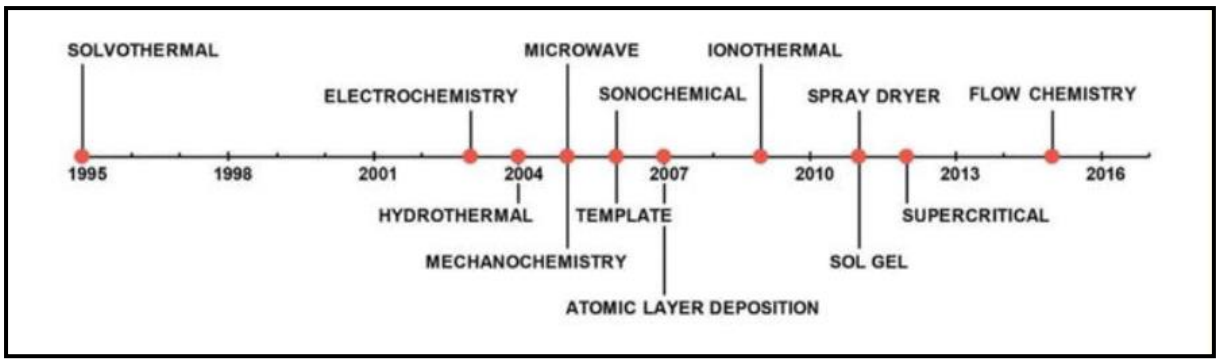

Figure 2.19: Timeline of the most common synthesis approaches for MOFs (*180*).

Several novel MOF structures have been created using these various techniques since their discovery. The "structure determines function" approach expressly states that it is critical to be able to control and tailor the morphology, size, and chemical functionalization of MOF crystals in order to achieve desired characteristics and performances of the resulting MOF materials. As a result, it is necessary to develop more advanced synthesis techniques based on knowledge of the mechanisms that cause crystallisation throughout the synthesis process (*103*).

MOF can be synthesised using methods that are classified into three types: Conventional Solvothermal Methods, Unconventional Solvothermal methods, and Alternative Solvothermal methods (*45*, *85*). Below sections contains a more detailed description of these three methods.

2.8.1 Conventional Solvothermal Method

Conventional solvothermal methods involve heating a mixture of metal ion (metal salts) and organic linkers in a solvent system containing formamide functionality (*104*), Scheme 2.2. This method makes use of materials that are thermally unstable or reactive to the solvent, which may result in bond breaking or the formation of metal sites through which guest species, such as gases, can enter the framework's macropores, mesopores, and micropores. In some cases, using assisted microwave-solvothermal synthesis, the temperature of the reaction can be monitored or controlled while it is taking place (*105*).

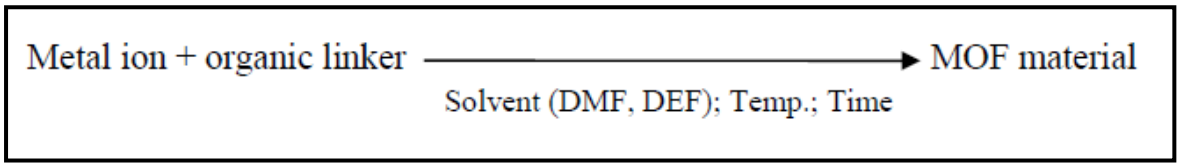

Scheme 2.2: Synthetic Route of the Conventional Solvothermal Method

2.8.2 Solvothermal Method

According to Gonzalez et al.'s investigation, a significant number of scientific studies that are currently available in the literature suggest that the solvothermal method of MOF synthesis is likely to be the most typical and straightforward way of material fabrication. When compared to other synthetic methods, this process produced the best results for crystallinity and morphological characteristics. The solvothermal method heats a solvent and its precursors above their boiling points in a closed system. Under supercritical conditions, the precursors are affected differently by increased pressure, high temperatures, and the type of solvent, which results in the synthesis of the desired product. Although the solvothermal method produces the best results, it frequently necessitates the use of hazardous and environmentally unfriendly solvents (*106*) (Figure 2.20).

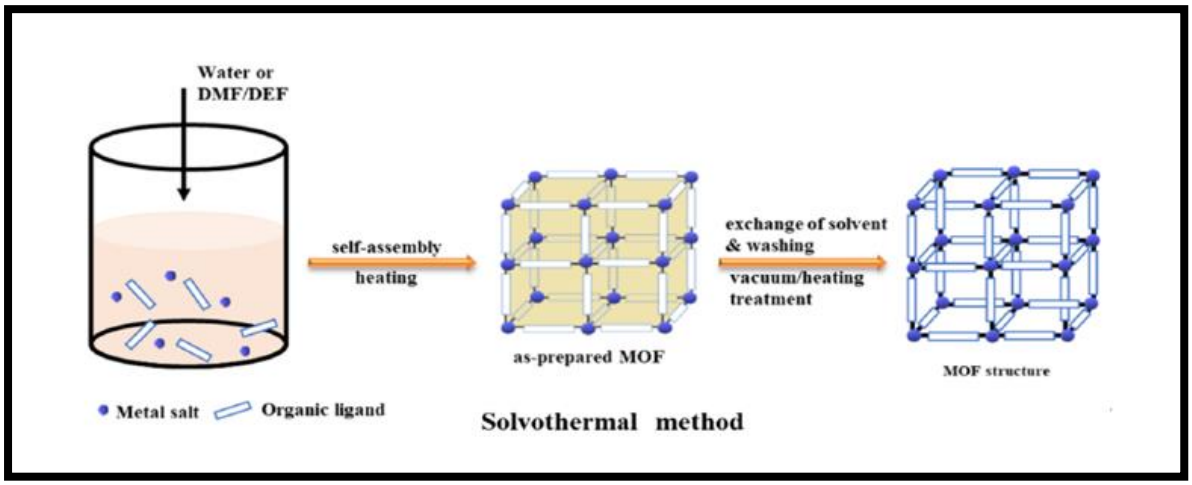

Figure 2.20: Conventional Solvothermal Synthesis of MOF structures (*42*).

For the solvothermal method, the normal thermal energy range is 353–453 K for 48–96 hours. Organic solvents such as ethanol, methanol, acetone, dimethylformamide (DMF), diethyl formamide (DEF), and others are widely used in solvothermal methods. To deal with the problem of solubility, which varies depending on the initial ingredient, solvent mixtures have been used. Depending on the reaction, solvothermal reactions can occur at a variety of temperatures (*107*).

A study by Senkovska, et al, provides information on the solvothermal method's synthesis route as well as on the solvent's key role in modifying MOFs' final structures. Senkovska et al synthesised the two aluminium-based metal-organic frameworks using the solvothermal method. They discovered Al(OH)(ndc) (ndc = 2,6-naphthalene dicarboxylate), a new porosity

modification of the non-porous MIL-69, using N,N-dimethylformamide as the solvent. They came to the conclusion that the structure is composed of ndc-connected chains of coordination octahedra constructed of aluminium. The material's specific pore volume was found to be 0.68 $cm^3\ g^{-1}$ after the solvent molecules were removed. They also discovered that once the solvent molecules are removed, the synthesised material has a specific pore volume of 0.68 cm^3g^{-1}. Furthermore, they discovered that the excess hydrogen saturation value of this compound at 30 bar and -196 °C is 2.1 wt.% (Vad, STP(H_2) = 247 $cm^3\ g^{-1}$) (*108*).

2.8.3 Hydrothermal and unconventional Methods

The hydrothermal method refers to several procedures for crystallising compounds from high-temperature aqueous solutions at high vapour pressures, as mentioned by Chen et al. The hydrothermal method relies on the solubility of minerals in hot water under high pressure and is a single crystal synthesis technique. The word hydrothermal refers to any heterogeneous reaction that takes place under high temperature and pressure conditions in aqueous solvents to dissolve and recrystallize materials that are relatively insoluble under normal conditions (*109*).

According to Gonzalez et al, the hydrothermal method is performed by using water as a solvent, which is known as the friendliest solvent; as a result, the hydrothermal method is considered a green method. It is possible to prepare a wide range of MOFs containing carboxylates, imidazole, transition metals, alkaline earth metal ions, and to synthesise several MOFs with 1D, 2D, and 3D structures using the hydrothermal method (*106*).

An unconventional synthesis frequently performed is grinding an organic linker and metal salt mixture in the absence of solvent in an agate mortar and pestle or in a ball mill. This is referred to as the mechanochemical method (*105*).

2.9 Applications of MOF

MOFs are one of the primary porous crystalline materials. Every year, new MOF structures are discovered. Due to their evolution, the new structures have distinct properties such as persistent porosity, changeable composition, and specific surface properties. By altering the linker geometry, ratio, length, or functional group, a MOF's shape, size, and internal surface properties can be tuned for a specific application. These features make MOF significantly more likely to be used in a range of applications (*110*). MOFs are widely used in applications,

including gas adsorption and separation, photocatalysis, electrochemical applications, supercapacitors, hazardous material removal and separation, drug delivery, catalysis, rechargeable batteries, sensing, bio-related applications, separation membranes, and toxic compound detection. This is due to the benefits of combining all these properties into a single framework; as a result, MOF is more popular (*111*, *112*).

2.9.1 Hydrogen Adsorption

MOFs can store hydrogen because they have a huge, accessible surface area. Due to their hybrid metallic and molecular structure, they can be modified in many ways, such as by functionalizing potential ligands and storing them at different temperatures. In the process of hydrogenation synthesis, MOFs may also take the place of expensive metals such as platinum (Pt). Despite Pt's high cost and lower yields in hydrogen trapping, it is the most widely used metal for this application. It is suggested that this hybrid MOF can be employed in straightforward applications because it has pores that serve as "gas pockets", which hold hydrogen atoms for synthesis (*113*).

Cu-BTC is an excellent model for hydrogen adsorption. Cu-BTC is a copper-based MOF with benzene-1,3,5-tricarboxylate (BTC) linkers connecting Cu (II) metal units, is a substance that has undergone extensive research. The coordinated water molecule that is in the axial position of the paddlewheel Cu^{2+} centres of the structure that can be removed by heating. As a result, active sites with hydrogen adsorption potential are produced (*114*). Several instances of MOFs being employed to store hydrogen are shown in Table 2.3 below.

Table 2.3: Applications of MOFs for hydrogen storage (*105*).

MOF	Surface area (BET) [m^2g^{-1}]	Surface area (Langmuir) [m^2g^{-1}]	H_2 Uptake at 77 k (wt.%)	Pressure (bar)	Max ΔH° adsorption
$NaNi_3(OH)(sip)_2$	700	-	0.94	1	6.8
$Cu_3(btc)_2$	1507	2175	2.5	1	6.8
$Ni_{20}(OH)_{12}[(HPO_4)_8(PO_4)_4]$	500	-	0.53	0.79	-
$Zn_2(dhpt)$	870	-	2.8	30	8.8
$HCu[Cu_4Cl)_3(btt)_8].3.5HCl$	1710	1710	4.2	90	9.5

Abbreviation: sip = 5-sulfoisophthalate; btc = 1,3,5-benzenetricarboxylate; dhpt = 2,5-dihyroxyterephthalate; btt = 1,3,5-benzenetristetrazolate

2.9.2 CO_2 Adsorption and storage application

MOFs are ideal for environmental applications due to their structural properties and high level of stability. MOFs keeps their stability even when heated or chemically treated. Current research suggests that MOFs can absorb toxic gases like CO_2, CO, NO_2, and H_2S.

CO_2 sequestration is required to decrease anthropogenic greenhouse gas emissions. After combustion, one key strategy for limiting the effects of global warming is CO_2 separation from plant flue gases. The typical flue gas contains CO_2 at a partial pressure of about 0.15 bar, which is below atmospheric pressure. Using both simulation and experiments, researchers looked for MOFs with the highest CO_2 capacities at around 0.1 atm.

At 0.1 atm and 298 K, Emam et al. discovered that Ni-MOF-74 and Mg-MOF-74, or CPO-27-Ni and CPO-27-Mg, have the highest CO_2 capacities of 5.95 mol/kg and 4.07 mol/kg, respectively (*115*).

MOFs have a high potential for CO_2 adsorption. Bordiga et al. performed a spectroscopic examination on CO_2 interaction with the metallic Cu^{2+} centre of a MOF by loading 9 mbar of CO_2 into a HKUST-1 sample at 150 K and gradually lowering the equilibrium pressure to 0 as the temperature rose to 300 K. The presence of the Cu^{2+} interaction with carbon dioxide was identified by a red shift in the CO_2 gas phase frequency from 2349 cm^{-1} to 2333 cm^{-1}, which

was distinct from the interaction of the bare Cu^{2+} cation with CO_2 at low coverage (which bears a typical blue shift). They observed that the HKUST-1 reacted with 13 CO_2 because it contained roughly 1% of its natural isotope. Hence, HKUST-1 featured two relatively unique Cu^{2+} adsorption sites. These spots were typically attributed to structural defects or Cu^{2+} on the MOF's outer surface. XAFS findings indicated that CO_2 physisorption occurred when the CO_2 molecule binds to the HKUST-1 Cu^{2+} centre (*116*).

Qasem et al., suggested that MOF-5 and MOF-177 are promising CO_2 storage materials. MOF-5 is better suited for low-pressure storage (under 5 bar), while MOF-177 excels at high pressures (10 bar and above). Both perform optimally at 30 bar, with MOF-5 capturing 21.07 mmol g^{-1} (0.93 $kgCO_2$ /kgMOF) and consuming 231 kJ/tonneCO_2 and MOF-177 capturing 32.5 mmol g^{-1} (1.43 $kgCO_2$ /kgMOF) and consuming 233 kJ/tonneCO_2 (*117*).

2.9.3 Sensor Application

MOFs have found significant use in sensor-based applications. MOF is a simple tool to use in the manufacture of chemical sensors. The resistance of a chemical sensor can vary as a result of analytes adhering to the surface of pure MOFs; this is entirely dependent on the electrolyte's participation. Depending on whether the adsorption sites emit or absorb electrons, the sensor resistance may vary.

When compared to traditional porous materials, MOFs have a much larger surface area and greater gas accessibility. The ability of a MOF to sense and transmit signals over its whole surface considerably increases variations in resistance, or gas responsiveness.

ZIF-67, a co-based zeolite imidazole framework composed of co-ions and methylimidazole linkers, was used as a formaldehyde sensor. Zr-based MOFs with amine functionalization [$Zr_6(O)_4(OH)_4$(1,4-benzenedicarboxylate-$NH_2)_6$, NH_2-UiO-66] At 150°C in an Ar atmosphere, it also demonstrated chemiresistive sensing to sulphur dioxide (SO_2) (*118*).

2.10. Metal organic frameworks for the electrocatalytic reduction of CO_2

Carbon dioxide (CO_2) is one such gas that exists in trace amounts in the Earth's atmosphere. The unique quality of this gas is that it plays an essential role in preserving the equilibrium of multiple important planetary processes, including photosynthesis, the greenhouse effect, the

carbon cycle, and the marine carbon cycle. CO_2 gas should only be present at trace levels on Earth; otherwise, the delicate balance of the environment is disrupted (*119,120*).

CO_2 has long been seen as a waste product due to its prevalence as the most abundant greenhouse gas (GHG) in the Earth's atmosphere. It mostly enters the environment through breathing and human activities (*121*). Apart from human activity (the combustion of coal, oil, and petrol), deforestation is a major contributor to rising CO_2 levels in the atmosphere. As a result, cutting down forests not only diminishes the number of trees but also raises CO_2 levels in the atmosphere because plants absorb extra carbon from the atmosphere since trees are natural carbon sinks. As a result, the presence of a large number of trees on land will help to balance the atmospheric carbon cycle by absorbing excess CO_2 (*122, 123*).

Despite the fact that CO_2 is a minor component of the atmosphere's air, a recent study found that its concentration is increasing. All of the explanations described in the preceding paragraph highlight the fact that CO_2 concentrations are increasing on a daily basis. Furthermore, estimated data from NOAA's global monitoring laboratories indicates that CO_2 levels have grown significantly. According to the yearly report of the NOAA Global Monitoring Laboratory, the average atmospheric carbon dioxide concentration is predicted to reach 417.06 parts per million (ppm) within a few years, which would be extremely high and would break the previous record (*124*).

In order to reduce the quantity of CO_2 in the atmosphere through collection, storage, and use, both the scientific community and the general public are now equally concerned (*125*). The Paris Agreement, which sets strategies for international action to tackle climate change unanimously agreed upon by 197 member parties of the United Nations Framework Convention on Climate Change (UNFCCC). As part of the Paris Agreement (Agreement 2015), to take measures to limit the rise in global temperature to between 1.5 and 2 °C (*126*).

In order to solve this issue, the scientific community is attempting to develop and use a methodology or approach to reduce CO_2 emissions directly from the source of carbon. The most often used methods right now are CO_2 capture and utilisation, as well as CO_2 storage and usage to convert CO_2 into various chemicals and fuels with additional value (*127*). However, the utilisation of CO_2 in thermochemical, radiochemical, biochemical, photochemical, and electrochemical processes to convert high-value compounds and fuels, including carbon

monoxide, ethanol, methanol, and formic acid, has attracted considerable attention from across the world (*127*).

Out of all the methods recommended in the paragraph above, the electrochemical CO_2 reduction reaction methodology offers the most promise for turning CO_2 into chemicals with added value. This method can be used to reduce anthropogenic activities that result in excessive CO_2 emissions.

Since CO_2 molecules are chemically inert and the conversion process is sluggish, efficient electrocatalysts are required to speed it up. The electrochemical CO_2 reduction reaction (ECRR) technique has lately grown in favour because of its numerous benefits (*128*). These techniques have the following advantages:

- This method employs highly adaptable reaction steps, allowing electrochemical parameters to be modified while maintaining a very high conversion efficiency (*129*).
- It can reduce carbon dioxide in mild conditions (*128*).
- In this technique (ECRR), several renewable energy sources, such as, wind energy, biomass energy, solar energy, and water energy, are used as a power source for electrocatalysis to store energy in synthetic molecules (*130, 131*).
- The electrochemical reactors utilised in this technique have allowed for large-scale industrial applications due to their compactness and versatility (*128*).

Therefore, the scientific community has made several attempts to develop effective catalysts for CO_2 conversion. Some of the catalysts that are widely used in the conversion of CO_2 into various chemical compounds include zeolites, metal oxides, nanomaterials, and ionic liquids (*132*). Due to its chemical inertness and thermodynamic stability, the CO_2 molecule has a high bond enthalpy of +850 KJ mol^{-1}. Hence, in CO_2 utilisation, considerable pressure and energy input are often required for bond cleavage (*132, 133*).

MOF materials have been intensively investigated as heterogeneous catalysts in a range of processes. Some examples of processes include hydrogenation, oxidation, cyclization, coupled reactions, electrocatalytic reactions, and photocatalytic reactions (*134, 135*).

MOF materials have the following advantages, which makes them ideal for catalytic applications (*136*).

- The solid catalyst may be easily recovered and used a number of cycles (*136*).
- By providing inner holes with the appropriate hydrophilic or hydrophobic properties, MOF can interact more easily with reactant molecules, which would boost catalytic effectiveness (*136*).
- Functional groups present on the pore surfaces can interact with active sites to improve catalytic efficiency (*136*).
- The periodically dispersed active sites in the pore surface or space can synergistically work to improve the catalytic efficiency (*136*).
- The confined pore widths can transport substrate molecules selective for size-selective catalysis (*136*).
- The high density of catalytic sites and uniform distribution of pores may increase utility (*136*).
- Due to their nanosized pore space, MOFs may be able to withstand a variety of catalytic conditions, such as the stereochemical confinement effect, quantum size confinement, and the electron-rich or electron-deficient situations. This microscopic nanopore can also change the reactivity of reactant molecules (*136*).

According to Chuan-De Wu and Min Zhao, MOF materials with increased porosity, sizable surface areas, and changeable hydrophilic and hydrophobic holes have the potential to exhibit specialised enzyme-like characteristics for extraordinarily efficient catalysis in benign conditions. The crystal structures of MOFs and their positioning of the catalytic sites on or in the pore surface or space allow direct observation of the binding interactions between the catalytic sites and reactant molecules. This is essential for fully comprehending the catalytic processes. The aforementioned qualities also make MOF materials a highly promising class of heterogeneous catalysts for a number of catalytic processes. This finding is supported by several studies in the areas of organic, inorganic, catalytic, materials, and other forms of chemistry (*136*).

The use of CO_2 as a cheap material C1 feedstock for creating useful chemicals and fuels based on MOF catalysts is also one of the most active research fields currently (*132*).

For example,

- The conversion of CO_2 to methanol has attracted a lot of interest since methanol may be employed as a liquid fuel in industrial applications (*132*).

- Cyclic carbamates can be created by carboxylic cyclization of propargylic amines with CO_2, a green chemical method for synthesising antibiotics (*132*).

2.10.1. Electrochemical reduction of CO_2

CO_2 molecules are centrosymmetric and linear. The bonding electrons of the CO_2 molecule are more strongly bonded to oxygen than to carbon because of the difference in electron negativities. CO_2, a very stable form of carbon, has a C=O bond energy of 805 kJ mol^{-1}. Therefore, the direct conversion of CO_2 into any other chemical composition hence requires a large enthalpy under ideal conditions (*137*). For instance, at standard conditions (1 atm, 298.15 K), the direct breakdown of CO_2 into CO and O_2 results in a considerable enthalpy change ((ΔH°) of 283.0 kJ mol-1), Equation (*137,138*).

$$CO_2\ (g) \longrightarrow CO\ (g) + ½\ O_2\ (g) \quad \{\Delta H° = 283.0\ KJ\ mol^{-1}\}$$

In an electrochemical reduction process, a chemical change is made at the electrode surface by electrocatalysis. It may be viewed as a particular type of heterogeneous catalysis in which reactants interact and exchange electrons with an electrocatalyst, which is frequently the electrode or a component of the electrode (*138*).

As CO_2 is a thermodynamically stable molecule with a high kinetic and thermodynamic energy barrier and an average production enthalpy of 393.5 kJ mol^{-1}, converting CO_2 molecules into a variety of chemical compounds with added value is quite challenging (*139*). As a result, a potent catalyst is required. It could reduce activation energy, lowering the amount of energy required for completing the reaction. As a result, many catalysts are being investigated in an effort to boost CO_2 conversion while also regulating selectivity towards certain target products (*140*). The activation barriers for the conversion of CO_2 to CO in a protic environment are schematically illustrated Figure 2.21 below. In a protic environment, the illustrated solids exhibit the activation barriers for CO_2 reduction to CO. The catalytic species are shown by their absence (solid line).

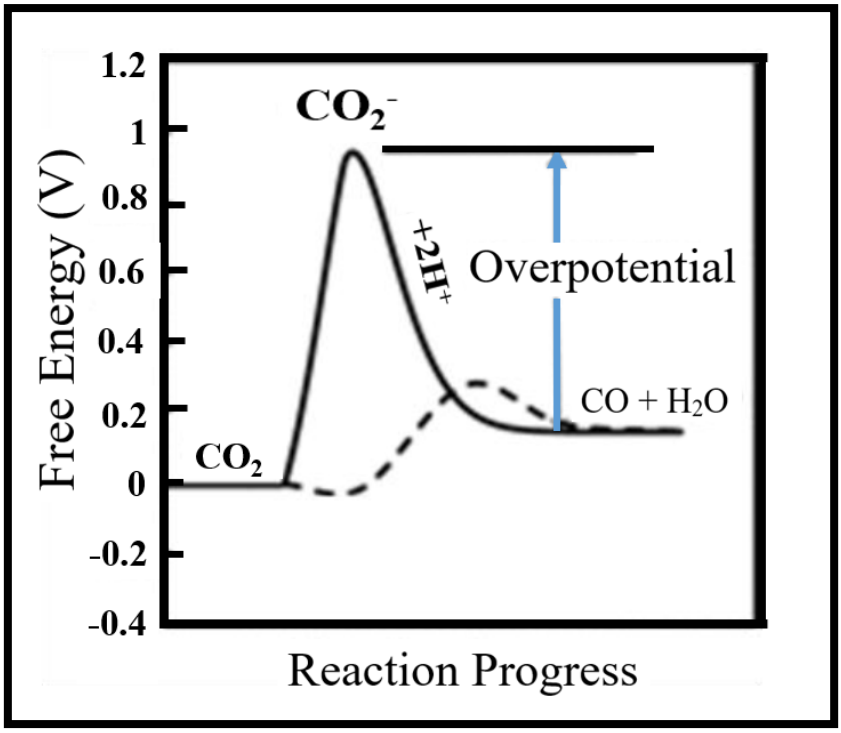

Figure 2.21: An illustration of the activation barrier for CO_2 reduction.

Figure 2.21 demonstrates how the system has been impacted by a reduction in CO_2's free energy. The solid line indicates that the reaction has ended in a protic environment, whereas the absence of a solid line indicates the presence of the catalytic species (*141*).

However, several proton and electron exchanges are required for CO_2 to go through chemical conversion. Many complex intermediates are used in this chemical process. The reaction route, selectivity, and faradic efficiency (FE) are all significantly affected by them (*142*). That is why a wide variety of the catalysts' properties affect selectivity and activity. The number of surface-active sites, coordination geometry, surface electronic structure, atom distribution, and chemical composition are important considerations (*142, 143*). In regard to the topic of high-performance electrocatalysts, it is necessary to comprehend the relationship between reaction mechanism and catalyst structure (*142*).

As a result, the ideal catalyst would allow for a reduction in the excess potential required for CO_2 reduction. Furthermore, it makes possible the production of specific molecules with high effectiveness, an acceptable rate, and stability, all of which permit the synthesised product to be easily separated. Many of these needs have been addressed in various ways, but no research has been able to properly meet all of them *(142*).

In CO_2RR, the reduction of CO_2 molecules is accomplished by chemisorption. This procedure involves the chemical attachment of a CO_2 molecule to an electrode surface. After that, a chemical bond is created, and the process of redistributing electrons starts. After the catalyst surface chemisorbs CO_2 molecules, electrons are redistributed and new chemical bonds are formed. This mechanism is well explained by the molecular orbital diagram of CO_2, which is displayed in Figure 2.22. The CO_2 molecule has $1\pi_g$ and $2\pi_u$ highest-occupied and lowest-unoccupied molecular orbitals, respectively (*137*).

The HOMO and LUMO energy levels of CO_2 molecules have a considerable impact on the chemistry of the adsorbate surface, and chemical-sorption has a strong direct effect on all chemical bonds. Chemisorbed adsorbates (chemisorbates) afterwards adhere to certain areas, and the orientation in which they are in reference to the surface is a crucial element in this binding interaction. The relationship between the HOMO and LUMO and the surface determines the kind of bonding (*137*).

Additionally, the 1pg and 2pu orbitals are distributed symmetrically along the molecule's axis. The fully occupied 1 pg orbital interacts considerably with the electronic states of a metallic electrode. By efficiently donating the electron density of the 1 pg orbital to the electrode, a new hybrid electronic state is produced. The 2p orbital accepts electrons from the electrode. It generates brand-new hybrid electronic states, often close to the CO_2 molecule. This process is fascinating because of the bent structure of the chemisorbed CO_2 molecule. Therefore, there are three possible configurations for CO_2 molecules when they chemisorb to a metal surface. The three possible configurations of CO_2 molecules are shown in Figure 2.22 (b) below (*137).*

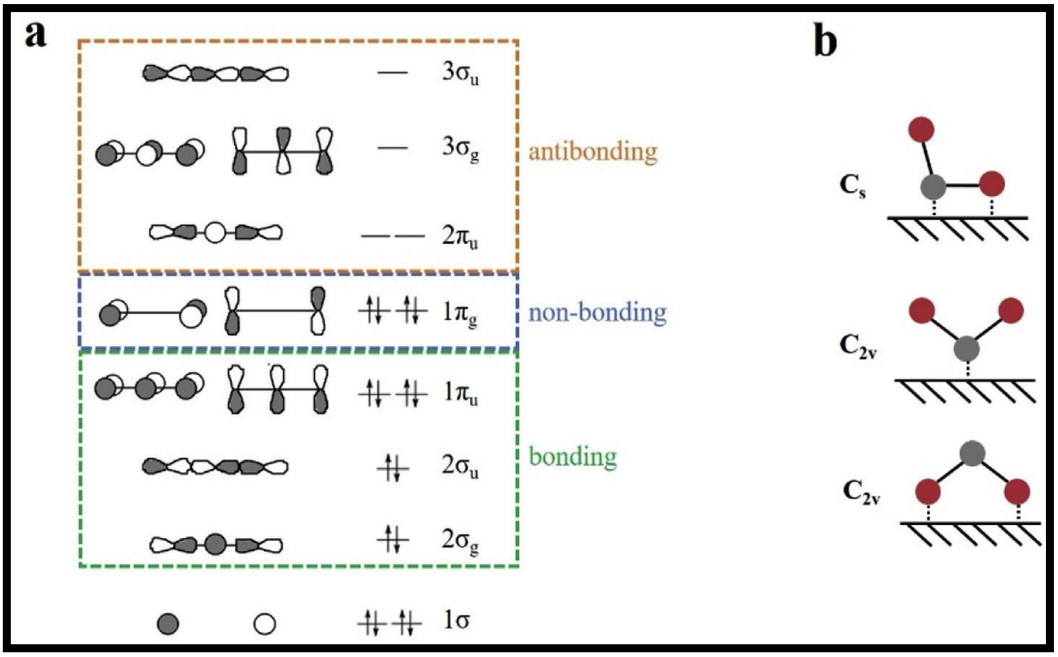

Figure 2.22: Displays the (a) Energy levels for the orbitals of the CO_2 molecule. (b) Possible CO_2 coordination modes that might exist on a metallic surface (*137*).

Table 2.4 shows some of the MOF-based catalysts used for the conduct reduction of CO_2.

Table 2.4: Some MOF-based electrocatalysts for CO2 reduction are listed below (*144*).

MOF-based electrocatalysts	**Resultant Products**	**Faradic Efficiency (FE) (%)**	**Potential**
ZIF-8	CO	65.5	-1.8 V vs SCE
Zn-BTC	CH_4	80.1 $\pm$ 6.6	-2.2 V vs. Ag/AgCl
Ru(III)-doped HKUST-1	CH_3OH, C_2H_5OH	47.2	20mA cm^{-2}
M-PMOF	CO	98.7	-0.8 V vs. RHE[1]
Re-SURMOF	CO	93 $\pm$ 5	-1.6 V vs NHE

Note: The terms used in Table RHE[1] are reversible hydrogen electrode, normal hydrogen electrode (NHE), and saturated calomel electrode (SCE).

2.11 An overview of selected MOFs

2.11.1 MOF-5 ($Zn_4O(BDC)_3$)

MOF-5, or IRMOF-1, is a cubic metal-organic framework molecule with the formula $Zn_4O(BDC)_3$, where BDC_2=1,4-benzodicarboxylate (MOF-5). Omar M. Yaghi was the discoverer. MOF-5 has one of the highest surface areas to volume ratios among metal-organic frameworks, with a surface area to volume ratio of 2200 m^2/cm^3. It was also the first metal-organic framework for hydrogen gas storage to be researched (*160*, *145*).

Figure 2.23 shows the framework of MOF-5 a ball and a stick indicate the metal node in the upper left corner. Grey represents carbon (C), blue represents zinc (Zn), and green represents oxygen (O). The core of the tetrahedron is made up of $Zn_4(O)$ tetrahedrons, and the blue one is also a ZnO_4 tetrahedron, as may be seen in the top right corner of the image (*146*, *147*). The MOF-5 framework is decorated with eight clusters; however, only seven of them may be observed from a distance, (146,*147*). A yellow sphere with a diameter of 18.5 Å in contact with 72 C atoms (grey) serves as a sign of the massive cavity that is surrounded by all clusters, which together form a unit cell of MOF-5 (*146*, *147*).

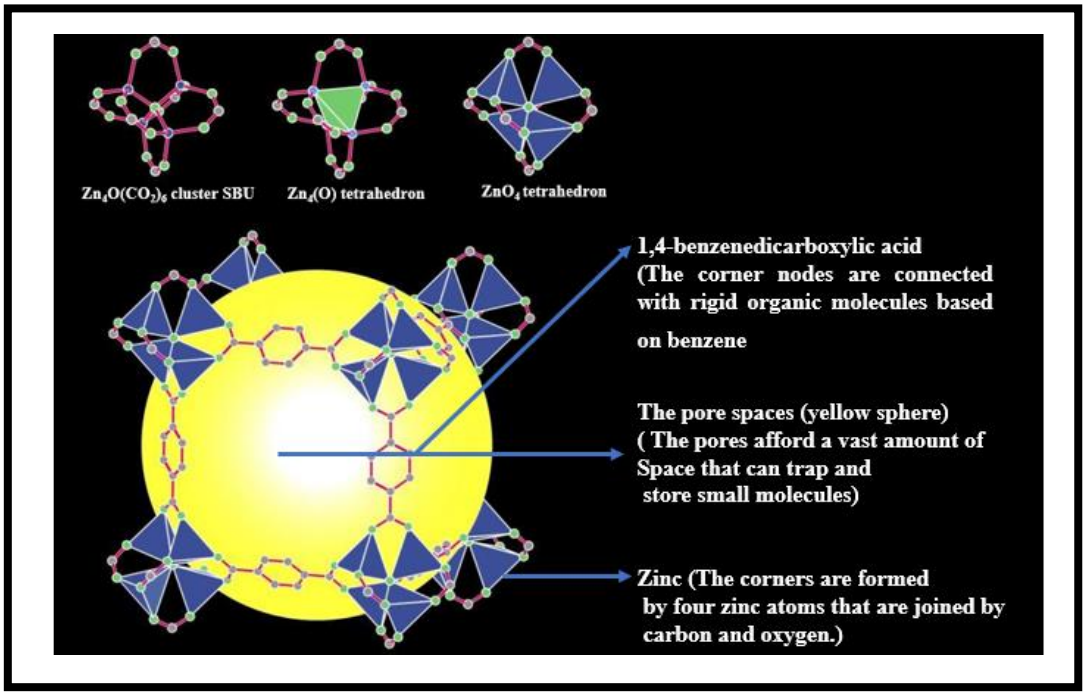

Figure 2.23: The MOF-5 framework's development: $Zn_4(O)O_{12}C_6$ cluster at the top left, in the shape of a ball and stick (Zn, blue; O, green; C, grey). The $Zn_4(O)$ tetrahedron is shown in

green in the middle. On the right, the same, but now with the ZnO4 tetrahedra indicated in blue. One of the cavities in the $Zn_4(O)(BDC)_3$, MOF-5, framework is shown at the bottom. A unit cell is made up of eight clusters (only seven of which are visible), and this cell has a sizable cavity that is enclosed by a yellow sphere with a diameter of 18.5A that is in contact with 72 C atoms (*147*).

MOF-5 is appropriate for use in quantum applications because of its adaptable three-dimensional structure and internal pore size. MOF-5 molecules exhibit properties such as thermal stability up to 400 °C, a BET surface area of 260 to 4400 $m^2\ g^{-1}$, micropore widths of 0.92-1 $cm^3\ g^{-1}$, and more (*146, 147*). The framework of MOF-5 has two kinds of cavities, lined with C and H atoms, with an aperture of 8 nm between them. These cavities may each accommodate guest molecules with Van der Waals radii of 11.0 and 15.1 Å, respectively. (*146-148*).

There are several techniques to make MOF-5; however, when it is made using a solution assembly method, guest solvent molecules can fill the pores in the structure. Numerous studies on MOF synthesis have been conducted, which are crucial for the synthesis of MOF-5, with the goal of increasing the structural characteristics, surface area, and single crystal size of MOF materials while also reducing the total time required for the synthesis process (*149*). The schematic representation of MOF-5 synthesis on the basis of reported literature (*150*) is represented in figure 2.24 below.

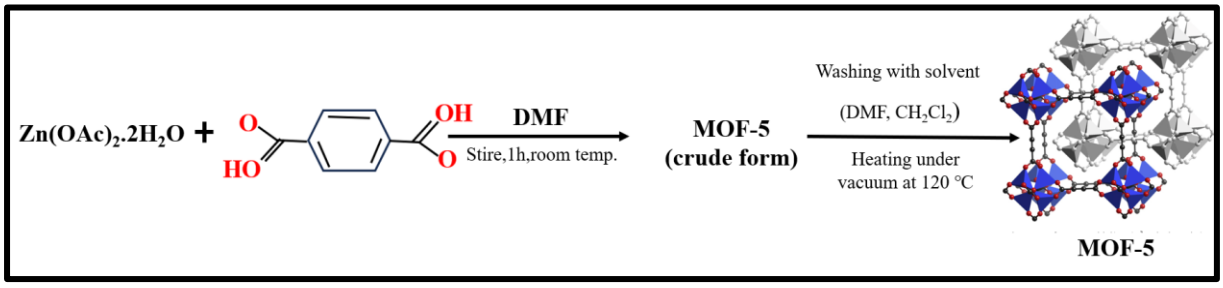

Figure 2.24: The schematic representation of MOF-5 synthesis.

2.11.2. Copper benzene-1,3,5-tricarboxylate, Cu-BTC MOF, HKUST-1, MOF-199

Cu-BTC MOF, sometimes called HKUST-1 or MOF-199 was initially reported by Chui et al. Each copper ion in this MOF forms a dimer with four oxygen atoms from the 1,3,5-benzene tricarboxylate (BTC) molecule (*151*). Cu-BTC is one of the MOF family's more rigid members

and is simple to synthesise. The three-dimensional structure of the Cu-BTC MOF has open metal sites, a decent surface area, and a sufficient pore volume. CuBTC was selected due to its great thermal stability and reversible adsorption-desorption properties without any evidence of crystal structure degradation (*152*).

HKUST-1 is chemically characterised as $[Cu_3(BTC)_2(H_2O)_3]$. The network structure is maintained by SBUs of the $Cu_2(OAc)_4$ paddlewheel type (Figure 2.25). Because of the labile and readily removed axial water molecules, the $Cu_2(OAc)_4$ SBUs have open metal sites that can be employed for catalysis or replaced with various metal-binding groups (*153*).

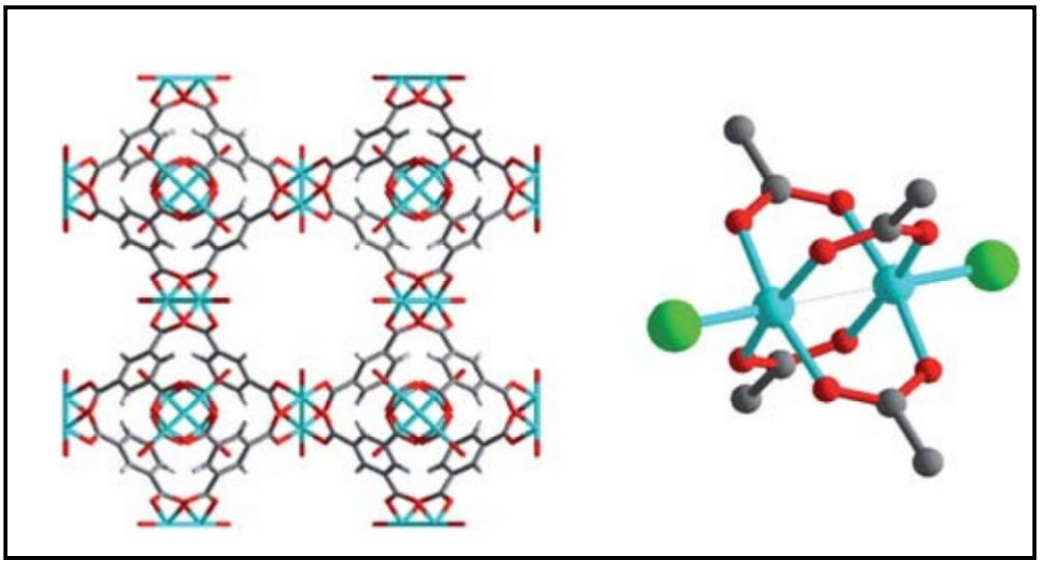

Figure 2.25: Structures of the HKUST-1 cubic metal-organic framework and the paddlewheel secondary building unit (SBU), respectively. Oxygen is represented by red, hydrogen by light grey, carbon by grey, and copper by light blue. The adjustable axial positions of the SBU are shown in the right-hand image by the larger green spheres (*153*).

Cu-BTC has outstanding thermal stability, crystallinity, and porosity. Due to its regular and tiny pore volume, it has a high ability to adsorb small molecules (*154*). Cu-BTC has a lot of potential for molecule adsorption in addition to having high surface activity. Due to these qualities, Cu-BTC is a great candidate for uses like environmental cleaning (*154*). It has also been widely used in the fields of hydrogen storage, hydrocarbon separation, and hazardous gas eradication.

Cu-BTC is a powerful catalytic material due to its high-water sensitivity. It may undergo irreversible degradation because of interactions with polar molecules on the active Cu (II)

surface (*154*). The colour change that occurs after activation indicates a decrease in water molecules caused by the Cu coordination, as indicated in Scheme 2.3 (*155).* According to Kumar, R.S. et al. (2013), the loss of water in the Cu (II) condition is referred to as a weight loss. They asserted that when there are fewer water molecules in the Cu(II) coordination, weight loss occurs. Catalysis is made possible in the open structure by the presence of Cu^{2+} (*155*). CuBTC is typically synthesized following Scheme 2.4 (*156*).

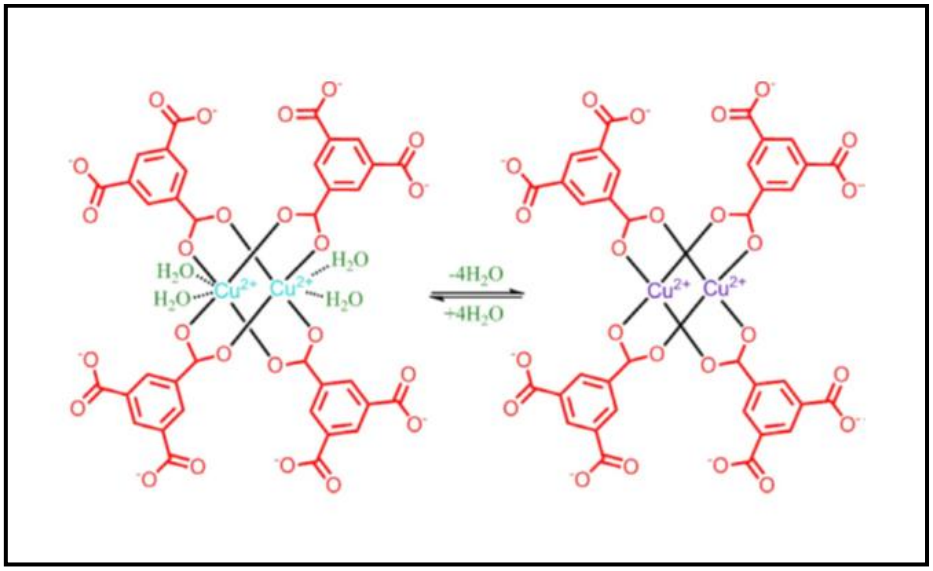

Scheme 2.3: CuBTC colour change demonstration (*155*).

CuBTC is typically synthesized following scheme 2.4.

$$2Cu(NO_3)_2 + 2H_3BTC + 3H_2O \longrightarrow [Cu_3(BTC)_2].3H_2O + 6HNO_3$$

Scheme 2.4: The procedure used in the lab for synthesising of Cu-BTC (*156*).

2.11.3. Iridium (III)-bipyridine Metal-Organic Framework (Ir(III)Cp*Cl@COMOC-4)

The iridium (III)-bipyridine Metal-Organic Framework (Ir(III)Cp*Cl@COMOC-4) is a Ga-based MOF that is used as a heterogeneous catalyst. COMOC-4 is an abbreviation for the University of Ghent's Centre for Ordered Materials, Organometallics, and Catalysis. The gallium 2,2′-bipyridine-5,5′-dicarboxylate (H_2bpydc) MOF, Ga(OH)(bpydc), also known as COMOC-4, was used as the host matrix to create a MOF-supported iridium catalyst (*157*).

These nanoporous materials have generated a great deal of attention because of their large specific surface area, regular, accessible pores, and particularly their structural variation, which

makes them ideal supports for a range of active centres (*157, 158*). It is also feasible to add various functional groups to the framework by prefunctionalization, which requires employing the changed ligands right away in the solvothermal synthesis. Another benefit of creating sophisticated MOF materials suitable for more specific applications is the chemical alteration of the framework after synthesis, or post-synthetic modification (*157,159-160*).

The COMOC-4 is a gallium-based framework with 1D microporous channels, and it is the most basic version. The bipyridine sites of the H_2bpydc linkers located on the channel walls allow coordination of a second metal site. The figure 2.26 demonstrates the general functionalization of MOFs with transition metal complexes using post- or pre-functionalization methods. In this instance, pre-functionalization and post-synthetic modification methods were performed to use $[IrCp^*Cl_2]_2$ as an iridium precursor to bind to the bipyridine moiety of the 2,2′-bipyridine-5,5′-dicarboxylate linkers (*157*).

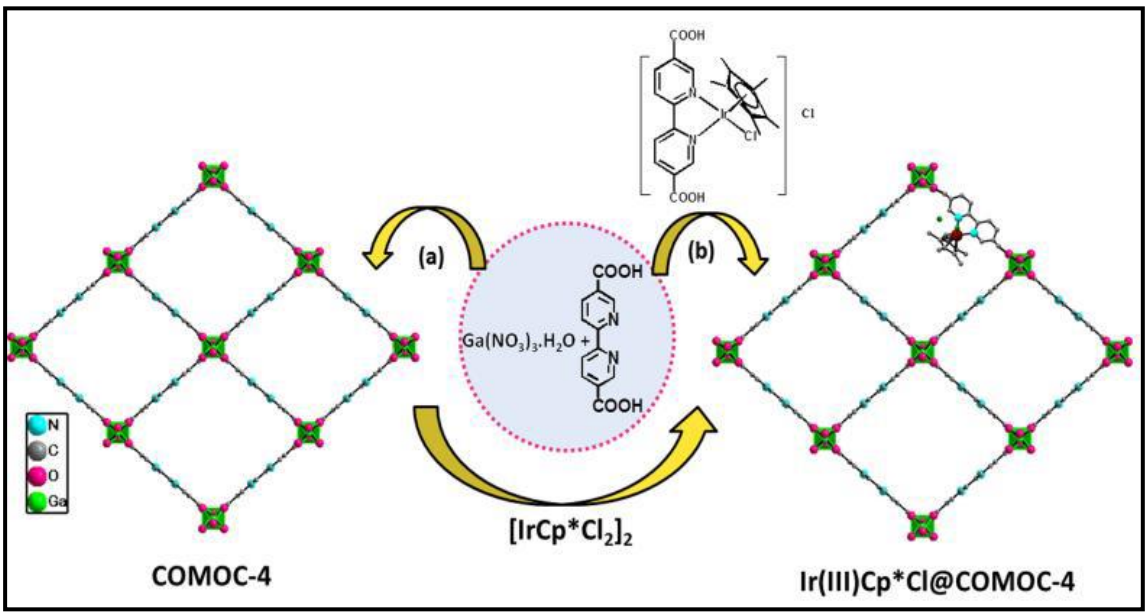

Figure 2.26: The schematic representation for the synthesis of Ir (III)Cp*Cl@COMOC-4 (a) post-functionalization and (b) pre-functionalization is illustrated (*157*).

2.12. Electrochemical Analysis

Electrochemical methods are often used in analytical measurements. Various electrochemical methods with varied degrees of value can be utilised for quantitative and qualitative analysis. However, in this study, the cyclic voltammetry (CV) technique was used to define and evaluate the performance of synthesised MOF-based electrocatalysts. CV was used to investigate the general properties of MOFs on electrodes, as well as the electrochemical behaviour of CO_2 diffusing to an MOF based electrode surface and the interfacial phenomena at the electrode surface (*161*).

2.12.1 Principles of Cyclic Voltammetry (CV)

Cyclic voltammetry is a well-liked dynamic electrochemical method that scans the voltage supplied to an electrochemical cell. The resulting cell current is shown as output versus potential. A three-electrode cell suitable for material study consists of a reference electrode, a counter electrode, and a working electrode. Cyclic voltammetry equipment is built on the three-electrode potentiostat that modifies the working electrode potential in relation to the reference electrode while accounting for as much of the cell resistance as is practical. Due to the potentiostat and cell design, events at the working electrode may be seen during the experiment (*161*).

Randles suggested CV study the electrochemical behaviour of a substrate in an electrolytic medium. CV has evolved as a useful tool for understanding electrochemical processes and electroanalytical methods in a wide range of chemistry domains, including pharmaceutical analysis and biological material. A cyclic voltammogram is formed by applying a linear potential sweep to the working electrode. As a result of the electrode's current, which sweeps the potential, the analyte is reduced or oxidised (*162*).

A cyclic voltammogram's primary characteristics are the scales of the, cathodic peak current (Ipc), anodic peak current (Ipa), cathodic peak potential (Epc), and anodic peak potential (Epa) (*162*). In the CV depicted in figure 2.27, as the species in solution oxidise, a concentration gradient is produced, the potential is elevated beyond its starting value (E_0), the current rises, and the potential is further raised. I_{pa} and E_{pa} represent the maximum current and potential values, respectively, where all reduced species have undergone oxidation. At this time, if the potential application is maintained, the current will start to fall. The current loss is attributed to

the dropping and depleted reduced species. Once E_f is achieved, the now-oxidised species will be reduced back to its original state on the reverse of the potential sweep until E_0 is reached (*163*).

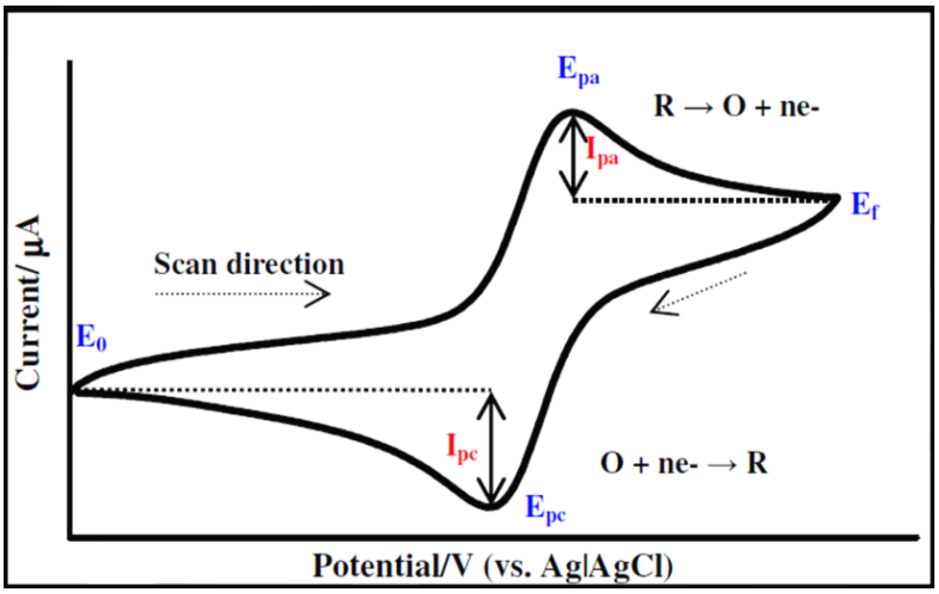

Figure 2.27: A typical cyclic voltammogram (*163*).

The cyclic voltammetry is the potential plot that emerges from the excitation-potential signal, and it can be either (a) reversible, (b) quasi-reversible, or (c) irreversible cycles, as seen in figure 2.28 and defined in Table 2.5. Anodic (Epa), cathodic (Epc), and anodic (Ipa) peak potentials as well as anodic (Ipa) and cathodic (Ipa) peak current information may be obtained from a cyclic voltammogram (*164).*

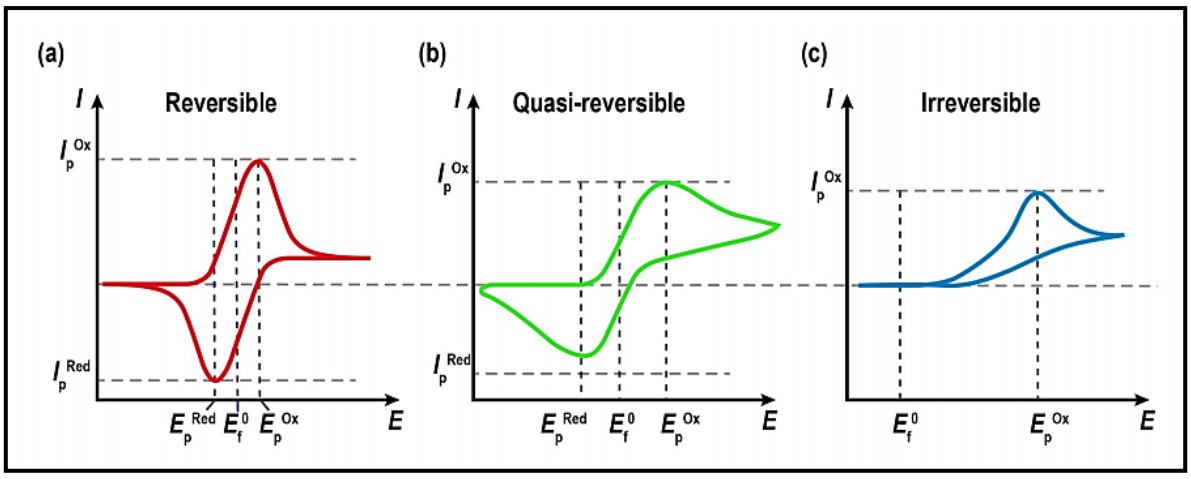

Figure 2.28: Cyclic voltammograms of reversible, quasi-reversible, and irreversible cycles, respectively (*164*).

Table 2.5: Properties of the three categories of cycles (*164*).

Reversible Cyclic Voltammetry	**Quasi-reversible Cyclic Voltammetry**	**Irreversible Cyclic Voltammetry**
Epa and Epc are close to each other	Epa and Epc are away from each other	Only one peak (Epa/Epc) is observed
E^0 = (Epa + Epc)/2 is half way between Epa and Epc	E^0 is not half way between Epa and Epc	E^0 shifts with scan rate
ΔEp = 59/n mV	ΔEp > 59/n mV	No reverse peak
|ipa/ipc| = 1	|ipa/ipc| = 1 when α is 0.5	No reversible peak
Obeys the Nernst equation	The Nernst equation is not maintained	Electron transport is explained by Nicolson equation
ip=(2.69x10^5)AD$^{0.5}$C$*\nu$0.5n$^{1.5}$	$i$pa and $i$pc ∝ to scan rate and not linearly ∝ $\nu^{1/2}$	ip=(2.69x10^5)n[(1−α)n]$^{0.5AC}$ $(Dv)^{0.5}$

If the concentrations in the bulk solution and near the electrode surface are identical, the current induced by analyte oxidation or reduction will be zero. According to the Nernst equation, the applied potential controls the concentrations of redox species at the electrode surface (*162*,*165*).

$$E = E^o + \frac{RT}{nF} \ln\left[\frac{Ox}{Red}\right]$$

where R is the molar gas constant (8.314 $Jmol^{-1}K^{-1}$), T the absolute temperature in K, n the number of electrons transferred, F the Faraday constant (96.485 C/equivalent) and E_o the redox couple standard reduction potential.

To provide evidence of an electrochemically reversible redox process the Randles-Sevcik equation shown below is used. Linear plots of Ip vs $\nu^{1/2}$ at peak potential (Ep) show confirmation of reversible redox process.

$$Ip = (2.69 \times 10^5) n^{3/2} AD^{1/2} C \nu^{1/2}$$

Where Ip is the current maximum (A), n the number of electrons transferred, A the electrode area (cm^2), D the diffusion coefficient (cm^2/s), C the concentration in (mol/cm^3) and ν the scan rate (V/s)

In electrochemical cells, charge transfer processes between an electrode and a reactant molecule can occur by one of three main ways. The three potential charge transfers are shown using an energy diagram, figure 2.29. When an electrode is put into a redox electrolyte, the electrode potential, which is connected to the Fermi Level, equilibrates with the chemical potential of the redox couple, which is located between the HOMO and LUMO levels, as illustrated (*164*). However, by adding a significant quantity of negative potential Φ, the electrode's electrochemical potential ($\mu = E_F + \Phi$) climbs above the LUMO level of the redox molecule even though there is no longer any electron transfer taking place (*164*). Therefore, it is possible for an electron to be transported from the electrode to the redox electrolyte (Figure 2.29 b). In this instance, electrostatic repulsion reduces the redox molecule and causes it to be ejected off the surface. A redox molecule can also be oxidised by applying enough positive potential. When the electrode's electrochemical potential falls below the HOMO level, this reaction takes place. Then, a transfer of electrons from the molecule to the electrode occurs (Figure 2.29 c) (*164*).

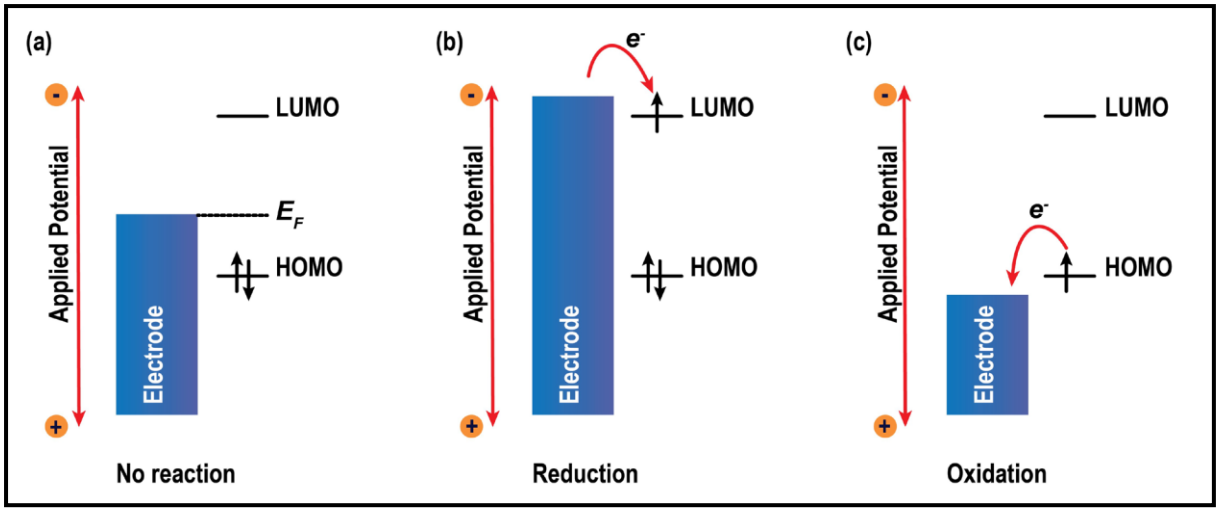

Figure 2.29: Electrode electron transfer process (*273*).

Typically, the electrochemical cell utilised in the CO_2 reduction process is shown in figure 2.30 and is made up of a cathode, an anode, and an ion-exchange membrane. The initial stage in electrochemical CO_2 reduction is the diffusion of CO_2 molecules from the solution to the surface of the cathode prepared with a suitable catalyst. A single electron transfer to CO_2 is one of the proposed methods for activating the CO_2 molecule, resulting in the formation of a CO_2**.** radical anion. A single electron addition causes the linear molecule to bend because of the repulsion between the gained electron over the electrophilic carbon atom and the free electron pairs on the oxygen atom. The disadvantage of this approach is that it requires a very high redox potential (1.9 V against NHE) for such a reaction to take place (*166*).

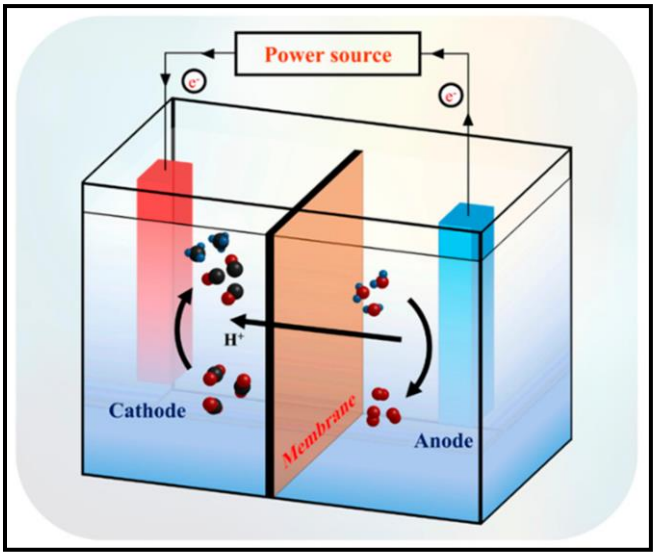

Figure 2.30: Schematic representation of CO_2 reduction using an electrochemical cell (*166*).

The electrocatalytic reduction of CO_2 makes use of a wide variety of surface reaction intermediates for multi-electron and proton reduction. Aqueous solutions can thus possibly produce a variety of reduction products, including hydrogen, formaldehyde, carbon monoxide,, formic acid, methanol, methane, and ethene.

Table 2.6: CO_2 reduction products

Chemical reactions and resulted in CO_2-reduced products.	**The standard hydrogen electrode (SHE) at pH 7**	**Equation Number**
$CO_2 + 2H^+ + 2e^- \rightarrow CO + H_2O$	$E^0 = -0.52$ V	(1)
$CO_2 + 4H^+ + 4e^- \rightarrow HCHO + H_2O$	$E^0 = -0.51$ V	(2)
$CO_2 + e^- \rightarrow CO_2\cdot^-$	$E^0 = -1.9$ V	(3)
$CO_2 + 8H^+ + 8e^- \rightarrow CH_4 + 2H_2O$	$E^0 = -0.24$ V	(4)
$CO_2 + 6H^+ + 6e^- \rightarrow CH_3OH + H_2O$	$E^0 = -0.38$ V	(5)
$CO_2 + 2H^+ + 2e^- \rightarrow HCOOH$	$E^0 = -0.61$ V	(6)
$2CO_2 + 12H^+ + 12e^- \rightarrow C_2H_4 + 4H_2O$	$E^0 = -0.34$ V	(7)
$2H^+ + 2e^- \rightarrow H_2O$	$E^0 = -0.42$ V	(8)

Compared to equilibrium potentials, greater negative potentials are needed for successful electrochemical reduction of CO_2. The following are the main causes: First, as demonstrated

in Eq. (1), the CO_2 molecules are adsorbed onto the catalyst's surface and converted to CO_2 by electron transfer, which necessitates a strong negative potential to disassemble the molecules' stable linear structure. Second, CO_2 is further transformed into various chemical intermediates at the catalyst's surface and then desorbed off the catalyst (Figure 2.31). The electrolyte system of the aqueous solution in the reactor must use energy throughout this process to enhance mass and electron movement on top of overcoming complicated kinetic hurdles. Thirdly, the hydrogen evolution process (HER) is a supplementary reduction reaction since most CO_2 reduction reactions use aqueous solutions as electrolytes (Eq. 8). (*142,167*).

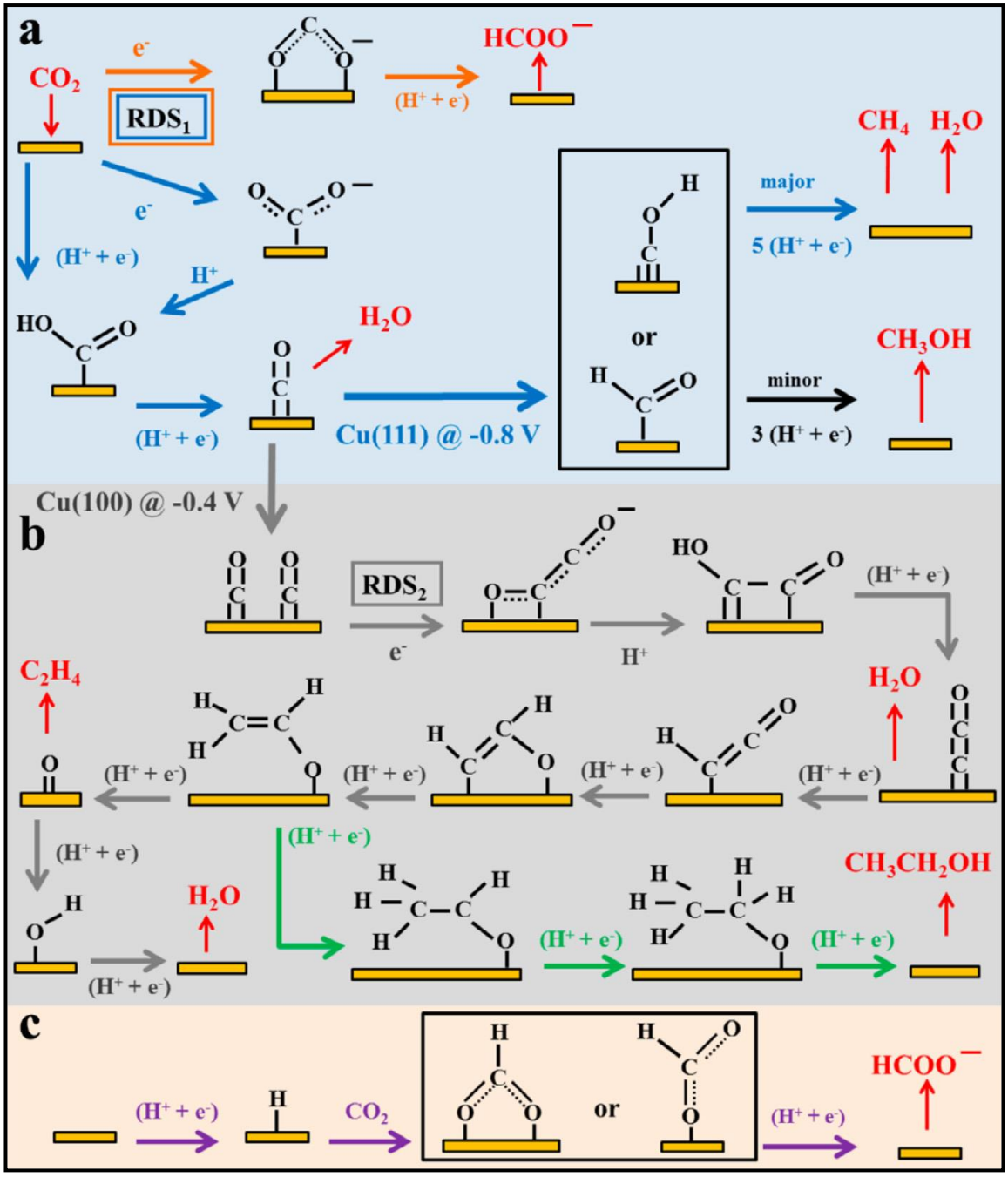

Figure 2.31: Reaction paths for the electrocatalytic reduction of CO_2 to products over catalysts: (a) CO_2 paths to CO, CH_4 (blue arrows), CH_3OH (black arrows), and HCOO (orange arrows); (b) CO_2 pathways to ethylene (grey arrows) and ethanol (green arrow); and (c) CO_2 insertion into a metal H bond-generating formate (purple arrows). Species in black are adsorbates, whereas those in red are reactants or products in solution. Potentials are presented vs. RHE, where RDS denotes rate-determining steps and (H^+ + e) denotes steps involving either concerted or separated proton-electron transfer (*167*).

References

1. Weisz, P.B., Basic choices and constraints on long-term energy supplies, *Physics Today* **57**, 47–52 (2004).
2. Asif, M., and Muneer, T., Energy supply, its demand and security issues for developed and emerging economies. *Renewable and Sustainable Energy Reviews* **11**, 1388–1413 (2007).
3. Canadell, J.G., Le Quere, C., Raupach, M.R., Field, C.B., Buitenhuis, E.T., Ciais, P., Conway, T.J., Gillett, N.P., Houghton, R.A., and Marland, G., Contributions to accelerating atmospheric CO_2 growth from economic activity, carbon intensity, and efficiency of natural sinks, *Proceedings of the National Academy of Sciences* **104**, 18866–18870 (2007).
4. Dresselhaus, M.S., and Thomas, I.L., Alternative energy technologies. *Nature* **414**, 332–337 (2001).
5. Barbir, F., Veziroglu, T.N. and Plass Jr, H.J., Environmental damage due to fossil fuels use. *International Journal of Hydrogen Energy*, **15**, 739–749 (1990).
6. Godbold, J.A. and Calosi, P., Ocean acidification and climate change: advances in ecology and evolution. *Philosophical Transactions of the Royal Society B: Biological Sciences* **368**, 20120448-20120453 (2013).
7. Gomes, V.G. and Kornienko, N. Metal-based nanomaterials for efficient CO_2 electroreduction: Recent advances in mechanism, material design and selectivity. *Nano Energy* **78**, 105311-105329 (2020).
8. Hunt, A.J., Sin, E.H., Marriott, R. and Clark, J.H., Generation, capture, and utilization of industrial carbon dioxide. *ChemSusChem: Chemistry & Sustainability Energy & Materials* **3**, 306-322 (2010).
9. D'Alessandro, D.M., Smit, B. and Long, J.R., Carbon dioxide capture: prospects for new materials. *Angewandte Chemie International Edition* **49**, 6058-6082 (2010).
10. Perera, F. Pollution from fossil-fuel combustion is the leading environmental threat to global pediatric health and equity: Solutions exist. *International journal of environmental research and public health*, **15**, 16-33 (2018).
11. Centi, G., Quadrelli, E.A. and Perathoner, S., Catalysis for CO_2 conversion: a key technology for rapid introduction of renewable energy in the value chain of chemical industries. *Energy & Environmental Science* **6**, 1711-1731 (2013).

12. Liu, H., Zhu, Y., Ma, J., Zhang, Z. and Hu, W., Recent advances in atomic-level engineering of nanostructured catalysts for electrochemical CO_2 reduction. *Advanced Functional Materials* **30**, 1910534-1910558 (2020).
13. Ma, S. and Kenis, P.J., Electrochemical conversion of CO_2 to useful chemicals: current status, remaining challenges, and future opportunities. *Current Opinion in Chemical Engineering* **2**, 191-199 (2013).
14. Song, Y., Chen, W., Wei, W. and Sun, Y., Advances in clean fuel ethanol production from electro-, photo-and photoelectron-catalytic CO_2 reduction. *Catalysts* **10**, 1287-1312 (2020).
15. Zhang, W., Hu, Y., Ma, L., Zhu, G., Wang, Y., Xue, X., Chen, R., Yang, S. and Jin, Z., Progress and perspective of electrocatalytic CO_2 reduction for renewable carbonaceous fuels and chemicals. *Advanced Science* **5**, 1700275-1700299 (2018).
16. Zhang, B., Jiang, Y., Gao, M., Ma, T., Sun, W. and Pan, H., Recent progress on hybrid electrocatalysts for efficient electrochemical CO_2 reduction. *Nano Energy* **80**, 105504-105567 (2021).
17. Nitopi, S., Bertheussen, E., Scott, S.B., Liu, X., Engstfeld, A.K., Horch, S., Seger, B., Stephens, I.E., Chan, K., Hahn, C. and Norskov, J.K., Progress and perspectives of electrochemical CO_2 reduction on copper in aqueous electrolyte. *Chemical reviews* **119**, 7610-7672 (2019).
18. Bigdeli, F., Lollar, C.T., Morsali, A. and Zhou, H.C., Switching in metal–organic frameworks. *Angewandte Chemie International Edition* **59**, 4652-4669 (2004).
19. Singh, C., Mukhopadhyay, S. and Hod, I., Metal–organic framework derived nanomaterials for electrocatalysis: recent developments for CO_2 and N_2 reduction. *Nano Convergence* **8**, 1-10 (2021).
20. Adegoke, K.A. and Maxakato, N.W., Porous metal-organic framework (MOF)-based and MOF-derived electrocatalytic materials for energy conversion. *Materials Today Energy* **21**,100816-100903 (2021).
21. Kumar, R.S., Kumar, S.S. and Kulandainathan, M.A., Highly selective electrochemical reduction of carbon dioxide using Cu based metal organic framework as an electrocatalyst. *Electrochemistry Communications* **25**, 70-73 (2012).
22. Hinogami, R., Yotsuhashi, S., Deguchi, M., Zenitani, Y., Hashiba, H. and Yamada, Y., Electrochemical reduction of carbon dioxide using a copper rubeanate metal organic framework. *ECS Electrochemistry Letters* **1**, 17-20 (2012).

23. Pan, F. and Yang, Y., Designing CO_2 reduction electrode materials by morphology and interface engineering. *Energy & Environmental Science* **13**, 2275-2309 (2020).
24. Durst, J., Rudnev, A., Dutta, A., Fu, Y., Herranz, J., Kaliginedi, V., Kuzume, A., Permyakova, A.A., Paratcha, Y., Broekmann, P. and Schmidt, T.J., Electrochemical CO_2 Reduction–A Critical View on Fundamentals, Materials and Applications. *Chimia*, **69**, 769-769 (2015).
25. Chen, Y.Z., Zhang, R., Jiao, L. and Jiang, H.L., Metal–organic framework-derived porous materials for catalysis. *Coordination Chemistry Reviews* **362**, (2018).
26. Derick's, C.S., Kalmutzki, M.J., Diercks, N.J. and Yaghi, O.M., Conceptual advances from Werner complexes to metal–organic frameworks. *ACS Central Science* **4**, 1457-1464 (2018).
27. Alamer, B. Design, Synthesis and Characterization of Functional Metal-Organic Framework Materials, 1-83 (2015).
28. Pentyala, V., Design and functionalization of metal-organic frameworks for chemical gas sensor applications, Royal Society of Chemistry **49**, 1-171 (2019).
29. Hofmann, K.A. and Kuspert, F.A., Z. Compounds of hydrocarbons with metal salts. *Anorg. Allg. Chem*, **15**, 204-207 (1897).
30. Rayner, J.H. and Powell, H.M., Structure of molecular compounds. Part X. Crystal structure of the compound of benzene with an ammonia–nickel cyanide complex. *Journal of the Chemical Society*, 319-328 (1952).
31. Davis, M.E., Saldarriaga, C., Montes, C., Garces, J. and Crowdert, C., A molecular sieve with eighteen-membered rings. *Nature* **331,** 698-699 (1988).
32. Yaghi, O.M., Li, G. and Li, H., Selective binding and removal of guests in a microporous metal–organic framework. *Nature* **378**, 703-706 (1995).
33. Yaghi, O.M. and Li, H., Hydrothermal synthesis of a metal-organic framework containing large rectangular channels. *Journal of the American Chemical Society* **117**, 10401-10402 (1995).
34. Li, H., Eddaoudi, M., Groy, T.L. and Yaghi, O.M., Establishing microporosity in open metal− organic frameworks: gas sorption isotherms for Zn (BDC)(BDC= 1, 4-benzenedicarboxylate). *Journal of the American Chemical Society* **120**, 8571-8572 (1998).
35. Yaghi, O.M., Reticular chemistry in all dimensions. *ACS Central Science* **5**, 1295-1300 (2019).

36. Sharanyakanth, P.S. and Radhakrishnan, M., Synthesis of metal-organic frameworks (MOFs) and its application in food packaging: A critical review. *Trends in Food Science & Technology* **104**, 102-116 (2020).
37. Moghadam, P.Z., Li, A., Liu, X.W., Bueno-Perez, R., Wang, S.D., Wiggin, S.B., Wood, P.A. and Fairen-Jimenez, D., Targeted classification of metal–organic frameworks in the Cambridge structural database (CSD). *Chemical science* **11**, 8373-8387 (2020).
38. Daglar, H. and Keskin, S., Recent advances, opportunities, and challenges in high-throughput computational screening of MOFs for gas separations. *Coordination Chemistry Reviews* **422**, 213470-213490 (2020).
39. Hoskins, B.F. and Robson, R., Design and construction of a new class of scaffolding-like materials comprising infinite polymeric frameworks of 3D-linked molecular rods. A reappraisal of the zinc cyanide and cadmium cyanide structures and the synthesis and structure of the diamond-related frameworks $[N(CH_3)_4][CuIZnII(CN)_4]$ and CuI [4, 4', 4", 4"'-tetracyanotetraphenylmethane] $BF_4.xC_6H_5NO_2$. *Journal of the American Chemical Society* **112**, 1546-1554 (1990).
40. Hoskins, B.F. and Robson, R., Infinite polymeric frameworks consisting of three dimensionally linked rod-like segments. *Journal of the American Chemical Society* **111**, 5962-5964 (1989).
41. Zhang, X., Chen, Z., Liu, X., Hanna, S.L., Wang, X., Taheri-Ledari, R., Maleki, A., Li, P. and Farha, O.K., A historical overview of the activation and porosity of metal–organic frameworks. *Chemical Society Reviews* **49**, 7406-7427 (2020).
42. Yusuf, V.F., Malek, N.I. and Kailasa, S.K., Review on Metal–Organic Framework Classification, Synthetic Approaches, and Influencing Factors: Applications in Energy, Drug Delivery, and Wastewater Treatment. *ACS Omega* **7**, 44507-44531 (2022).
43. Chen, L., Zhang, X., Cheng, X., Xie, Z., Kuang, Q. and Zheng, L., The function of metal–organic frameworks in the application of MOF-based composites. *Nanoscale Advances* **2**, 2628-2647 (2020).
44. Ling, P., Lei, J. and Ju, H., Porphyrinic metal-organic framework as electrochemical probe for DNA sensing via triple-helix molecular switch. *Biosensors and Bioelectronics* **71**, 373-379 (2015).
45. Abedi, S., Tehrani, A.A. and Morsali, A., Mechanochemical synthesis of isoreticular metal–organic frameworks and comparative study of their potential for nitrobenzene sensing. *New Journal of Chemistry* **39**, 5108-5111 (2015).

46. Zhu, M., Wu, X., Niu, B., Guo, H. and Zhang, Y. Fluorescence sensing of 2, 4, 6-trinitrophenol based on hierarchical IRMOF-3 nanosheets fabricated through a simple one-pot reaction. *Applied Organometallic Chemistry* **32**, 4333-4340 (2018).
47. Tong, P., Liang, J., Jiang, X. and Li, J., Research progress on metal-organic framework composites in chemical sensors. *Critical Reviews in Analytical Chemistry* **50**, 376-392 (2020).
48. Buser, H.J., Schwarzenbach, D., Petter, W. and Ludi, A.J.I.C., The crystal structure of Prussian blue: $Fe_4[Fe(CN)_6]_3.xH_2O$. *Inorganic chemistry* **16**, 2704-2710 (1977).
49. Hirai, K., Sumida, K., Meilikhov, M., Louvain, N., Nakahama, M., Uehara, H., Kitagawa, S. and Furukawa, S., Impact of crystal orientation on the adsorption kinetics of a porous coordination polymer–quartz crystal microbalance hybrid sensor. *Journal of Materials Chemistry C* **2**, 3336-3344 (2014).
50. Pan, Y., Zhan, S. and Xia, F., Zeolitic imidazolate framework-based biosensor for detection of HIV-1 DNA. *Analytical Biochemistry* **546**, 5-9 (2018).
51. Wang, Y., Yan, J., Wen, N., Xiong, H., Cai, S., He, Q., Hu, Y., Peng, D., Liu, Z. and Liu, Y., Metal-organic frameworks for stimuli-responsive drug delivery. *Biomaterials* **230**, 119619-119687 (2020).
52. Han, T.T., Yang, J., Liu, Y.Y. and Ma, J.F., Rhodamine 6G loaded zeolitic imidazolate framework-8 (ZIF-8) nanocomposites for highly selective luminescent sensing of Fe^{3+}, Cr^{6+} and aniline. *Microporous and Mesoporous Materials* **228**, 275-288 (2016).
53. Han, T.T., Bai, H.L., Liu, Y.Y. and Ma, J.F., Two host-guest hybrids by encapsulation AlQ_3 in zeolitic imidazolate framework-8 as luminescent sensors for Fe^{3+}, $CrO_4^{2-}$and acetone. Journal of Solid-State Chemistry **269**, 588-593 (2019).
54. Yu, H., Zhang, W., Lv, S., Han, J., Xie, G. and Chen, S., A one-step structure-switching electrochemical sensor for transcription factor detection enhanced with synergistic catalysis of PtNi@ MIL-101 and Exo III-assisted cycling amplification. *Chemical Communications* **54**, 11901-11904 (2018).
55. Duan, S. and Huang, Y., Electrochemical sensor using NH_2-MIL-88 (Fe)-rGO composite for trace Cd^{2+}, Pb^{2+}, and Cu^{2+} detection. *Journal of Electroanalytical Chemistry* **807**, 253-260
56. Nabipour, H., Mozafari, M. and Hu, Y., Nomenclature of MOFs. In *Metal-Organic Frameworks for Biomedical Applications*, 1-9 (2020).
57. Alhumaimess, M.S., Metal–organic frameworks and their catalytic applications. *Journal of Saudi Chemical Society* **24**, 461-473 (2020).

58. Pham, M.H., Vuong, G.T., Vu, A.T. and Do, T.O. Novel route to size-controlled Fe–MIL-88B–NH_2 metal–organic framework nanocrystals. *Langmuir* **27**, 15261-15267 (2011).
59. Pham, H.Q., Mai, T., Pham-Tran, N.N., Kawazoe, Y., Mizuseki, H. and Nguyen-Manh, D., Engineering of band gap in metal–organic frameworks by functionalizing organic linker: A systematic density functional theory investigation. *The Journal of Physical Chemistry C* **118**, 4567-4577 (2014).
60. Mai, Z. and Liu, D., Synthesis and Applications of Isoreticular Metal–Organic Frameworks IRMOFs-n (n= 1, 3, 6, 8). *Crystal Growth & Design* **19**, 7439-7462 (2019).
61. Eddaoudi, M., Kim, J., Rosi, N., Vodak, D., Wachter, J., O'Keeffe, M. and Yaghi, O.M., Systematic design of pore size and functionality in isoreticular MOFs and their application in methane storage. *Science* **295**, 469-472 (2002).
62. Butova, V.V.E., Soldatov, M.A., Guda, A.A., Lomachenko, K.A. and Lamberti, C., Metal-organic frameworks: structure, properties, methods of synthesis and characterization. *Russian Chemical Reviews* **85**, 280-309 (2016).
63. Bucior, B.J., Rosen, A.S., Haranczyk, M., Yao, Z., Ziebel, M.E., Farha, O.K., Hupp, J.T., Siepmann, J.I., Aspuru-Guzik, A. and Snurr, R.Q., Identification schemes for metal–organic frameworks to enable rapid search and cheminformatics analysis. *Crystal Growth & Design* **19**, 6682-6697 (2019).
64. Lin, Z.J., Lu, J., Hong, M. and Cao, R., Metal–organic frameworks based on flexible ligands (FL-MOFs): structures and applications. *Chemical Society Reviews* **43**, 5867-5895 (2014).
65. Meyer, K., Ranocchiari, M. and van Bokhoven, J.A., Metal organic frameworks for photo-catalytic water splitting. *Energy & Environmental Science* **8**, 1923-1937 (2015).
66. Batten, S.R., Champness, N.R., Chen, X.M., Garcia-Martinez, J., Kitagawa, S., Ohrstrom, L., O'Keeffe, M., Suh, M.P. and Reedijk, J., Coordination polymers, metal–organic frameworks and the need for terminology guidelines. *CrystEngComm* **14**, 3001-3004 (2021).
67. O'Keeffe, M., Peskov, M.A., Ramsden, S.J. and Yaghi, O.M., The reticular chemistry structure resource (RCSR) database of, and symbols for, crystal nets. *Accounts of Chemical Research* **41**, 1782-1789 (2008).

68. Rana, A., A Review on Metal-Organic Frameworks: Synthesis and Applications. *Asian Journal of Chemistry* **33**, 1-8 (2021)
69. Baumann, A.E., Burns, D.A., Liu, B. and Thoi, V.S., Metal-organic framework functionalization and design strategies for advanced electrochemical energy storage devices. *Communications Chemistry* **2**, 86-100 (2019).
70. Wu, H.B. and Lou, X.W., Metal-organic frameworks and their derived materials for electrochemical energy storage and conversion: Promises and challenges. *Science Advances* **3**, 9252-9321 (2017).
71. Cao, X., Tan, C., Sindoro, M. and Zhang, H., Hybrid micro-/nano-structures derived from metal–organic frameworks: preparation and applications in energy storage and conversion. *Chemical Society Reviews* **46**, 2660-2677 (2017).
72. Liu, J., Zhu, D., Guo, C., Vasileff, A. and Qiao, S.Z., Design strategies toward advanced MOF-derived electrocatalysts for energy-conversion reactions. *Advanced Energy Materials* **7**, 1700518- 1700537 (2017).
73. Lee, H.J., We, J., Kim, J.O., Kim, D., Cha, W., Lee, E., Sohn, J. and Oh, M., Morphological and structural evolutions of metal–organic framework particles from amorphous spheres to crystalline hexagonal rods. *Angewandte Chemie*, **127**, 10710-10714 (2015).
74. Saraci, F., Quezada-Novoa, V., Donnarumma, P.R. and Howarth, A.J., Rare-earth metal–organic frameworks: from structure to applications. *Chemical Society Reviews* **49**, 7949-7977 (2020).
75. Luebke, R., *Metal-Organic Frameworks: Building Block Design Strategies for the Synthesis of MOFs*, [PhD] King Abdullah University of Science and Technology (2014). https://repository.kaust.edu.sa/bitstreams/6c2d0230-0b80-4435-8376-36bb312af0a1/download
76. Rowsell, J.L. and Yaghi, O.M., Metal Organic Frameworks: A New Class of Porous Materials. *Microporous and mesoporous materials* **73**, 3-14 (2004).
77. James, S.L., Metal-organic frameworks. *Chemical Society Reviews* **32**, 276-288 (2003).
78. Eddaoudi, M., Moler, D.B., Li, H., Chen, B., Reineke, T.M., O'keeffe, M. and Yaghi, O.M., Modular chemistry: secondary building units as a basis for the design of highly porous and robust metal organic carboxylate frameworks. *Accounts of chemical research* **34**, 319-330 (2001).
79. Rowsell, J.L. and Yaghi, O.M., Strategies for hydrogen storage in metal–organic frameworks. *Angewandte Chemie International Edition* **44**, 4670-4679 (2005).

80. Eubank, J.F., Wojtas, L., Hight, M.R., Bousquet, T., Kravtsov, V.C. and Eddaoudi, M., The next chapter in MOF pillaring strategies: trigonal heterofunctional ligands to access targeted high-connected three-dimensional nets, isoreticular platforms. *Journal of the American Chemical Society* **133**, 17532-17535 (2011).
81. Nouar, F., Eckert, J., Eubank, J.F., Forster, P. and Eddaoudi, M., Zeolite-like metal− organic frameworks (zmofs) as hydrogen storage platform: Lithium and magnesium ion-exchange and H_2-(rho-ZMOF) interaction studies. *Journal of the American Chemical Society* **131**, 2864-2870 (2009).
82. Wade, C.R. and Dinca, M. Investigation of the synthesis, activation, and isosteric heats of CO_2 adsorption of the isostructural series of metal–organic frameworks $M_3(BTC)_2$ (M= Cr, Fe, Ni, Cu, Mo, Ru). *Dalton Transactions* **41**, 7931-7938 (2012).
83. Seetharaj, R., Vandana, P.V., Arya, P. and Mathew, S., Dependence of solvents, pH, molar ratio and temperature in tuning metal organic framework architecture. *Arabian journal of chemistry* **12**, 295-315 (2019).
84. Castillo-Blas, C. and Gándara, F., Metal-organic Frameworks Incorporating Multiple Metal Elements. *Israel Journal of Chemistry* **58**, 1036-1043 (2018).
85. Soni, S., Bajpai, P.K. and Arora, C., A review on metal-organic framework: Synthesis, properties and application. *Characterization and Application of Nanomaterials* **3**, 87-106 (2020).
86. Vilela, S.M.F. Metal-Organic Frameworks Based on Phosphonate Linkers. *Universidade de Aveiro*, 1-24 (2016).
87. Lu, W., Wei, Z., Gu, Z.Y., Liu, T.F., Park, J., Park, J., Tian, J., Zhang, M., Zhang, Q., Gentle III, T. and Bosch, M., Tuning the structure and function of metal–organic frameworks via linker design. *Chemical Society Reviews* **43**, 5561-5593 (2014).
88. Hardian, R., Interplay between structure, texture, and reactivity in MOFs in the case of amorphous, defective, and composite materials. *Theses.Fr*, 1- 194 (2018).
89. Zacher, D., Shekhah, O., Woll, C., and Fischer, R.A., Thin films of metal–organic frameworks. *Chemical Society Reviews*, **38**, 1418-1429 (2009).
90. De Meneses Precker, R.L. Metal-organic Frameworks as Drug Delivery System for Cancer Therapy, 1-157 (2022).
91. Wu, H., Zhou, W. and Yildirim, T., High-capacity methane storage in metal− organic frameworks M_2 (dhtp): the important role of open metal sites. *Journal of the American Chemical Society* **131**, 4995-5000 (2009).

92. Platero Prats, A.E., de la Pena-O'Shea, V.A., Iglesias, M., Snejko, N., Monge, A. and Gutierrez-Puebla, E., Heterogeneous Catalysis with Alkaline-Earth Metal-Based MOFs: A Green Calcium Catalyst. *ChemCatChem* **2**, 147-149 (2010).
93. Yang, L.M., Vajeeston, P., Ravindran, P., Fjellvag, H. and Tilset, M., Revisiting isoreticular MOFs of alkaline earth metals: A comprehensive study on phase stability, electronic structure, chemical bonding, and optical properties of A–IRMOF-1 (A= Be, Mg, Ca, Sr, Ba). *Physical Chemistry Chemical Physics* **13**, 10191-10203 (2011).
94. Maark, T.A. and Pal, S., A model study of effect of M= Li^{+}, Na^{+}, Be^{2+}, Mg^{2+}, and Al^{3+} ion decoration on hydrogen adsorption of metal-organic framework-5. *International Journal of Hydrogen Energy* **35**, 12846-12857 (2010).
95. Serre, C. and Ferey, G., Hydrothermal synthesis, thermal behaviour and structure determination from powder data of a porous three-dimensional europium trimesate: $Eu_3(H_2O)(OH)_6[C_6H_3(CO_2)_3]\cdot 3H_2O$ or MIL-63. *Journal of Materials Chemistry* **12**, 3053-3057(2002).
96. Reineke, T.M., Eddaoudi, M., O'keeffe, M. and Yaghi, O.M., A microporous lanthanide–organic framework. *Angewandte Chemie International Edition* **38**, 2590-2594 (1999).
97. Dey, C., Kundu, T., Biswal, B.P., Mallick, A., and Banerjee, R., Crystalline metal-organic frameworks (MOFs): synthesis, structure and function. *Crystal Engineering and Materials* **70**, 3-10 (2014).
98. Demazeau, G., Solvothermal reactions: an original route for the synthesis of novel materials. *Journal of Materials Science* **43**, 2104-2114 (2008).
99. Sun, Y.X., and Sun, W.Y., Influence of temperature on metal-organic frameworks. *Chinese Chemical Letters* **25**, 823-828 (2014).
100. Li, Y., Gan, D., Deng, X., Jiang, L., Xie, C. and Lu, X., Preparation of metal-organic frameworks and their derivatives for supercapacitors. *Biosurface and Biotribology* **8**, 151-164 (2022).
101. Chu, Q., Liu, G.X., Okamura, T.A., Huang, Y.Q., Sun, W.Y. and Ueyama, N., Structure modulation of metal–organic frameworks via reaction pH: Self-assembly of a new carboxylate containing ligand N-(3-carboxyphenyl) iminodiacetic acid with cadmium (II) and cobalt (II) salts. *Polyhedron* **27**, 812-820. (2008).
102. Rubio-Martinez, M., Avci-Camur, C., Thornton, A.W., Imaz, I., Maspoch, D. and Hill, M.R., New synthetic routes towards MOF production at scale. *Chemical Society Reviews* **46**, 3453-3480 (2017).

103. Tao, A.R., Habas, S. and Yang, P., Shape control of colloidal metal nanocrystals. S*mall* **4**, 310-325 (2008).

104. Long, J.R. and Yaghi, O.M., The pervasive chemistry of metal–organic frameworks. *Chemical Society Reviews* **38**, 1213-1214 (2009).

105. Tella, A.C. and Aaron, I.Y., Syntheses and applications of metal–organic frameworks materials: a review. *Acta Chim Pharm Indica* **2**, 75-81(2012).

106. Gonzalez, C.M.O., Morales, E.M.C., Tellez, A.D.M.N., Quezada, T.E.S., Kharissova, O.V., and Méndez-Rojas, M.A., CO_2 capture by MOFs. In Handbook of Greener Synthesis of Nanomaterials and Compounds. *Elsevier* **2**, 407-448 (2021).

107. Gupta, C., Pant, P., and Rajput, H., Strategies to Synthesize Diverse Metal–Organic Frameworks (MOFs). In Metal-Organic Frameworks (MOFs) as Catalysts Singapore: Springer Nature Singapore, 69-97 (2022).

108. Senkovska, I., Hoffmann, F., Froba, M., Getzschmann, J., Bohlmann, W. and Kaskel, S., New highly porous aluminium-based metal-organic frameworks: Al (OH)(ndc) (ndc=2,6-naphthalene dicarboxylate) and Al(OH)(bpdc)(bpdc=4,4′-biphenyl dicarboxylate). *Microporous and Mesoporous Materials*, **122**, 93-98 (2009).

109. Chen, W., Du, L., and Wu, C., Hydrothermal synthesis of MOFs. In Metal-Organic Frameworks for Biomedical Applications. *Woodhead Publishing*, 141-157 (2020).

110. Kumar, S., Vijayan, S., Goyal, K., Kathuria, M., and Gulati, S., Functionalization Strategies of Metal–Organic Frameworks (MOFs): Diverse Ways to Versatile MOFs. In Metal-Organic Frameworks (MOFs) as Catalysts. *Springer Nature Singapore*, 99-123 (2022).

111. Hu, M.L., Razavi, S.A.A., Piroozzadeh, M. and Morsali, A., Sensing organic analytes by metal–organic frameworks: a new way of considering the topic. *Inorganic Chemistry Frontiers* **7**, 1598-1632 (2020).

112. Pettinari, C., Marchetti, F., Mosca, N., Tosi, G., and Drozdov, A., Application of metal−organic frameworks. *Polymer International* **66**, 731-744 (2017).

113. Silva, A.R., Alexandre, J.Y., Souza, J.E., Neto, J.G.L., de Sousa Junior, P.G., Rocha, M.V., and Dos Santos, J.C., The Chemistry and Applications of Metal–Organic Frameworks (MOFs) as Industrial Enzyme Immobilization Systems. *Molecules* **27**, 4529-4557 (2022).

114. Peedikakkal, A.M.P., and Aljundi, I.H., Mixed-Metal Cu-BTC metal-organic frameworks as a strong adsorbent for molecular hydrogen at low temperatures. *ACS omega* **5**, 28493-28499 (2020).

115. Emam, H.E., Abdelhameed, R.M., and Ahmed, H.B., Adsorptive performance of MOFs and MOF containing composites for clean energy and safe environment. *Journal of Environmental Chemical Engineering* **8**, 104386- 104399 (2020).

116. Bordiga, S., Regli, L., Bonino, F., Groppo, E., Lamberti, C., Xiao, B., Wheatley, P.S., Morris, R.E., and Zecchina, A., Adsorption properties of HKUST-1 toward hydrogen and other small molecules monitored by IR. *Physical Chemistry Chemical Physics* **9**, 2676-2685 (2007).

117. Qasem, N.A., Ben-Mansour, R., and Habib, M.A., An efficient CO_2 adsorptive storage using MOF-5 and MOF-177. *Applied Energy* **210**, 317-326 (2018).

118. Koo, W.T., Jang, J.S., and Kim, I.D., Metal-organic frameworks for chemiresistive sensors. *Chem* **5**, 1938-1963 (2019).

119. Keller, D.P., Lenton, A., Littleton, E.W., Oschlies, A., Scott, V., and Vaughan, N.E., The effects of carbon dioxide removal on the carbon cycle. *Current Climate Change Reports* **4**, 250-265 (2018).

120. Houghton, R.A., Balancing the global carbon budget. *Annu. Rev. Earth Planet. Sci*. **35**, 313-347 (2007).

121. Yoro, K.O. and Daramola, M.O., CO_2 emission sources, greenhouse gases, and the global warming effect. In Advances in carbon capture. *Woodhead Publishing*. 3-28 (2020).

122. Le Quéré, C., Andres, R.J., Boden, T., Conway, T., Houghton, R.A., House, J.I., Marland, G., Peters, G.P., Van der Werf, G., Ahlström, A., and Andrew, R.M., The global carbon budget 1959–2011. *Earth System Science Data Discussions* **5,** 1107-1157 (2012).

123. Houghton, R.A., How well do we know the flux of CO_2 from land-use change? *Tellus B: Chemical and Physical Meteorology* **62** 337-351(2010).

124. Das, S., Carbonate Chemistry of Water. In An Introduction to Water Quality Science: Significance and Measurement Protocols. *Cham: Springer International Publishing*. 79-101(2023).

125. Markewitz, P., Kuckshinrichs, W., Leitner, W., Linssen, J., Zapp, P., Bongartz, R., Schreiber, A. and Müller, T.E. Worldwide innovations in the development of carbon capture technologies and the utilization of CO_2. Energy & environmental science **5**, 7281-7305 (2021).

126. Chen, L., Msigwa, G., Yang, M., Osman, A.I., Fawzy, S., Rooney, D.W. and Yap, P.S., Strategies to achieve a carbon neutral society: a review. Environmental Chemistry Letters **20**, 2277-2310 (2022).

127. Khezri, B., Fisher, A.C., and Pumera, M., CO_2 reduction: the quest for electrocatalytic materials. *Journal of Materials Chemistry A* **5**, 8230-8246 (2017).

128. Zhao, Y., Zheng, L., Jiang, D., Xia, W., Xu, X., Yamauchi, Y., Ge, J., and Tang, J. Nanoengineering metal–organic framework-based materials for use in electrochemical CO_2 reduction reactions. *Small* **17**, 06590-2006608 (2021).

129. Wang, Z., Hou, P., Wang, Y., Xiang, X., and Kang, P., Acidic electrochemical reduction of CO_2 using nickel nitride on multiwalled carbon nanotube as selective catalyst. *ACS Sustainable Chemistry & Engineering* **7**, 6106-6112 (2019).

130. Whipple, D.T., and Kenis, P.J., Prospects of CO_2 utilization via direct heterogeneous electrochemical reduction. *The Journal of Physical Chemistry Letters* **1**, 3451-3458 (2010).

131. Aresta, M., Dibenedetto, A., and Angelini, A., Catalysis for the valorization of exhaust carbon: from CO_2 to chemicals, materials, and fuels. Technological use of CO_2. *Chemical reviews* **114**, 1709-1742 (2014).

132. Hou, S.L., Dong, J., and Zhao, B., Formation of C-X Bonds in CO_2 Chemical Fixation Catalyzed by Metal− Organic Frameworks. *Advanced Materials* **32**, 1806163-1806177 (2020).

133. Sakakura, T., Choi, J.C., and Yasuda, H. Transformation of carbon dioxide. *Chemical Reviews* **107**, 2365-2387 (2007).

134. Shen, Y., Pan, T., Wang, L., Ren, Z., Zhang, W., and Huo, F., Programmable logic in metal–organic frameworks for catalysis. *Advanced Materials* **33**, 2007442- 2007472 (2021).

135. Hutchings, G.J. Heterogeneous catalysts-discovery and design. *Journal of materials Chemistry* **19**, 1222-1235 (2009).

136. Wu, C.D., and Zhao, M. Incorporation of molecular catalysts in metal–organic frameworks for highly efficient heterogeneous catalysis. Advanced Materials 29, 1605446-1605467 (2017).

137. Zhang, X., Guo, S.X., Gandionco, K.A., Bond, A.M. and Zhang, J., Electrocatalytic carbon dioxide reduction: From fundamental principles to catalyst design. *Materials Today Advances* **7**, 100074- 100098 (2020).

138. Diwakar, V.D., Harinipriya, S., and Subramanian, V.R. A review of Continuum Electrochemical Engineering Models and a Novel Monte Carlo Approach to Understand Electrochemical Behavior of Lithium-Ion Batteries. *Theory and Experiment in Electrocatalysis*, 315-349 (2010).

139. Alvarez, A., Borges, M., Corral-Pérez, J.J., Olcina, J.G., Hu, L., Cornu, D., Huang, R., Stoian, D., and Urakawa, A. CO_2 activation over catalytic surfaces. *ChemPhysChem* **18**, 3135-3141 (2017).

140. Whang, H.S., Lim, J., Choi, M.S., Lee, J., and Lee, H. Heterogeneous catalysts for catalytic CO_2 conversion into value-added chemicals. *BMC Chemical Engineering* **1**, 1-19 (2019).

141. Rosen, B.A., Salehi-Khojin, A., Thorson, M.R., Zhu, W., Whipple, D.T., Kenis, P.J., and Masel, R.I. Ionic liquid–mediated selective conversion of CO_2 to CO at low overpotentials. *Science* **334**, 643-644 (2011).

142. Shao, P., Yi, L., Chen, S., Zhou, T., and Zhang, J. Metal-organic frameworks for electrochemical reduction of carbon dioxide: The role of metal centres. *Journal of Energy Chemistry* **40**, 156-170 (2020).

143. Aran-Ais, R.M., Gao, D., and Roldan Cuenya, B. Structure-and electrolyte-sensitivity in CO_2 electroreduction. *Accounts of Chemical Research* **51**, 2906-2917 (2018).

144. Elhenawy, S.E.M., Khraisheh, M., AlMomani, F., and Walker, G., Metal-organic frameworks as a platform for CO_2 capture and chemical processes: Adsorption, membrane separation, catalytic-conversion, and electrochemical reduction of CO_2. Catalysts **10**, 1293-1326 (2020).

145. Rosi, N.L., Eckert, J., Eddaoudi, M., Vodak, D.T., Kim, J., O'Keeffe, M. and Yaghi, O.M. Hydrogen storage in microporous metal-organic frameworks. Science **300**, 1127-1129 (2003).

146. Gangu, K.K., Maddila, S., and Jonnalagadda, S.B. The pioneering role of metal–organic framework-5 in ever-growing contemporary applications–a review. RSC advances **12**, 14282-14298 (2022).

147. Li, H., Eddaoudi, M., O'Keeffe, M., and Yaghi, O.M. Design and synthesis of an exceptionally stable and highly porous metal-organic framework. Nature **402**, 276-279 (1999).

148. Khan, S.A. Metal-Organic Frameworks (MOFs): Synthesis, Characterization, and Potential Application. Middle East Technical University. 1-148 (2022).

149. Qiu, S., and Zhu, G. Molecular engineering for synthesizing novel structures of metal–organic frameworks with multifunctional properties. *Coordination Chemistry Reviews*, **253**, 2891-2911 (2009).

150. Tranchemontagne, D.J., Hunt, J.R., and Yaghi, O.M., Room temperature synthesis of metal-organic frameworks: MOF-5, MOF-74, MOF-177, MOF-199, and IRMOF-0. *Tetrahedron* **64**, 8553–8557 (2008).

151. San Ho, P., Chong, K.C., Lai, S.O., Lee, S.S., Lau, W.J., Lu, S.Y., and Ooi, B.S. Synthesis of Cu-BTC Metal-Organic Framework for CO_2 Capture via Solvent-free Method: Effect of Metal Precursor and Molar Ratio. *Aerosol and Air Quality Research*, **22**, 220235-220249 (2022).

152. Nobar, S.N. Cu-BTC synthesis, characterization and preparation for adsorption studies. *Materials Chemistry and Physics* **213**, 343-351 (2018).

153. O'Neill, L.D., Zhang, H., and Bradshaw, D. Macro-/microporous MOF composite beads. *Journal of Materials Chemistry* **20**, 5720-5726 (2010).

154. Kim, D., Kim, I.J., Kwon, H.T., Paeng, K., and Lee, H. CuBTC Metal–Organic Framework Decorated with FeBTC Nanoparticles with Enhance Water Stability for Environmental Remediation Applications. *ACS omega* **8**, 14900-14906 (2023).

155. Kumar, R.S., Kumar, S.S., and Kulandainathan, M.A. Efficient electrosynthesis of highly active $Cu_3(BTC)_2$-MOF and its catalytic application to chemical reduction. *Microporous and Mesoporous Materials* **168**, 57-64 (2013).

156. Kim, J., Cho, H.Y., and Ahn, W.S. Synthesis and adsorption/catalytic properties of the metal organic framework CuBTC. *Catalysis Surveys from Asia* **16**, 106-119 (2012).

157. Abednatanzi, S., Derakhshandeh, P.G., Abbasi, A., Van Der Voort, P., and Leus, K. Direct synthesis of an iridium (III) bipyridine metal–organic framework as a heterogeneous catalyst for aerobic alcohol oxidation. *ChemCatChem* **8**, 3672-3679 (2016).

158. Yang, D., Odoh, S.O., Wang, T.C., Farha, O.K., Hupp, J.T., Cramer, C.J., Gagliardi, L., and Gates, B.C. Metal–organic framework nodes as nearly ideal supports for molecular catalysts: NU-1000-and UiO-66-supported iridium complexes. *Journal of the American Chemical Society* **137**, 7391-7396 (2015).

159. Kim, D., Kang, M., Ha, H., Hong, C.S., and Kim, M. Multiple functional groups in metal–organic frameworks and their positional regioisomerism. *Coordination Chemistry Reviews* **438**, 213892-213913 (2021).

160. Wang, Z., and Cohen, S.M. Postsynthetic modification of metal–organic frameworks. *Chemical Society Reviews* **38**, 1315-1329 (2009).

161. Rusling, J.F., and Suib, S.L. Characterizing materials with cyclic voltammetry. *Advanced Materials* **6**, 922-930 (1994).

162. Sharma, S., Mehtab, S., and Zaidi, M.G. Voltammetry: An Electrochemical Analytical Method. *Chemical Sciences* **1**, 1-140 (2020).

163. Nombona, N., (2009) *Electrochemical studies of titanium, manganese and cobalt phthalocyanines*. [MSc] Rhodes university .

164. Wijeratne, K. Conducting Polymer Electrodes for Thermogalvanic Cells. *Linkoping University Electronic Press* **1971**, 1-114 (2019).

165. Hussam, A., Voltammetry: Dynamic electrochemical techniques. *Comprehensive Analytical Chemistry* **47**, 661-689 (2006).

166. Hiragond, C.B., Kim, H., Lee, J., Sorcar, S., Erkey, C., and In, S.I.Electrochemical CO_2 reduction to CO catalyzed by 2D nanostructures. *Catalysts* **10**, 98-119 (2020).

167. Kortlever, R., Shen, J., Schouten, K.J.P., Calle-Vallejo, F., and Koper, M.T. Catalysts and reaction pathways for the electrochemical reduction of carbon dioxide. *The journal of physical chemistry letters* **6**, 4073-4082 (2015).

Chapter 3: Materials and Methods

3.1 Introduction

This chapter provides information on the methods, instruments, and materials, as well as chemical inventories, that were used in the synthesis of MOFs. The MOF materials used in this study were synthesised using existing methods from literature. In this chapter, methods and procedures are thoroughly explained. The synthesised MOFs were characterised using X-ray diffraction (XRD), scanning electron microscopy (SEM), energy dispersive X-ray spectroscopy (EDX), Brunauer, Emmett, and Teller (BET), and cyclic voltammetry for electrochemical analysis.

The materials and methods section is an essential component of any formal laboratory testimony. This part deals with a comprehensive explanation of the process that was followed in completing the methodologies employed and instrumental conditions for electrochemical reduction of CO_2 using MOF catalysts. Not only does such a design aid in distributing a clear knowledge of the analytical research, but a fine explanation of the materials and methods section also serves as a set of guidelines for anybody wishing to replicate the study in the near future.

3.2 Materials

All reagents and solvents were obtained from accredited suppliers. Copper(II)acetate monohydrate ($Cu(C_2H_3O_2)_2H_2O$), benzene-1,3,5-tricarboxylic acid (C_6H_3-1,3,5-$(COOH)_3$), triethylamine ($(C_2H_5)_3N$), terephthalic acid ($C_6H_4(CO_2H)_2$), zinc acetate dihydrate ($Zn(CH_3CO_2)_2.2H_2O$), gallium(III)nitrate hydrate ($Ga(NO_3)_3H_2O$), 2,2′-bipyridine-4,4′-dicarboxylicacid or H_2bpydc ($C_{12}H_8N_2O_4$), pentamethylcyclopentadienyl iridium dichloride ($(IrCp^*Cl_2)_2$), diethyl ether or Et_2O ($(C_2H_5)_2O$), and pentane ($CH_3(CH_2)_3CH_3$), were purchased from Sigma Aldrich. N, N-Dimethylformamide or (DMF) $(CH_3)_2NC(O)H$), dichloromethane (CH_2Cl_2), methanol (CH_3OH), acetone ($(CH_3)_2CO$), tetrahydrofuran or THF ($(CH_2)_3CH_2O$), and molecular sieves were purchased from Radchem (Pty) LTD or Merck. All solvents were used without further purification, with the exception of DMF, which required distillation before use. Molecular sieves were used to dry solvents. Millipore water was used for aqueous solutions.

3.3 Instrumentation

The following instruments were used to characterise the synthesised MOFs: Fourier transform infrared spectroscopy (FT-IR), X-ray diffraction (XRD), scanning electron microscopy (SEM), energy dispersive X-ray spectroscopy (EDX), and Brunauer, Emmett, and teller (BET).

- FTIR spectroscopy was used to identify the chemical fingerprints of the MOFs. FTIR was conducted on a Bruker Alpha Fourier transform spectroscopy with platinum attenuated total reflectance (ATR) sampling accessory.
- XRD was used to study the structural characteristics of synthesised MOF materials. XRD patterns of the MOFs were obtained using Cu-K radiation (0.15418) and a Bruker D2 PHASER-e diffractometer.
- SEM was used for morphological analysis. The morphology of the MOFs was examined using a cross-beam 540 FEG SEM microscope from Zeiss at various magnifications.
- EDX was used to determine the elemental composition of the samples using a cross-beam 540 FEG SEM microscope from Zeiss.
- The BET surface area analysis was carried out using the Quantachrome (NOVAtouch NT 2LX-1, Volts 220, USA), a gas sorption analyzer operated with Quantachrome TouchWin Software Version 1.22. degassing the samples at 150 °C.

3.4 Electrochemical analysis

The electrochemical analysis of MOFs was performed using cyclic voltammetry (CV). A Versa STAT 3F potentiostat from Princeton Applied Research using Versa Studio software and utilizing the three-electrode system was used to collect the data.

The CV three-electrode system was made up of the following components:

- As a working electrode, a glassy carbon GCE with a diameter of 3 mm was used. This working electrode was modified by the drop-casting of concentrated MOF composites on the surface of the GCE.
- An Ag/AgCl wire was used as the reference electrode and
- Platinum wire as the counter electrode.

For electrochemical experiments, phosphate buffered saline (PBS) at pH 7.4 was used as the supporting analyte. The GCE was rinsed with Millipore water and polished with an alumina slurry on a Buehler felt pad prior to the experiment. The electrocatalytic reduction of MOFs was measured in an aqueous solution containing a saturated amount of the analyte.

3.5 MOF Synthesis

3.5.1 Synthesis of Copper-Benzene-1,3,5-tricarboxylate Metal Organic Framework (Cu-BTC MOF)

The Cu-BTC MOF was synthesised using a previously reported method (*1*). In a round-bottom flask, solid mixtures of copper(II)acetate monohydrate (0.725 g, 3.631 mmol) and benzene-1,3,5-tricarboxylic acid (BTC) (0.42 g, 1.998 mmol) were dissolved in 40 ml of DMF. The prepared solution was mixed and stirred thoroughly until homogeneous.

Following that, the reaction vial was tightly sealed and placed in a 140 °C oven for 24 hours. Furthermore, the sample was removed from the oven and allowed to cool at room temperature resulting in a blue precipitate. The light blue precipitate was washed three times with solvent (methanol and DMF).

The crystal was activated by immersing the light blue precipitate in methanol overnight and drying under vacuum at 140 °C to form a dark blue crystalline product (Cu-BTC MOF). Yield: 0.502 g

3.5.2 Synthesis of MOF-5 ($Zn_4O(BDC)_3$)

MOF-5 was prepared according to the method reported in the literature (*3*). In a round-bottom flask, a solid mixture of terephthalic acid (2.532 g, 15.24 mmol) was added to 200 ml of DMF. After stirring for ten minutes, 4.25 ml of triethylamine was added slowly. After that, the mixture was stirred continuously for another 20 minutes. This prepared solution mixture is the organic solution. In another round-bottom flask, zinc acetate dihydrate (8.495 g, 38.69 mmol) was dissolved in 250 ml of DMF. The zinc salt solution was gradually added to the organic solution and the resulting solution was stirred and refluxed at 120 °C for 1 hour.

The white precipitates formed were collected and filtered. The white powder (MOF-5) was washed using dichloromethane and DMF and dried overnight in a vacuum at 120 °C. Yield: 0.108 g

3.5.3 Ir(III)CP*Cl@COMOC-4 (Iridium (III)-bipyridine MOF) Synthesis

The iridium (III)-bipyridine MOF was synthesised using a previously reported method, as described in literature (5).

3.5.3.1 Synthesis of $Ga(OH)(C_{12}H_6N_2O_4)_2$•7 H_2O, (COMOC-4) (Step-I)

Solid mixtures of $Ga(NO_3)_3{\cdot}H_2O$ (1.2 g, 4.4 mmol) and H_2bpydc (1.22 g, 5 mmol) were dissolved in a two-neck round-bottom flask in 120 ml of DMF. This reaction was heated at 150 °C under reflux for 48 hours before being cooled to room temperature. By reacting resin with acetone, methanol, and DMF, an orange precipitate was formed. This resin process is repeated until no unreacted linkers remain. The orange precipitate was washed with DMF for two hours at 80 °C under reflux. The reaction mixture was washed with methanol and refluxed at 120 °C for 48 hours. Finally, at 150 °C, the yellow product, $Ga(OH)(C_{12}H_6N_2O_4)_2.7H_2O$ (COMOC-4), was vacuum dried overnight.

3.5.3.2 Modification of COMOC-4 (Step-II)

COMOC-4 was modified in the following ways: $[IrCP^*Cl_2]_2$ (0.037 g, 0.044 mmol) was added to 45 ml of dry THF in a two-necked round-bottom flask. The mixture was stirred under nitrogen (N_2) for 15 minutes to produce a clear orange solution. This solution was stirred continuously at room temperature for 20 hours with COMOC-4 (0.1 g, 0.264 mmol). The finished product, Ir(III) CP*Cl@COMOC-4, was collected and filtered. Acetone was used to clean the obtained product. Finally, the functionalized Ir(III) CP*Cl@COMOC-4 was vacuum dried overnight at 150 °C.

3.5.3.3 Synthesis of metallo-linker ($C_{22}H_{23}Cl_2IrN_2O_4$) (Step-III)

In a two-neck round-bottom flask with 60 ml of DMF, a mixture of $[IrCp^*Cl_2]_2$ (0.398 g, 0.5 mmol) and H_2bpydc (0.244 g, 1 mmol) was added. This reaction mixture was stirred at room temperature for 24 hours under nitrogen atmosphere. After 30 minutes, the mixture was added to 60 ml of diethyl ether to produce an orange-coloured solid precipitate, the metallo-linker ($C_{22}H_{23}Cl_2IrN_2O_4$). The metallo-linker was washed with pentane and diethyl ether and thereafter vacuum dried for eight hours at 150 °C.

*3.5.3.4 Synthesis of prefunctionalied Ir(III)Cp*Cl@COMOC-4 (Step-IV)*

In a two-necked round-bottom flask, solid mixtures of H_2bpydc (0.075 g, 0.31 mmol), metallo-linker (0.056 g, 0.088 mmol), and $Ga(NO_3)_3{\cdot}H_2O$ (0.096 g, 0.352 mmol) were suspended in 9.6 ml of dry DMF. This solution mixture was heated at 150 °C for 48 hours while being constantly stirred resulting in an orange precipitate. The orange precipitate was washed with methanol for 48 hours at 120 °C under N_2 atmosphere. Finally, the product was vacuum-dried to obtain pre-functionalized Ir(III)Cp*Cl@COMOC-4. Yield: 0.005 g

References

1. Nobar, S.N., Cu-BTC synthesis, characterization and preparation for adsorption studies. *Materials Chemistry and Physics* **213**, 343–351 (2018).
2. Da Silva, G.G., Machado, F.L.A., Junior, S.A., and Padron-Hernandez, E., Metal-organic framework: Structure and magnetic properties of $[Cu_3(BTC)_2(L)x.(CuO)\ y]n$ (L= H_2O, DMF). *Journal of Solid State Chemistry* **253**, 1–5 (2017).
3. Tranchemontagne, D.J., Hunt, J.R., and Yaghi, O.M., Room temperature synthesis of metal-organic frameworks: MOF-5, MOF-74, MOF-177, MOF-199, and IRMOF-0. *Tetrahedron* **64**, 8553–8557 (2008).
4. Tirmizi, S.A., Badshah, A., Ammad, H.M., Jawad, M., Abbas, S.M., Rana, U.A., and Khan, S.U.D., Synthesis of highly stable MOF-5@ MWCNTs nanocomposite with improved hydrophobic properties. *Arabian Journal of Chemistry* **11**, 26–33 (2018).
5. Abednatanzi, S., Derakhshandeh, P.G., Abbasi, A., Van Der Voort, P., and Leus, K., Direct synthesis of an iridium (III) bipyridine metal–organic framework as a heterogeneous catalyst for aerobic alcohol oxidation. *ChemCatChem* **8**, 3672–3679 (2016).

Chapter 4: Results and Discussion

4.0 Synthesis and characterization

In this study, three distinct types of metal-organic framework (MOF) materials were synthesised using the solvothermal technique in a simple, cost-effective, and highly efficient manner. The MOFs are described using chemical composition (FT-IR), structure identification (XRD), morphological analysis (SEM), elemental analysis (EDX) and surface area analysis, or textural features of surface area/pore volume (BET).

4.1 Copper Benzene-1,3,5-tricarboxylate Metal Organic Framework (Cu-BTC MOF) Synthesis and Fourier transform infrared spectroscopy (FT-IR)

The synthesis of Cu-BTC MOF was carried out in accordance with previously referenced literature (*1*), as shown in Scheme (4.1). Cu-BTC MOF was made up using copper (II) acetate monohydrate as a metal (I) and benzene-1,3,5-tricarboxylic acid (BTC) as a linker (II). These two components were mixed in DMF and methanol, and the complete reaction was carried out at 140 °C for 24 hours. A dark blue Cu-BTC MOF powder product was subsequently formed (*1*).

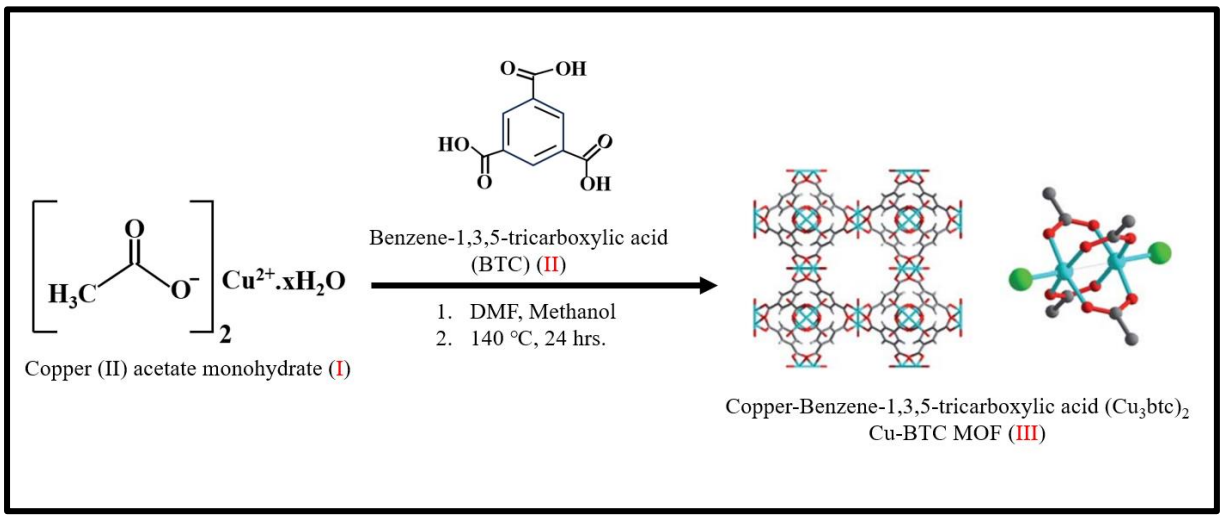

Scheme 4.1: Synthetic route to Cu-BTC MOF preparation.

Figure 4.1 shows the FT-IR spectrum of Cu-BTC. The peaks at 727 cm^{-1}, 595 cm^{-1}, 479 cm^{-1} are attributed to Cu-O stretching and vibration. The peak at 1370 cm^{-1} corresponds to C-C stretching and the peak at 1650 cm^{-1} is attributed to C=C stretching and vibration.

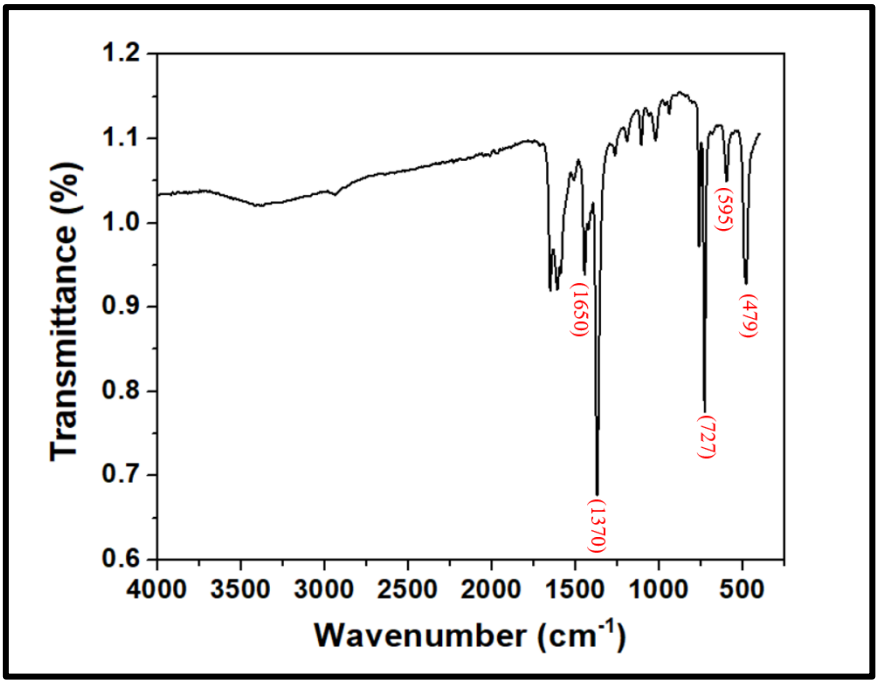

Figure 4.1: FT-IR spectra of Cu-BTC MOF

4.1.1 Powder X-ray diffraction (PXRD) of Cu-BTC MOF

The crystal structures of the Cu-BTC MOFs were investigated using XRD. Cu-BTC exhibited typical XRD patterns with characteristic diffraction peaks consistent with previous research reports (*2*, *3*). The Cu-BTC MOF diffractogram (Figure 4.2) shows peaks at 2θ = 6.8°, 9.5°, 11.6°, 13.5°, 14.9°, 16.6°, 17.5°, 19.0°, 20.2°, 24.1°, 25.9°, 29.3°, 35.3°, and 39.1° corresponding to the crystal planes (200), (220), (222), (400), (420), (422), (511), (440), (442), (551), (731), (751), (773), and (882), respectively.

The obtained intensities and the represented peak locations correlate well with known data and literature. The data includes Cambridge crystallographic information data with deposit number 112954, JCPDS-card file number 05-661, and reported literature (*2*, *3*). The synthesised Cu-BTC MOFs also show high crystallinity. The occurrence of this discovery is supported by the demonstration of sharper diffraction peaks, which is consistent with previous studies (*2*). Moreover, Figure 4.2 displayed a large number of tiny peaks in the 35°–45° range, which could be signs of trace amounts of CuO, Cu_2O, and Cu (*1*, *4*). All of the aforementioned data show that the experimental XRD pattern and the published ones (*1*, *5*) are similar.

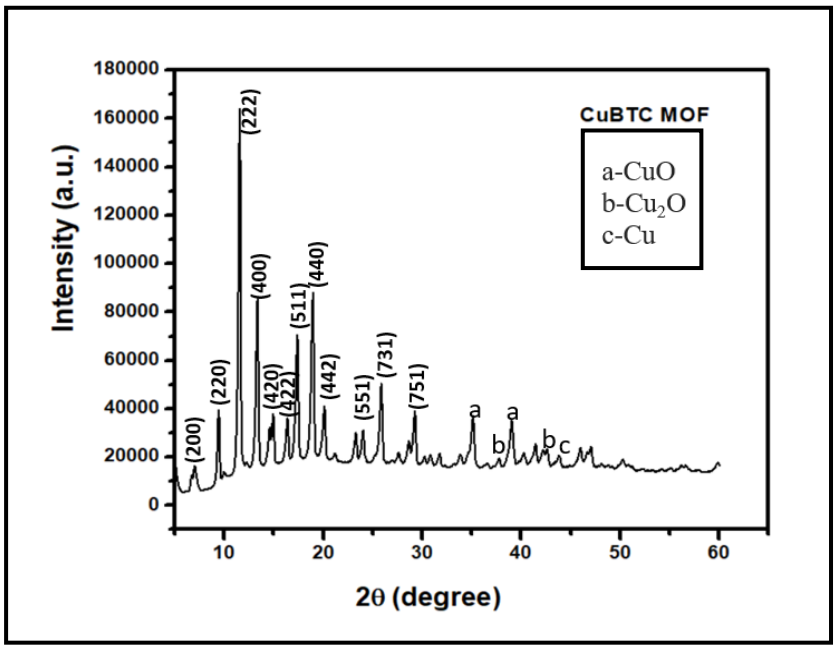

Figure 4.2: Diffractogram of synthesized Cu-BTC MOF.

4.1.2 Scanning electron microscopy (SEM) and energy dispersive X-ray spectroscopy (EDX) of Cu-BTC MOF

The morphology of the synthesized Cu-BTC MOF was investigated using SEM. Figure 4.3(a) depicts the SEM image of Cu-BTC MOF. The image shows small, irregularly shaped Cu-BTC MOF crystals, along with larger crystals that have a smooth surface and an almost cubo-octagonal shape similar to previous reports (*6, 7*). In the early stages of the reaction, the small Cu-BTC MOF crystals were formed. As the reaction time increased, copper ions in the solution became depleted. As a result, some of the small Cu-BTC MOF crystals dissolved providing a source of cupper ions for the growth of new and larger Cu-BTC MOF crystals (*8*).

The EDX spectrum was used to confirm the elemental composition of Cu-BTC MOF. The compounds were coated with carbon prior to examination. Hydrogen is too light for the equipment to detect during the examination, but oxygen may be detected from the environment. The interest was in the atomic mass of the cupper element. According to Figure 4.3(b), the material has a cupper composition of 26.2%, which is in agreement with previous research (*9*).

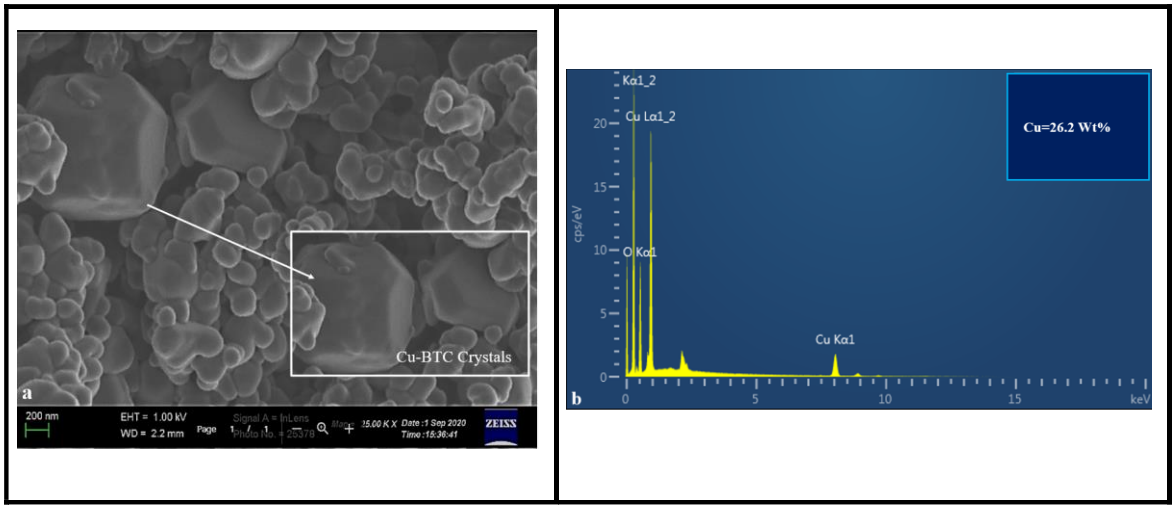

Figure 4.3: Cu-BTC MOF (a) SEM image and (b) EDX spectrum

4.2 Synthesis and FT-IR analysis of MOF-5

The schematic representation for the synthesis of MOF-5 is shown in Scheme 4.2. MOF-5 was synthesised following the described procedure in literature (*10*) using zinc acetate dihydrate as a metal source and terephthalic acid (II) as a linker. A white precipitate formed from the clear solution after the solvothermal process. The temperature and reaction time are known to affect the final MOF-5 product as higher surface areas are observed for MOF-5 produced at lower temperatures and slow reaction times. In this work, MOF-5 was synthesized at 120 °C for 1 hour using the solvothermal method. MOF-5 can be produced at room temperature however; this usually requires the use of a base to deprotonate the organic linker in order to precipitate MOF-5.

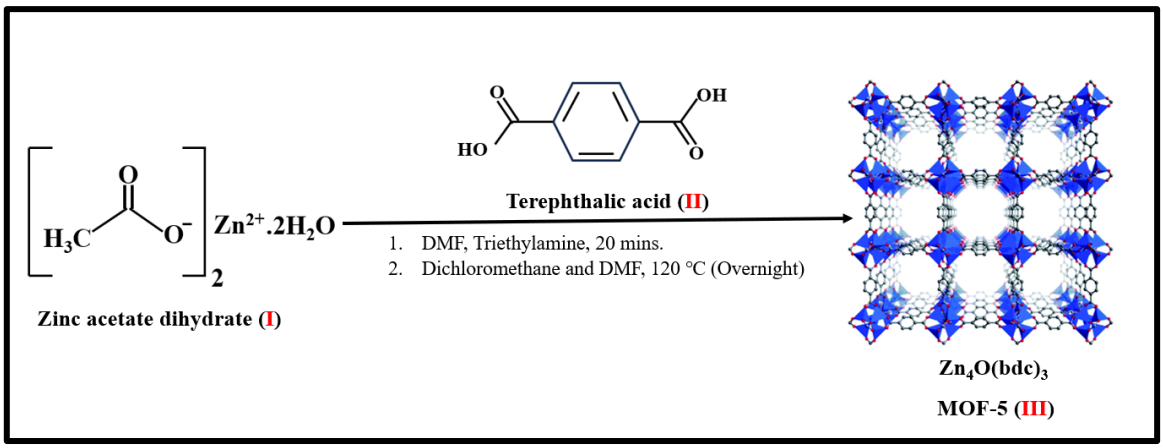

Scheme 4.2: Synthetic route to MOF-5 preparation

Figure 4.4 displays the FT-IR spectrum of MOF-5. The peak at 463 cm^{-1} is due to Zn-O stretching. The peaks at 747 cm^{-1} and 885 cm^{-1} are due to C-H vibrations of the benzene ring. Peaks at 1382 cm^{-1} and 1587 cm^{-1} are attributed to the asymmetric and symmetric stretching of the carboxylate groups.

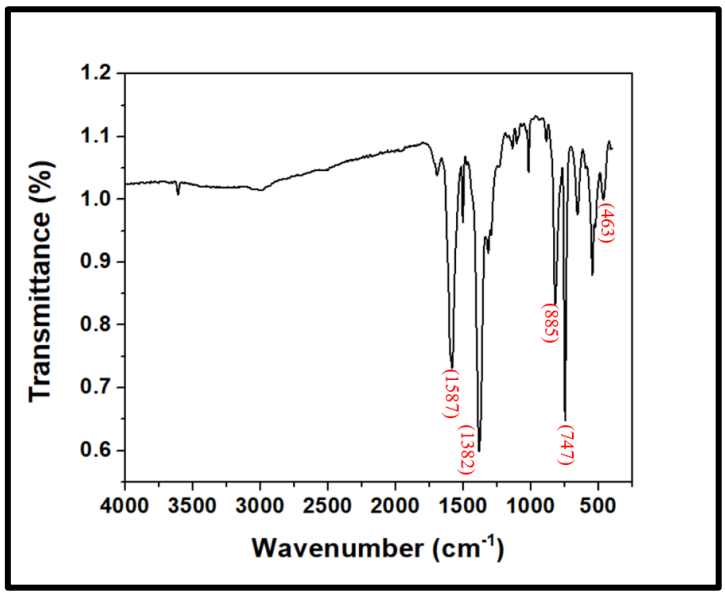

Figure 4.4: FT-IR of MOF-5

4.2.1 Powder X-ray diffraction (PXRD) of MOF-5

The MOF-5 crystal structures were subjected to XRD investigation. According to previously published research literature (*11, 12*), MOF-5 demonstrated typical XRD patterns and diffraction peaks as shown in Figure 4.5. Peaks at positions 6.8°, 9.6°, 13.8°, and 15.8° correspond to the crystal planes (200), (220), (400), and (420) respectively. The synthesised MOF-5 material show good crystallinity, as evidenced by the sharp diffraction peaks (*11, 12*).

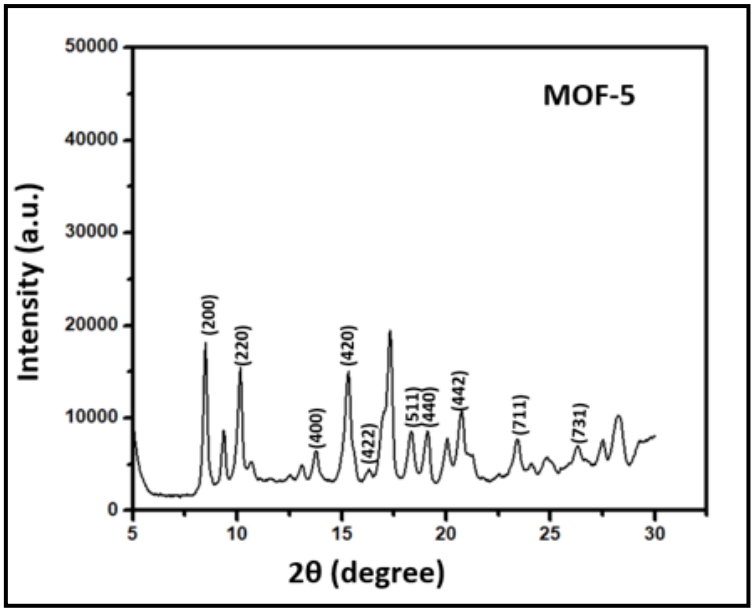

Figure 4.5: Diffractogram of synthesized MOF-5

4.2.2 Scanning electron microscopy (SEM) and energy dispersive X-ray spectroscopy (EDX) of MOF-5

A scanning electron microscope (SEM) was used to analyse the morphology of the synthesised MOF-5. Figure 4.6 (a) shows the SEM image of MOF-5 at three different scales: 3µ m, 1µm, and 200 nm. The figure depicts MOF-5 having a flat smooth surface with a cube morphology. Similar results have been previously reported for MOF-5 (*13, 14*). The elemental composition was confirmed using the EDX spectrum. The examination of zinc concentration was the major emphasis. According to the EDX study, MOF-5 contained 35.86% Wt. of zinc, figure 4.6 (b). The zinc content is similar to previous findings for MOF-5 (*15*).

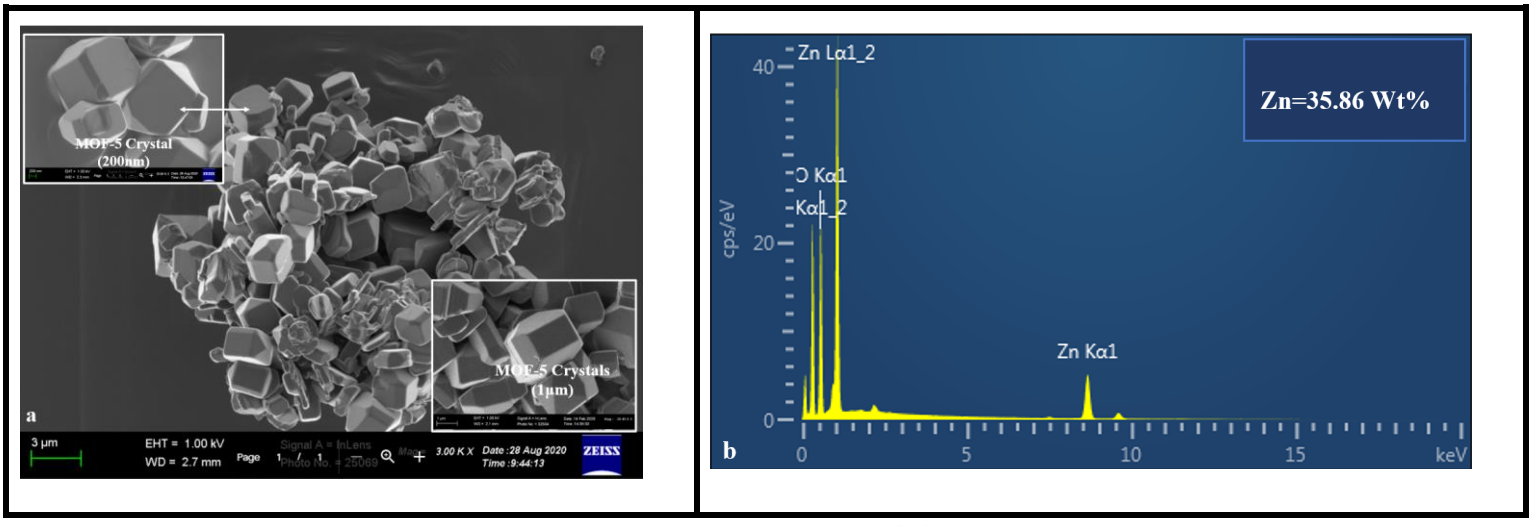

Figure 4.6: MOF-5 (a) SEM images and (b) EDX spectrum

4.3 Ir(III)CP*Cl@COMOC-4 (Iridium (III)-bipyridine MOF) Synthesis and FT-IR analysis

The synthesis of iridium (III)-bipyridine MOF was done following previously reported literature (*16*). The Ir-based MOF was completed in two steps: functionalized (I) and pre-functionalized (II) steps. The schematic synthetic process for Ir(III)Cp*Cl@COMOC-4 (functionalized) is shown in scheme 4.3 (a). This step results in the formation of COMOC-4, a 1D microporous gallium-based framework. During this step, an orange precipitate was formed instead of a green precipitate as reported in the literature. The complex arrangement can result in a blue, green or light orange compound as has been reported for Ga complexed with pyridine-based ligands (*17-18*). The next step, shown in scheme 4.3(b), immobilizes $[IrCp^*Cl_2]_2$ onto the COMOC-4 framework to form the pre-functionalized (Ir(III)Cp*Cl@COMOC-4)(II). This occurs due to the bipyridine functionalities of the H_2bpydc linker being on the COMOC-4 pore walls, which allows for coordination with a second metal. This synthesis is very challenging as decomposition of COMOC-4 can occur under the applied reaction conditions. An orange precipitate formed, deviating from the expected green colour reported in the literature. This discrepancy likely arises from variations in the coordination complex arrangement, which can result in blue, green, or light orange products.

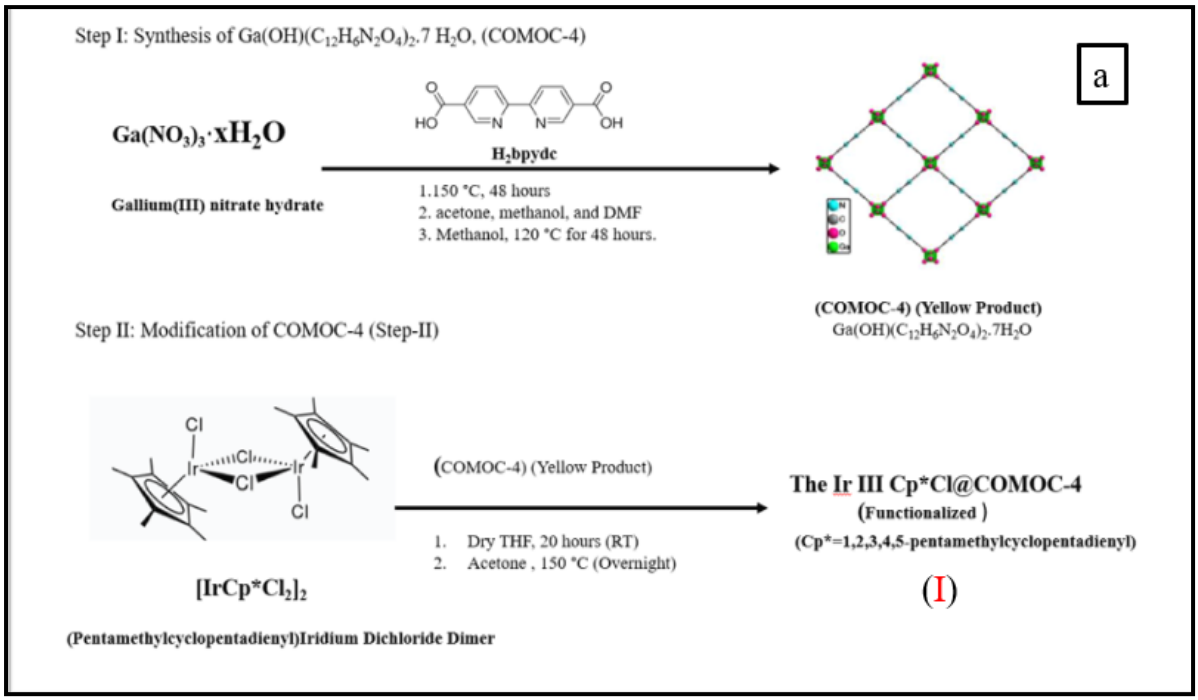

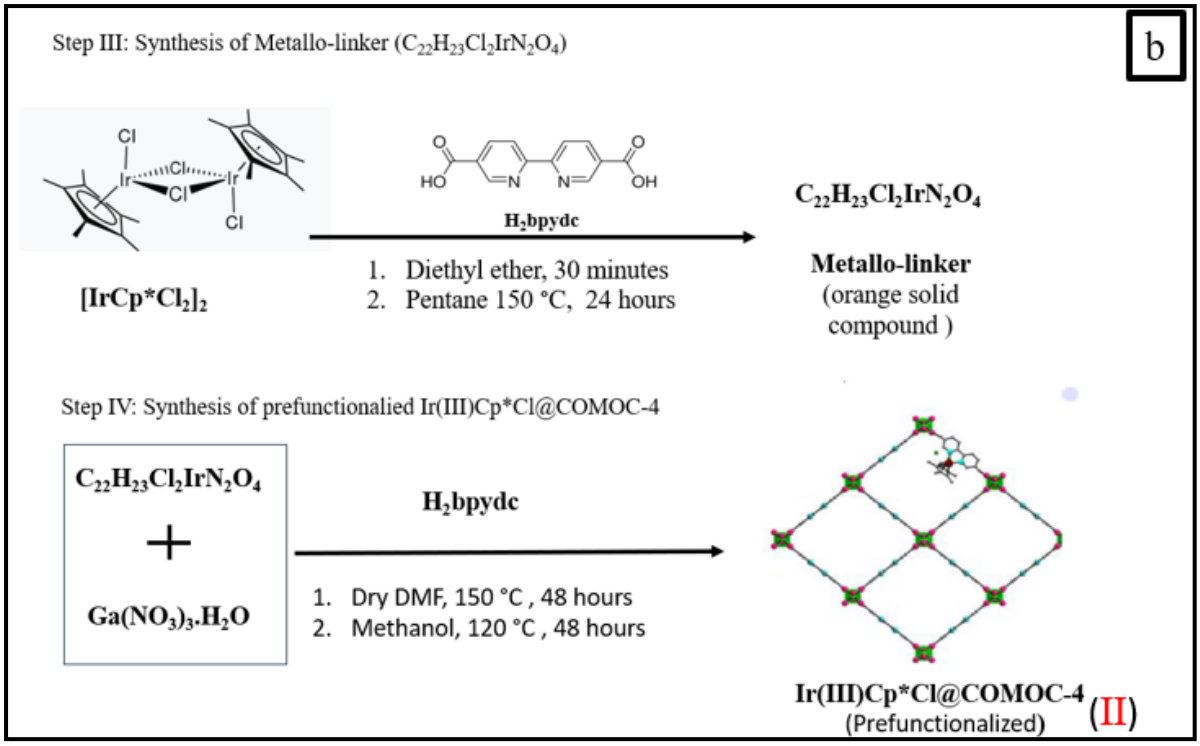

Scheme 4.3: Synthetic route of Ir(III)Cp*Cl@COMOC-4 (Iridium (III)-bipyridine MOF) (16)

Figure 4.7 depicts the FT-IR spectrum of the Ir-based MOF. The Ir-N and Ir-Cl stretching vibrations are expected in the far IR region between 190-260 cm^{-1} that are outside the limits of the instrument. Peaks between 1155 cm^{-1} and 707 cm^{-1} are attributed to aromatic C-H stretching. The peak at 1365 cm-1 is due to aromatic C=C stretching.

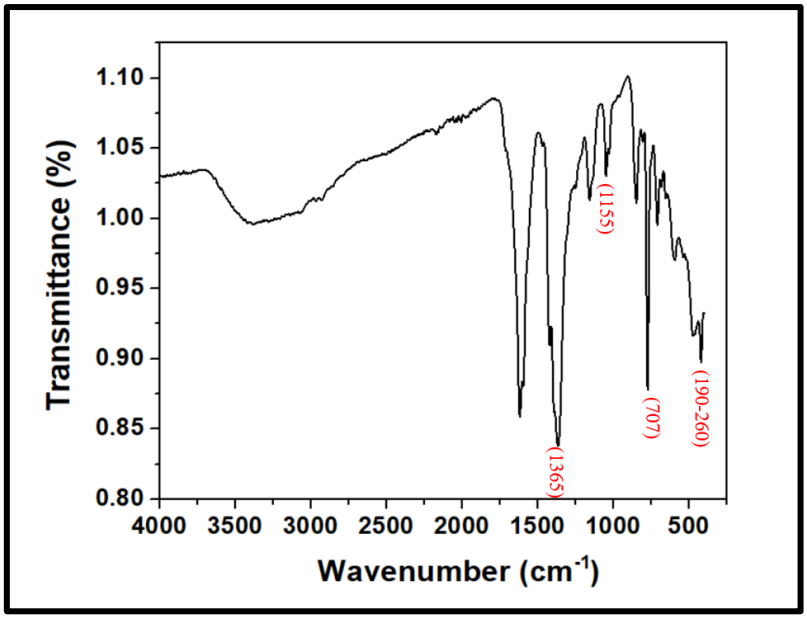

Figure 4.7: FT-IR of Ir(III)Cp*Cl@COMOC-4 MOF

4.3.1 Powder X-ray diffraction (PXRD) of Ir(III)Cp*Cl@COMOC-4 MOF

The XRD diffraction pattern for Ir(III)Cp*Cl@COMOC-4 is shown in Figure 4.8 and is similar to previous reports (*16*). This indicates that the Ir(III)Cp*Cl@COMOC-4 structure remained intact post modification.

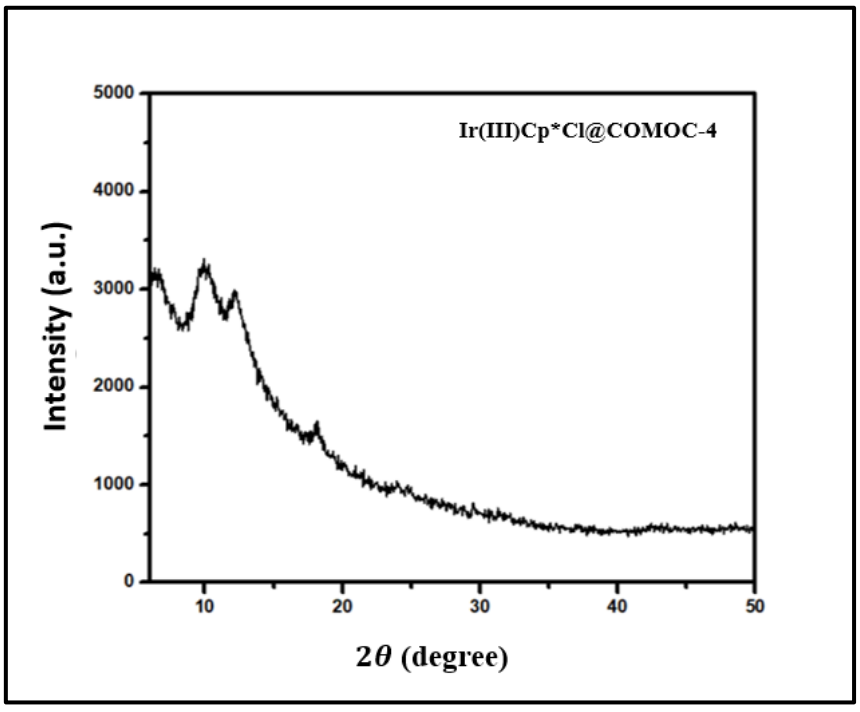

Figure 4.8: Diffractogram of Ir(III)Cp*Cl@COMOC-4

4.3.2 Scanning electron microscopy (SEM) and energy dispersive X-ray spectroscopy (EDX) of Ir(III)Cp*Cl@COMOC-4 MOF

Figure 4.9 (a) shows the SEM image of Ir(III)Cp*Cl@COMOC-4 MOF. The MOF has irregularly shaped crystals with visible pores on the surface as seen on the magnified view of the crystal. EDX spectrum was used to confirm the elemental composition of Ir(III)Cp*Cl@COMOC-4 MOF. The analysis shows that Ir(III)Cp*Cl@COMOC-4 MOF contains 5.0% wt. iridium and 4.1% wt. gallium, Figure 4.9 (b). The gallium proportion is due to the fact that Ir(III)Cp*Cl@COMOC-4 is a Ga-based MOF.

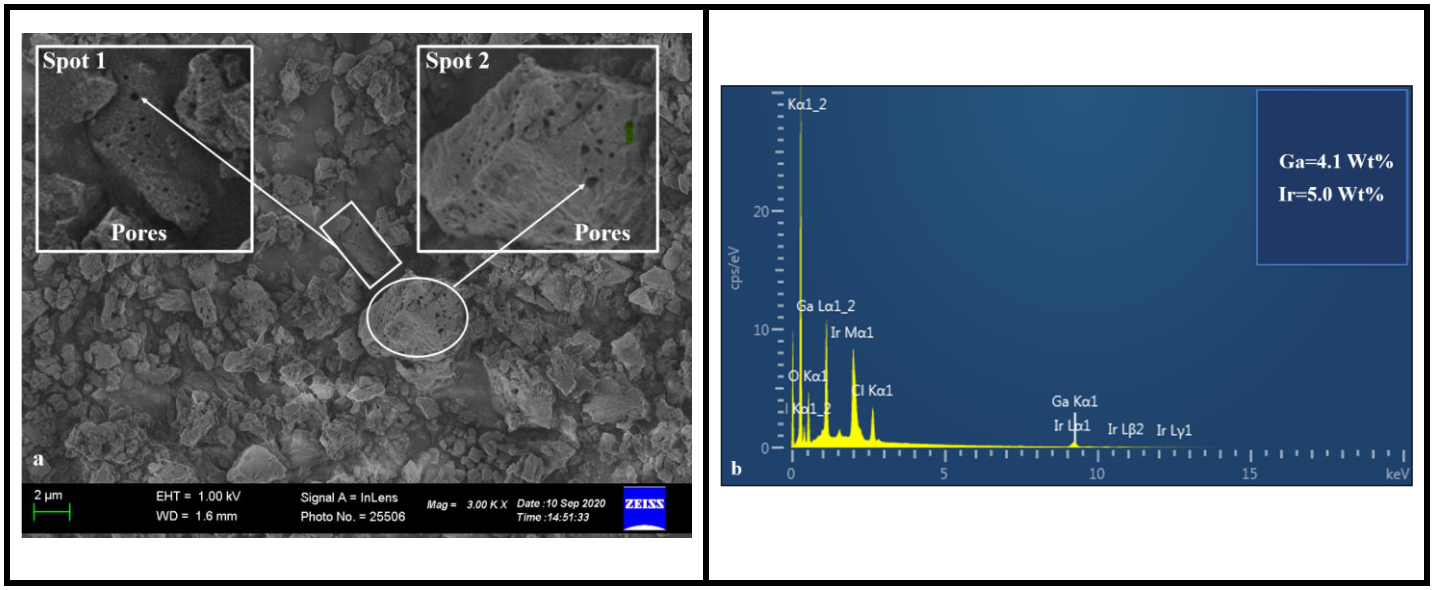

Figure 4.9: (a) SEM image and (b) EDX spectrum of Ir(III)Cp*Cl@COMOC-4 MOF

4.4 Brunaeur Emmett Teller (BET) analysis

The porosity of materials is a crucial parameter in catalytic applications. The pore volume and specific surface area of the three synthesized MOFs (Cu-BTC MOF, MOF-5, and Ir(III)Cp*Cl@COMOC-4 MOF) were analysed using BET. Cu-BTC MOF showed a surface area and pore volume of 634 m^2/g and 0.21 cc/g, respectively, whereas MOF-5 had a surface area and pore volume of 631 m^2/g and 0.22 cc/g, respectively. The results of this investigation support those of earlier research (*1*, *11*, *20*). Ir(III)Cp*Cl@COMOC-4 MOF exhibited a surface area of 272 m^2/g and a pore volume of 0.17 cc/g. The relatively low surface area is expected given the presence of the Ir complex on the pore walls. Nevertheless, compared to the previously published MOF (*16*), the synthesised MOF, Ir(III)Cp*Cl@COMOC-4, has a

smaller surface area. The surface characteristics of the three MOFs as confirmed by the BET study are summarised in Table 4.1.

Table 4.1: BET surface area and porosity measurements of Cu-BTC MOF, MOF-5, and Ir(III)Cp*Cl@COMOC-4 MOF.

Materials	**Specific surface area m^2/g**	**Pore volume cc/g**
Cu-BTC MOF	634	0.21
MOF-5	631	0.22
Ir(III)Cp*Cl@COMOC-4 MOF	272	0.17

The N_2 adsorption isotherms for Cu-BTC MOF (Figure 4.10(a)) and MOF-5 (Figure 4.10(c)) show a type II isotherm profile with an H_4 hysteresis loop. Type II N_2 adsorption isotherms is a feature for microporous materials. Furthermore, the Type H_4 hysteresis loop is caused by slit-shaped pores arising from particles of irregular shape with a broad pore size distribution (*21-22*). The SEM image confirmed the irregular shape of the Cu-BTC MOF. While most of the crystals were cubic, some of the MOF-5 crystals showed irregular shapes. The Ir(III)Cp*Cl@COMOC-4 MOF, shown in figure 4.10 (e) exhibits a type III isotherm with an H_3 hysteresis loop. These features imply a microporous material with non-rigid aggregates forming slit shaped pores (*21-23*). The microporous nature of this MOF is attributed to its parent compound, COMO-4 and the SEM image of this MOF revealed aggregates with irregular shapes.

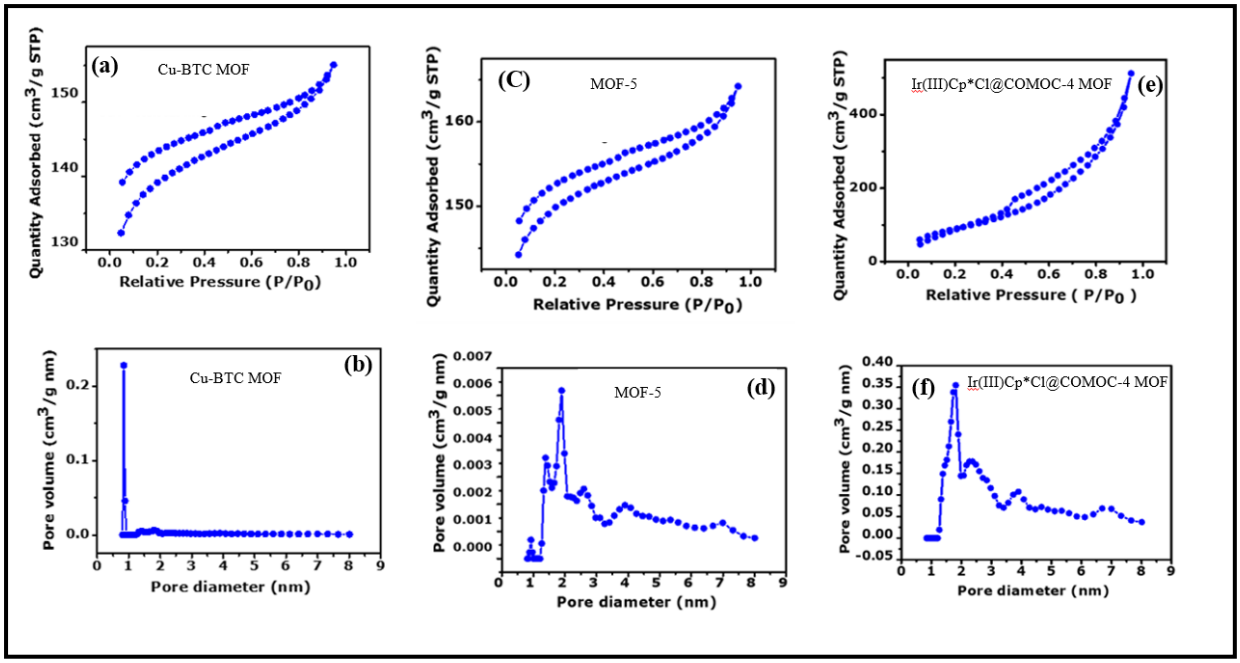

Figure 4.10: Adsorption isotherms of (a) Cu-BTC MOF, (c) MOF-5, (e) Ir(III)Cp*Cl@COMOC-4 MOF, and pore size distribution of (b) Cu-BTC MOF, (d) MOF-5, and (f) Ir(III)Cp*Cl@COMOC-4 MOF.

References

1. Nobar, S.N., Cu-BTC synthesis, characterization and preparation for adsorption studies. *Materials Chemistry and Physics* **213**, 343–351 (2018).
2. Da Silva, G.G., Machado, F.L.A., Junior, S.A., and Padrón-Hernández, E. Metal-organic framework: Structure and magnetic properties of $[Cu_3(BTC)_2(L)x\cdot(CuO)y]n$ (L= H_2O, DMF). *Journal of Solid-State Chemistry* **253**,1-5 (2017).
3. Kaur, R., Kaur, A., Umar, A., Anderson, W.A., and Kansal, S.K. Metal organic framework (MOF) porous octahedral nanocrystals of Cu-BTC: Synthesis, properties and enhanced adsorption properties. *Materials Research Bulletin* **109**, 124-133 ((2019).
4. Holder, C.F. and Schaak, R.E. Tutorial on powder X-ray diffraction for characterizing nanoscale materials. *Acs Nano* **13**, 7359-7365 (2019).
5. Cheng, J., Xuan, X., Yang, X., Zhou, J., and Cen, K. Preparation of a Cu(BTC)-rGO catalyst loaded on a Pt deposited Cu foam cathode to reduce CO_2 in a photoelectrochemical cell. *RSC Advances* **8**, 32296-32303 (2018).
6. Kar, A.K., and Srivastava, R. An efficient and sustainable catalytic reduction of carbon–carbon multiple bonds, aldehydes, and ketones using a Cu nanoparticle decorated metal organic framework. *New Journal of Chemistry* **42**, 9557-9567 (2018).
7. Peng, M.M., Jang, H.T., and Palanichamy, M. Selective Oxidation of Ethylbenzene over Transition Metal Organic Framework Cu-BTC. *International Journal of Control and Automation* **6**, 1-12 (2013).
8. Qu, Z.G., Wang, H., and Zhang, W., Highly efficient adsorbent design using a Cu-BTC/CuO/carbon fiber paper composite for high CH_4/N_2 selectivity. *Rsc Advances*, **7**, 14206-14218 (2017).
9. Nivetha, R., Sajeev, A., Paul, A.M., Gothandapani, K., Gnanasekar, S., Bhardwaj, P., Jacob, G., Sellappan, R., Raghavan, V., Pitchaimuthu, S., and Jeong, S.K. Cu based Metal Organic Framework (Cu-MOF) for electrocatalytic hydrogen evolution reaction. *Materials Research Express* **7**, 114001- 114013 (2020).
10. Tranchemontagne, D.J., Hunt, J.R., and Yaghi, O.M., Room temperature synthesis of metal-organic frameworks: MOF-5, MOF-74, MOF-177, MOF-199, and IRMOF-0. *Tetrahedron* **64**, 8553–8557 (2008).

11. Zhao, H., Song, H., and Chou, L. Nickel nanoparticles supported on MOF-5: Synthesis and catalytic hydrogenation properties. *Inorganic Chemistry Communications* **15**, 261-265 (2012).
12. Yang, H.M., Xian, L.I.U., Song, X.L., Yang, T.L., Liang, Z.H., and Fan, C.M. In situ electrochemical synthesis of MOF-5 and its application in improving photocatalytic activity of BiOBr. *Transactions of Nonferrous Metals Society of China* **25**, 3987-3994 (2015).
13. Greer, H.F., Liu, Y., Greenaway, A., Wright, P.A. and Zhou, W. Synthesis and formation mechanism of textured MOF-5. *Crystal Growth & Design* **16**, 2104-2111 (2016).
14. Mulyati, T.A., Ediati, R. and Rosyidah, A. Influence of solvothermal temperatures and times on crystallinity and morphology of MOF-5. *Indonesian Journal of Chemistry* **15**, 101-107 (2015).
15. Mulyati, T.A., Ediati, R. and Nadjib, M. Optimization of reaction conditions for synthesis of mof-5 using solvothermal method. *IPTEK Journal of Proceedings Series* **1**, 1-6 (2015).
16. Abednatanzi, S., Derakhshandeh, P.G., Abbasi, A., Van Der Voort, P., and Leus, K., Direct synthesis of an iridium (III) bipyridine metal–organic framework as a heterogeneous catalyst for aerobic alcohol oxidation. *ChemCatChem* **8**, 3672–3679 (2016).
17. Rendošová, M., Gyepes, R., Sovová, S., Sabolová, D., Vilková, M., Olejníková, P., Kello, M., Lakatoš, B., Vargová, Z., Ga(III) pyridinecarboxylate complexes: potential analogues of the second generation of therapeutic Ga(III) complexes? *Journal of Biological Inorganic Chemistry* **28**, 591-611 (2023).
18. Verderi, L., Scaccaglia, M., Rega, M., Bacci, C., Pinelli, S., Pelosi, G., Bisceglie, F., New Stable Gallium(III) and Indium(III) Complexes with Thiosemicarbazone Ligands: A Biological Evaluation. *Molecules* 29, 497-511 (2024).
19. Liu, Y., Ghimire, P., and Jaroniec, M. Copper benzene-1, 3, 5-tricarboxylate (Cu-BTC) metal-organic framework (MOF) and porous carbon composites as efficient carbon dioxide adsorbents. *Journal of colloid and interface science* **535**, 122-132 (2019).
20. Mirkovic, I., Lei, L., Ljubic, D., and Zhu, S. Crystal growth of metal–organic framework-5 around cellulose-based fibers having a necklace morphology. *ACS omega* **4**, 169-175 (2019).

21. Rahman, M.M., Shafiullah, A.Z., Pal, A., Islam, M.A., Jahan, I., and Saha, B.B. Study on optimum IUPAC adsorption isotherm models employing sensitivity of parameters for rigorous adsorption system performance evaluation. *Energies* **14**, 7478-7495 (2021).
22. Donohue, M.D., and Aranovich, G.L. Classification of Gibbs adsorption isotherms. *Advances in colloid and interface science* **76**, 137-152 (1998).
23. Xu, L., Zhang, J., Ding, J., Liu, T., Shi, G., Li, X., Dang, W., Cheng, Y., and Guo, R. Pore structure and fractal characteristics of different shale lithofacies in the dalong formation in the western area of the lower yangtze platform. *Minerals* **10**, 1-26 (2020).

Chapter 5 Electrocatalytic Reduction of CO_2

5.1 Introduction

Electrochemistry, studies the conversion of chemical energy to electrical energy and vice versa. Electrocatalysis is the process of accelerating electrochemical processes and lowering activation energy with a catalyst. This brings reactions closer to thermodynamic equilibrium. In the catalytic process shown in Figure 5.1, a catalyst (O) is reduced (R) on the electrode surface and interacts with a substrate (S) to generate a product (P) (*1-4*).

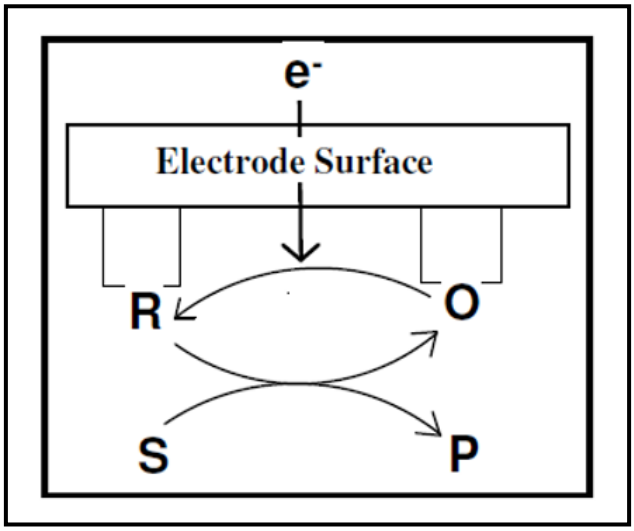

Figure 5.1: A schematic representation of electrocatalysis (*2*).

5.2 Electrochemical Methods

In this work, the synthesized MOFs were analysed using cyclic voltammetry (CV) in 2M phosphate buffer solution at pH 7.4, using a three-electrode electrochemical setup. Before modification, the bare glassy carbon electrode (GCE) was washed with Millipore water and polished using an alumina slurry on a polishing pad. The GCE was modified with MOFs using the drop-dry technique as shown in Figure 5.2. A suspension of the synthesised MOF was made by diluting in a designated solvent: DMF for Cu-BTC MOF and MOF-5, and methanol for Ir(III)Cp*Cl@COMOC-4 MOF. The shiny surface of the GCE was uniformly covered with the MOF suspension and dried at 100 °C. Cyclic voltammetry was used to investigate the electro-reduction of CO_2 using the modified electrode (*5*).

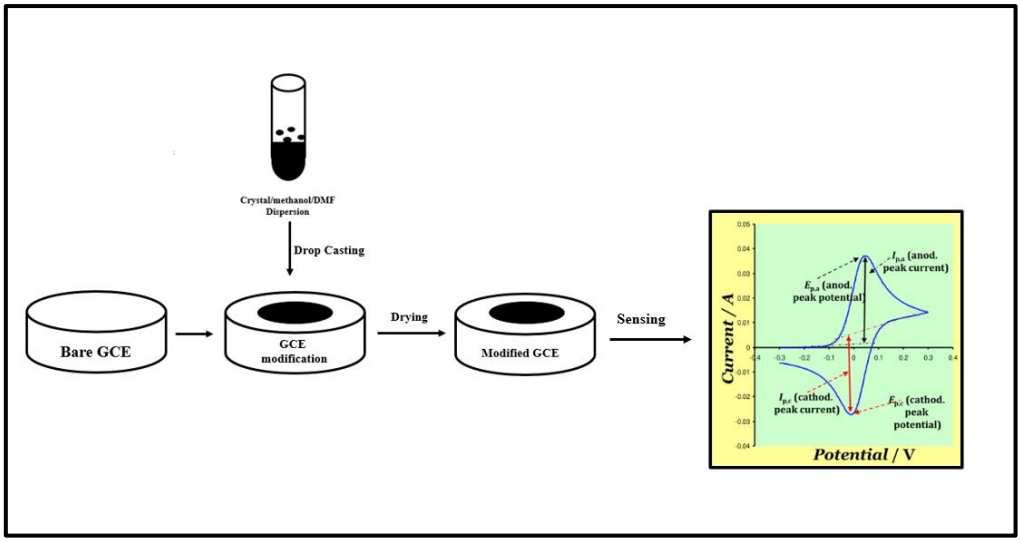

Figure 5.2: Drop drying method for electrode modification.

5.4 Electrochemical characterisation of synthesized metal organic frameworks

The redox properties of the MOFs where examined using CV in buffer solution. Figure 5.3a shows the cyclic voltammogram of MOF-5 coated GCE on a wide rage potential window (-1 V to +1 V). An irreversible reduction peak at ~ -0.5 V vs Ag|AgCl could be due to a ligand reduction process. Figure 5.3b shows the Cu-BTC modified GCE. Prominent peaks are observed as a result of the reduction of Cu(II) to Cu (I) at ~ 0.0 V and ~ +0.1 V vs Ag|AgCl. The oxidation peak at ~ +0.0 V vs Ag|AgCl is due to Cu-BTC MOF adsorption. A second reduction peak at ~ -0.4 V vs Ag|AgCl is due to the reduction of Cu (I). Figure 5.3c displays the Ir-MOF modified GCE. A faint reduction peak at ~ -0.5 V vs Ag|AgCl was observed (asterisk) and is possibly due to Ir reduction, which can only be confirmed using spectroelectrochemistry.

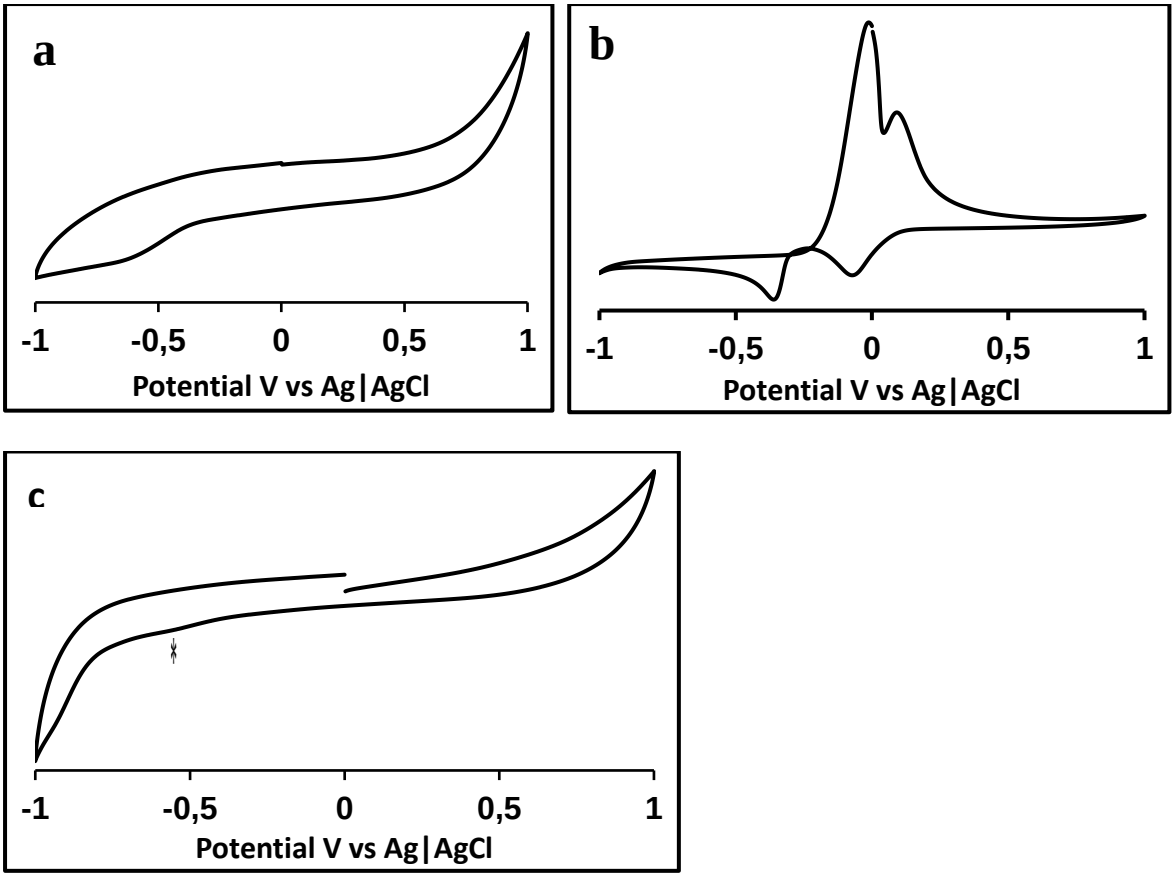

Figure 5.3: Cyclic voltammograms of (a) MOF-5-modified GCE (b) Cu-BTC MOF-modified GCE, and (c) Ir(III)Cp*Cl@COMOC-4 MOF-modified GCE in PBS. Scan rate 0.1 V/s.

5.5 Electrochemical reduction of CO_2

Understanding the modified electrode's response CO_2 reduction was the focus of this work. It was essential to use Ar or N_2 gas to purge the electrolyte solution before performing the experiments in order to remove oxygen. This step is crucial because any oxygen that remains in the solution might react within the potential window of study, which could affect the results. To overcome the -1.9 V barrier for CO_2 reduction, a $*CO_2^-$ intermediate is initially formed during the reduction process. This allows for further hydrogenation through different reaction pathways ultimately producing products like CO when two electrons are transferred.

For CO_2 reduction, cyclic voltammograms were recorded on modified MOF electrodes, covering a range from 0 V to -1 V (Figure 5.4).

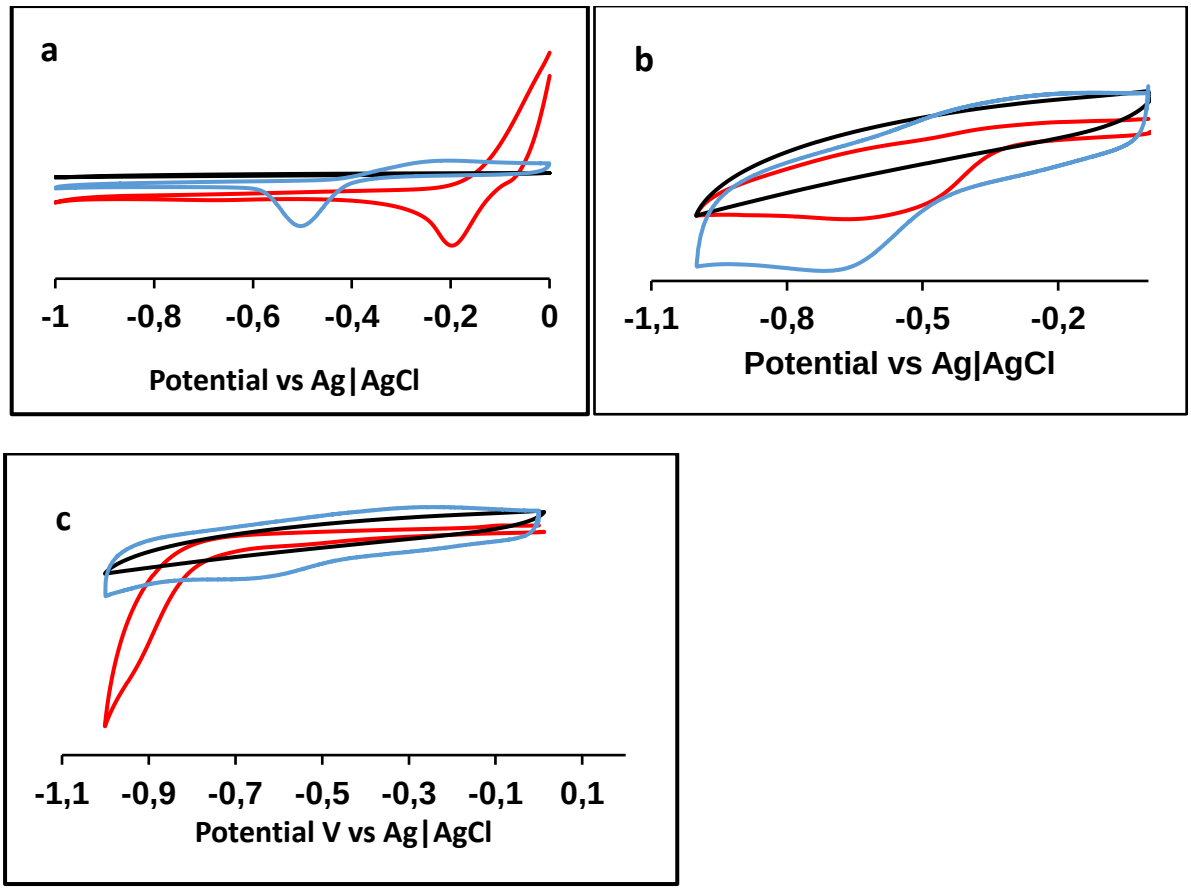

Figure 5.4: Cyclic voltammograms of bare GCE (black), (a) Cu-BTC MOF-modified GCE, (b) MOF-5-modified GCE and (c) Ir(III)Cp*Cl@COMOC-4 MOF-modified GCE in CO_2 saturated PBS (blue) and in PBS without CO_2 (red). Scan rate 0.1 V/s.

The catalytic responses from the CV's are shown in Table 5.1. In the presence of CO_2, the Cu-BTC MOF modified electrode (Figure 5.4a) shows a reduction peak at -473mV and an oxidation peak at -172mV. These peak potentials are that of copper, which confirm the deposition of CuBTC MOF on the electrode surface. However, the peak potentials have shifted when compared to potentials in the absence of CO_2. This shows that the MOF has catalytic active sites that are exposed for easy CO_2 adsorption which facilitates the interfacial reaction. Adsorption of CO_2 on Cu-BTC MOF immobilised on electrodes has been reported (*6*). The MOF-5 modified GCE (Figure 5.4b) shows a reduction peak at -684mV in the presence of CO_2. This peak is shifted and is at higher currents compared to the peak in the absence of CO_2. The peak shift is proof of CO_2 adsorption. The porous nature and the high surface area of the MOF contribute to increased currents. Zinc based MOFs have been reported to prefer the production of CO (*7*) via a two-electron reduction process. The Ir(III)Cp*Cl@COMOC-4 MOF modified GCE (Figure 5.4c) shows a peak at -297mV in the presence of CO_2 which not observed without

CO_2 confirming adsorption. To determine the products formed during the CO_2 reduction experiments a specialised electrochemical equipment (Differential electrochemical mass spectrometry) is required to determine the mass of the products produced.

Table 5.1: Electrochemical parameters for MOF modified GCEs in the reduction of CO_2.

Electrode	Epa (mV)	Epc (mV)	ΔEp (mV)	$E_{1/2}$	I_{pa}/i_{pc}
Cu-BTC MOF	-172.06	-473.92	-301.86	-323.99	-0.562
MOF-5	-279.71	-685.79	-406.08	-482.75	-0.372
Ir(III)Cp*Cl@COMOC-4 MOF	-238.00	-297.20	-228.58	-123.71	-0.539

Figure 5.5 was used for Randles-Sevcik analysis. The figure shows an increase in peak currents with increasing scan rate. This resulted in the plot of peak current versus the square root of the scan rate as shown in Figure 5.6. The linear trend indicate that the electrochemical process was diffusion controlled.

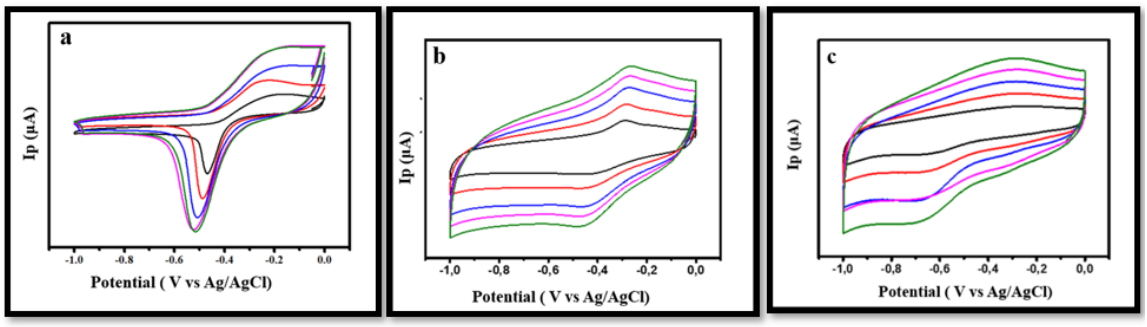

Figure 5.5: Effect of scan rate on CO_2 reduction on GCE modified with (a) Cu-BTC MOF, (b) MOF-5 and (c) Ir(III)Cp*Cl@COMOC-4 MOF in 0.2 M phosphate buffer (pH 7.4)

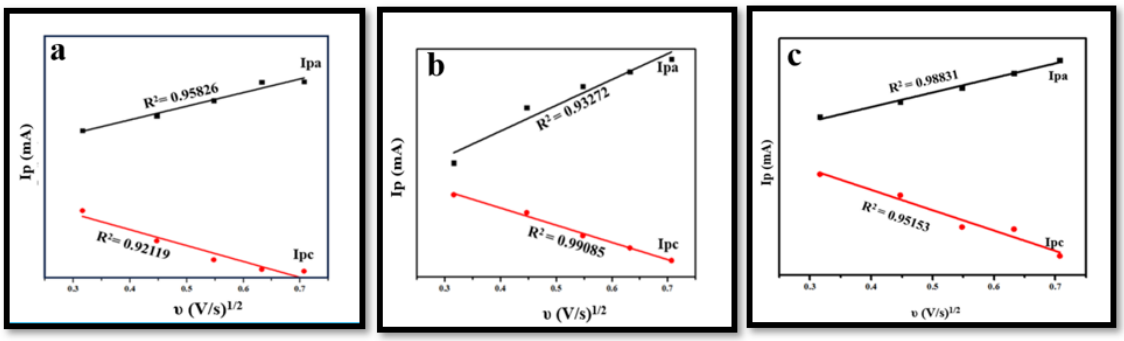

Figure 5.6: Peak current versus square root of scan rate for CO_2 reduction on (a) Cu-BTC MOF-modified GCE, (b) MOF-5-modified GCE, and (c) Ir(III)Cp*Cl@COMOC-4 MOF-modified GCE in CO_2 saturated 0.2 M phosphate buffer pH 7.4.

Further analyses of CO_2 electrocatalytic reduction was done using Equation 5.1 for an irreversible process

$$E_p = \frac{2.3RT}{2(1-\alpha)n_\alpha F} \log \upsilon + K = \frac{b}{2}\log \upsilon + K \qquad 5.1$$

where α is the transfer coefficient, n_α is the number of electrons involved in the rate determine step, υ is the scan rate, K is a constant, R is the gas constant, T is the temperature, F is Faraday's constant, Ep is the peak potential and b is the Tafel slope.

The Tafel slope is an indication of the activation energy of the reaction, as the slope becomes steeper; the activation energy required for the reaction to occur increases, resulting in a slower reaction rate (*8-10*). Tafel slopes determined from Figure 5.7 for Cu-BTC, MOF-5 and Ir(III)Cp*Cl@COMOC-4 modified GCE electrodes were calculated to be 169.97 mV/decade, 256.04 mV/decade, and 135.96 mV/decade respectively. These Tafel slopes suggest weak substrate-catalyst interaction.

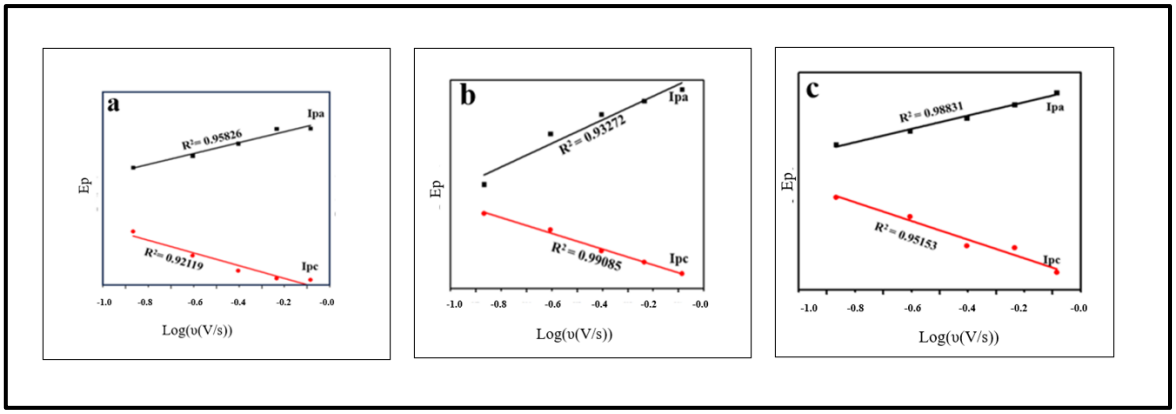

Figure 5.7: Peak potential vs log ν for the electroreduction of CO_2 on (a) Cu-BTC MOF-modified GCE, (b) MOF-5-modified GCE and (c) Ir(III)Cp*Cl@COMOC-4 MOF-modified GCE (c) in 0.2 M phosphate buffer pH 7.4.

It is concluded that all three MOFs (Cu-BTC, MOF-5, and Ir(III)Cp*Cl@COMOC-4) have potential as electrocatalysts for CO_2 reduction; their unique characteristics make them candidates for pursuing the goal of environmentally friendly CO_2 reduction.

References

1. Hassan, L., and Khan, K.A. Applications of PKL electricity for use in DC instruments. In Microelectronics, Circuits and Systems: Select Proceedings of 7th International Conference on Micro2020, *Springer Singapore*, 191-202 (2021).
2. Nombona, N. Electrochemical studies of titanium, manganese and cobalt phthalocyanines.1-208 (2009).
3. Bard, A.J., Faulkner, L.R. and White, H.S. *Electrochemical methods: fundamentals and applications*. *John Wiley & Sons*, 1-850 (2022).
4. Norskov, J.K., Bligaard, T., Rossmeisl, J. and Christensen, C.H. Towards the computational design of solid catalysts. *Nature chemistry* **1**, 37-46 (2009).
5. Firdous, N. and Janjua, N.K., CoPtx/γ-Al_2O_3 bimetallic nanoalloys as promising catalysts for hydrazine electrooxidation. *Heliyon*, **5**, 1-27 (2019).
6. Nambi A., Chatzitakiz A., Olsbye U., Hjelm J., Zhao Y., Kaiser A. Gas-phase electrochemical CO_2 reduction on silver-copper BTC MOF in a zero-gap membrane electrode assembly. *Electrochimica Acta* 506, 144763-144772 (2024).
7. Huang J.-M., Zhang X.-D., Huang J.-Y., Zheng D.-S., Xu M., Gu Z.-Y. MOF-based materials for electrochemical reduction of carbon dioxide. *Coordination Chemistry Reviews*, 495, 215333-215350 (2023).
8. Kear, G., and Walsh, F.C. The characteristics of a true Tafel slope. Corrosion and materials **30**, 51-55 (2005).
9. Yin, Q., Xu, Z., Lian, T., Musaev, D.G., Hill, C.L., and Geletii, Y.V., Tafel slope analyses for homogeneous catalytic reactions. *Catalysts* **11**, 87-98 (2021).
10. Lin, R., Guo, J., Li, X., Patel, P. and Seifitokaldani, A. Electrochemical reactors for CO_2 conversion. *Catalysts*, **10**, 473-08 (2020).

Chapter 6: Conclusion and future prospects

6.1 Conclusion

This study investigated the synthesis Cu-BTC, MOF-5, and Ir(III)Cp*Cl@COMOC-4 using the solvothermal method. The characterization of each MOF was performed using Fourier transform infrared spectroscopy (FT-IR), X-ray diffraction (XRD), scanning electron microscopy (SEM), energy dispersive X-ray spectroscopy (EDX), Brunauer-Emmett-Teller (BET) analysis, and cyclic voltammetry (CV). The electrochemical behaviour of the MOFs during CO_2 reduction was analysed using CV. Cu-BTC exhibited high crystallinity and octahedral crystal morphology, as confirmed by XRD and SEM analyses. FT-IR results confirmed the presence of copper-oxygen bonds, and BET analysis revealed a moderate surface area for this MOF. Cyclic voltammetry showed characteristic copper redox peaks. SEM analysis of MOF-5 revealed typical cube-shaped crystals often associated with MOF-5. FT-IR confirmed the presence of zinc-oxygen bonds, and a moderate BET surface area was recorded. The Ir(III)CpCl@COMOC-4 material displayed irregularly shaped crystals with a low surface area. SEM micrographs indicated the MOF possess porous structures, while the electrochemical behaviour showed Ir reduction. The MOFs showed shifts in peak potentials during CO_2 reduction indicating CO_2 adsorption and demonstrating catalytic behaviour with increased currents.

The results of this study highlight the potential of these MOFs in CO_2 reduction technologies, particularly in environmentally friendly applications for CO_2 capture and conversion. Cu-BTC and MOF-5 showed promise, especially due to their high surface areas and microporous structures, though further studies are needed to understand their catalytic efficiencies. Overall, this research contributes valuable insights into the development of MOFs for CO_2 electrocatalysis and offers a pathway toward creating more effective materials for environmental sustainability.

6.2 Future prospects

Future research should aim to enhance the catalytic performance of MOFs for CO_2 reduction by refining their structural properties and surface functionalities. One promising approach could be the incorporation of two metal centres within MOF structures to boost electron transfer rates and reduce activation barriers for CO_2 conversion. Additionally, post-synthetic modification strategies, such as immobilizing co-catalysts, could further improve the overall efficiency of CO_2 reduction. Furthermore, exploring alternative electrochemical systems including differential electrochemical mass spectrometry (DEMS) is crucial for validating the reduction reaction, its pathway and the resulting products.